Application of FBG-Based Sensors in Built Environment

By

Jackson Teck Leong Yeo

Thesis submitted for the degree of

Doctor of Philosophy

City University

Measurement and Instrumentation Centre

School of Engineering and Mathematical Sciences

Northampton Square, London EC1V 0HB

July 2007

Table of Contents

List of Figures

List of Tables

Acknowledgements

I would like to express my gratitude to Professor Grattan and Dr Sun for their guidance, support and encouragement throughout the course of my PhD work.

I would like to thank Rob and Dave for their valuable advice and those fruitful discussions that we had. Thanks for your time, support and the effort in making the research facilities available during my two weeks visit to Kidde Research. I would also like to acknowledge the kind support from Kidde Plc for the partial funding provided for my PhD studies.

I am also very grateful to Professor Boswell and Brett for initiating the work on moisture sensing in concrete. Many thanks also to Jim Hooker for the technical support throughout my research work. I would like to thank all my friends in our group for the time that we shared together.

I am also greatly indebted to my parents who raised and educated me with their humble salary. Finally, I would like to thank my wife Christabel for being so supportive over the years and my son Alastair for giving me that extra boost I needed to complete my PhD.

Copyright Declaration

Abstract

Fibre Bragg grating (FBG)-based optical fibre sensors have found numerous applications in various industries over nearly 20 years. This is due to their many advantageous features, which include those that are typical of fibre-optic sensors (FOSs), for example being light weight, compact, having immunity to electromagnetic fields and an ability to operate in harsh environment. In addition to that, FBG-based sensors offer intrinsic multiplexing capability and they operate using wavelength-encoded signals which are insensitive to the intensity variations that normally affect the performance of intensity-based FOSs.

One particular sector that is developing an interest in the use of FBG sensing technology is the civil engineering industry, where FBG-based sensors have begun to be used as physical sensors in a variety of civil structures, many of which are built using reinforced concrete. These sensors are used as part of structural health monitoring (SHM) systems which are effective in detecting possible damage in civil structures as a result of physical loading and corrosion which can lead to deformation, crack formation, fatigue and overloading. However, such sensors are incapable of providing information pertaining to chemical attacks that cause the degradation of the concrete structure before physical damages have been detected or observed.

Arising from this, the aim of this thesis is to address the technology gap identified through the exploration and development of a series of FBG-based sensors for structural health monitoring and required by industry. The primary objective of the work is to explore the use of polymer-coated FBGs as sensors in the cementious matrix to monitor moisture which is considered as a main agent involved in most of the chemical attacks, by transporting corrosive ions in concrete structures. The sensing concept used in this work exploits the inherent characteristics of the FBG and is based on the strain effect induced in the FBG through the swelling of the polymer coating. A direct indication of the moisture level is given by the shift of the Bragg wavelength caused by the expansion of the sensing material. The context of the work, both technical and applications-focused and the development and characterisation of the sensors are discussed extensively in this thesis. The effectiveness of the sensors developed was evaluated through a series of tests performed under various harsh conditions using a range of concrete specimens with different porosity and mix composition, designed in collaboration with civil engineers.

Results of the work are reported and relevant conclusions drawn for the use of this technology in the civil engineering sector, as well as incorporating a discussion of future trends and potential wider applications.

Chapter 1:

Introduction and Background

1.1. Introduction

The concept of guiding light using fibre optics can be traced back as early as 1870 when the Irish scientist, John Tyndall first gave a demonstration to prove that light can actually be guided and propagated along a curved path. This phenomenon has formed the basis of the design of optical fibres which have become one of key components employed in the field of telecommunications and sensing. The breakthrough in fibre optic technology, almost 100 years later, came from the work carried out by Kao and Hockham [1], exploring an alternative means to achieve a better transmission bandwidth in telecommunications, using optical frequencies. The solution they offered was a design using a dielectric transmission medium which consists of a glass core cladding with a coaxial layer of glass of a lower refractive index value. This light guiding medium thus created is what we now know as the optical fibre. With the advancement of research activities driven by the need of faster transmission capacity, this fibre optic technology soon became the backbone of modern telecommunications systems.

Along with the telecommunications sector, which has experienced an increase in the usage of fibre optic technology, the use of optical fibres in sensing application has also drawn a considerable attention because of its distinctive advantages over open air-path approaches. Fibre optic sensors (FOS) basically share the same technological platform as fibre optic

communications and it offers numerous benefits such as being lightweight, small size, having immunity to electromagnetic interference, and chemically and biological inert in nature, for example. They can be designed to operate either in intrinsic or extrinsic sensor mode, using a variety of techniques to probe the characteristics of the light propagating in the optical fibre such as intensity, polarisation state, phase or frequency [2]. Depending on the transduction mechanisms used, for example, be they microbending loss, fluorescence, absorption, rotation, a variety of physical and chemical sensors can be developed which have potential applications in a wide range of industries.

Among the different types of FOSs reported to date, the fibre Bragg grating (FBG), which operates as a notch filter that has a temperature/strain dependent spectral profile, is the one class of FOSs that has gained widespread popularity over the years and has been one of the most topical subjects in the optical fibre sensor community. This can be inferred from the number of contributions presented in the past international conferences of Optical Fibre Sensors (OFS), for example, OFS 15 (2002) – OFS 18 (2006), where the total number of FBG-related papers accounts for around 30% of the total contributions [3-5].

The creation of FBG would not be possible without the discovery of photosensitivity in optical fibres. This phenomenon was first discovered by Kenneth Hill [6] whilst performing an experiment at the Communication Research Centre (CRC), Ottawa, Canada in 1978. However, the "Hill grating" demonstrated has limited potential due to its operating wavelength in the visible range. The research interest on FBG however, was revived almost 10 years later when Meltz and his coworkers [7] at United Technologies Research Centre (UTRC) demonstrated a transverse holographic fabrication technique which allows FBG with operating wavelengths in the optical communication bandwidth (Infrared band) to be written through the side of the optical fibre. Soon after, there was an upsurge in research activities on FBGs due to their potential applications, particularly in the fibre optic communication sector where it is used as a filtering device in Dense Wavelength Division Multiplexing (DWDM) networks.

FBGs have been commonly employed as physical sensors in a number of applications due to their inherent sensitivity to strain and temperature [8, 9]. In addition to the numerous advantages offered by FOSs, FBG sensors use wavelength-encoded signals which are insensitive to intensity

fluctuation and their unique wavelength-multiplexing capability also allows an array of sensing elements (with different operating wavelengths) to be cascaded along a single strand of optical fibre, thus forming a sensor network which is particularly attractive for in-situ structural health monitoring (SHM) application. Such a quasi-distributed sensing network allows *in-situ* non-intrusive measurements to be performed, for example on civil structures such as bridges or buildings, the focus of the work of this thesis. An illustration of this is that under the Intelligent Sensing for Innovative Structures (ISIS) research initiative established in the early 1990s in Canada, a total of 16 bridges in the country were fitted with FBG sensors to monitor the health condition of these structures [10]. Similar examples where FBG sensors are installed in civil structures can also be found in USA, Europe and Asia [11-15].

The majority of the FBG sensors employed for SHM in civil structures are for strain sensing which gives information that can be related to deformation, crack formation, fatigue, overloading, etc. Sensors may be configured in a variety of ways so that the aforementioned information is "translated" into strain which can be readily detected by a FBG. However, there seem to have been limited work carried out to explore the use of FOSs, particularly FBG-based sensors as complementary chemical sensors (for example, pH, chloride ion, moisture sensors) that may be potentially useful for monitoring the decay of reinforced concrete structures at its early stage when physical deformation has not been detected or observed. When combined with the physical sensors in the SHM system, comprehensive information can be provided in order to allow the civil engineers to perform a more comprehensive structural health analysis and thus to take early action to mitigate the damage caused.

1.2. Structural Health Monitoring

1.2.1. Degradation of Concrete Structures

Concrete is a widely used construction material as it is cost effective, versatile and durable. However, one major drawback of concrete is that the cementious material is brittle and has low tensile strength. To overcome this problem, reinforcement steel bars ('rebars') are incorporated into concrete to improve the strength and thus the durability of the structure. The combination of

concrete and steel has thus become a very popular choice of construction material and can be found in most of today's civil structures. Although the integration of rebars helps to overcome the tensile weakness of concrete, it has brought about a new problem which has become a global issue that is putting a financial strain on economies and industries worldwide: the corrosion of the rebars in concrete structure due to environmental effects. This consequently leads to the reduction of the structure's service life and an increase in maintenance costs. In a worst case scenario, the disastrous consequences which arise from the structure failure lead to loss of life. The estimated cost of damage, repair and maintenance due to corrosion in the US alone has reached the mark of one billion US dollars per annum [16] and the cost could set to increase unless countermeasures are taken to minimise the impact of this problem.

In a fresh concrete, the hydration process which occurs releases calcium hydroxide as a result of the chemical reaction involving calcium silicates and water present in the concrete mixture. This gives concrete a highly alkalinity, with a typical pH value ranging from 12-13. With the rebars embedded into the concrete, this highly alkaline environment creates a very thin but dense passivating oxide layer on the surface of the rebar thus forming a protection barrier which reduces its corrosion rate to a very insignificant level [17]. The duration of this protection period however, depends on a number of factors, mainly the retention of this high pH level within the concrete and the integrity of the concrete that surrounds the rebars which prevents the ingress of harmful aggressive species that could trigger the onset of corrosion.

There are several mechanisms that could attack the protective barrier surrounding the rebar and expose it to corrosion [17]. Carbonation is one of the mechanisms responsible for the corrosion of the rebar. It takes place when the hydrated cement paste reacts with the aqueous solution formed by carbon dioxide and moisture present in the matrix. The resulting chemical reaction lowers the pH level down to 9-10, causes the breakdown of the passivating oxide layer and results in the formation of calcium carbonate. This strips the rebar of its protective layer and makes it vulnerable to corrosion when other agents such as oxygen and moisture is present. Another mechanism that can trigger the corrosion process is the ingress of chloride ions into a reinforced concrete structure. Chloride ions (for example originating from deicing salts, seawater, etc.) can penetrate into the concrete through the pores of hydrated cement paste and when accumulated to

a sufficient concentration level, the passivating oxide layer breaks down and the rebar starts to corrode.

The consequence of the corrosion process is the volumetric expansion induced on the rebar. This build-up of the corrosion product on the surface of the rebar induces pressure on the concrete and results in internal damage to the structure. Over time, this cumulative effect will lead to crack formation, spalling and delamination that may eventually lead to structural failure.

In the two main mechanisms that account for the corrosion of steel bars in reinforced concrete, moisture is one main agent that takes part in all chemical processes. The ingress of carbon dioxide and chloride ions depends on the presence of moisture in which the chemical species are dissolved and carried into the porous concrete. When the passivating oxide layer is broken down and leaving the rebar exposed, the presence of oxygen and moisture is required in order for the corrosion process to take place. In an environment where the supply of oxygen is limited (for example, when the structure is buried underground), corrosion can theoretically take place through the reduction of water to hydrogen but the speed of the process is very slow [17].

1.2.2. Effect of Moisture and Humidity on Concrete Structures

A recent report by Sergi and Dunster [18] from the Building Research Establishment (BRE), UK, has concluded that the moisture level (expressed in terms of relative humidity) has a significant influence on the rate of carbonation and corrosion. For example, the rate of carbonation in concrete is observed to be the fastest between 60%RH-80%RH (see figure 1-1(a)) and the rate of corrosion in reinforced concrete with different concentration of chloride ions is influenced by the internal RH level. Hence, it is evident that moisture plays a key role in the degradation of concrete structure and therefore, it will be useful for civil engineers to have some means to obtain real time information pertaining to moisture level in concrete.

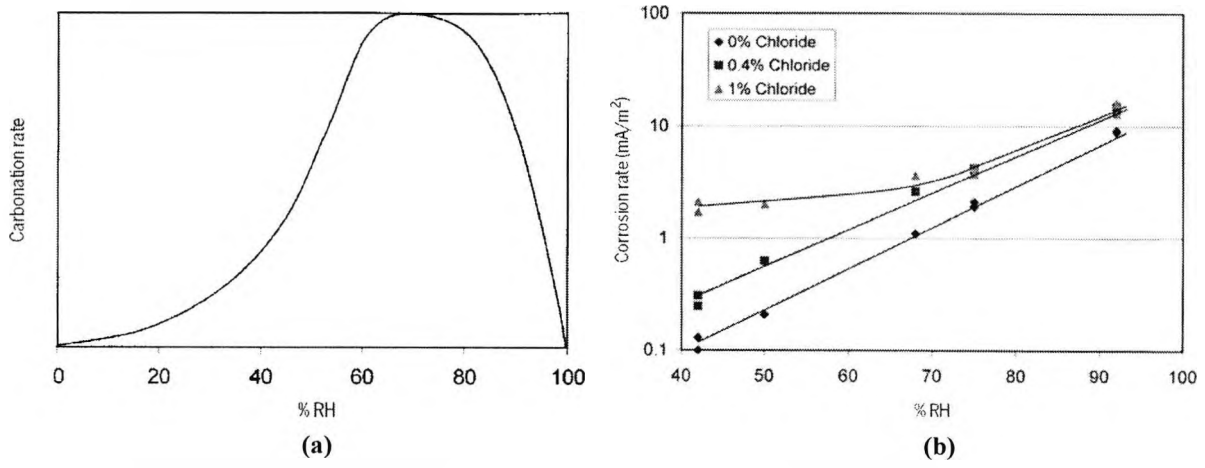

Figure 1-1: (a) Relationship between relative humidity and the rate of carbonation in concrete. (b) Influence of relative humidity on the corrosion rate of steel reinforcement obtained using carbonated mortars treated with chloride. [18]

1.2.3. Moisture Measurements

Various methods for moisture measurements have been considered and evaluated in the concrete industry [19, 20]. These include microwave absorption, magnetic resonance, neutron scattering and capacitance measurement using an electronic humidity sensor. These methods may be able to provide adequate measurements, thus giving information on the moisture level of the concrete structure at a specific position: however, it may not be feasible to form a sensor network using these methods to provide *in-situ* online monitoring of a civil structure. For example, the technique based on microwave absorption produces measurements that can be easily influenced by a great number of factors such as surface smoothness, salts dissolved within the matrix, concrete type. The neutron scattering technique requires the use of radioactive material, hence it raises health and safety concerns. The magnetic resonance technique is a highly sensitive method but it is expensive, bulky, easily susceptible to stray magnetic field and the tests can only be confined to the laboratory. The use of an electronic capacitive RH sensor may not be appropriate

as the device can corrode when embedded into concrete. In addition, it has shown limitations in terms of multiplexing and is susceptible to noise pickup if long electrical leads are used to cover the usually large concrete structures. Therefore, the choice of method that can be employed and implemented as part of structural health monitoring system for moisture sensing in concrete may seem to be limited.

1.2.4. Industrial Need for Chemical Sensors for Structural Health Monitoring

The need for chemical sensing is illustrated vividly by the photograph in figure 1-2, which shows a steel-reinforced concrete pedestrian bridge which collapsed after just 5 years into service [21]. The bridge which cost US$1 million to build collapsed in year 2000 due to the corrosion of the steel reinforcement bars in the bridge structure. The failure of this nearly new structure not only incurred a huge financial cost to the local authority but tragically it also resulted in more than 100 injuries.

Figure 1-2: Picture of a collapsed steel-reinforced concrete pedestrian bridge in North Carolina, USA. [21]

Below are some of the excerpts quoted from a news article that describes the incident-

Headline: ***"Dozens still hospitalized after walkway collapse"***

"Structural failure suspected in North Carolina accident"

(CNN News, 22 May 2000)

- ***"Some of the wires were rusted in two," said Don Idol, an engineer with the North Carolina Transportation Department.***
- ***"In my opinion, there probably was enough corrosion that could have caused the collapse," he told CNN on Monday.***
- ***"For corrosion, you need a combination of oxygen and moisture," Idol said. "At this point we do not know exactly how those items got to that steel."***
- ***"Cracks would have been a (warning) flag for us," he told The Charlotte Observer.***

It may be conferred from the above excerpts, the failure of the bridge was the result of corrosion to the steel bars in the reinforced concrete structure. The representative from the local authority concerned, however, was not certain about when the corrosion process started and how these deleterious agents penetrated into the concrete structure as there were no facilities onsite to monitoring the condition of the structure and routine inspection never took place during this short period of five years to identify signs which could help avert this catastrophic incident. This, therefore, emphasises the importance of investigating a structural health monitoring system which is designed to pick out not only the "physical" signals from the structure such as cracks which could possibly indicate advanced level of degradation but also "chemical" signals that could provide early warnings so that preventive measures can be carried out.

1.3. Aims and Structure of the Thesis

1.3.1. Aims and Objectives

In view of the discussions above, this thesis aims to address a gap in the area of FOS for structural health monitoring, in particular, fibre-optic-based moisture sensors that can be used as a complementary sensor to the FBG-based SHM systems. Therefore, the primary aims for this thesis are:

- To design and evaluate an FBG-based sensor scheme for moisture monitoring, suited to the needs of structural monitoring

- To conduct an experimentally-based programme with the objective of developing and characterising FBG-based sensors for the purpose of moisture detection and relating the data to the corrosion process analysis
- To work with civil engineers to test the sensors in concrete samples as a proof of concept to evaluate the effectiveness of the FBG-based moisture sensor developed in highly alkaline concrete environment.
- To draw relevant conclusions on the effectiveness of the sensors developed
- To report the results obtained in the peer reviewed literature and at conferences

1.3.2. Structure of the Thesis

The research work undertaken has been designed to fulfil the above aims and objectives and is discussed in detail in the following chapters, the contents of which can be summarized as follows:

Chapter 1 provides a brief introduction to the topic of the thesis and its aims, objectives and structure.

Chapter 2 incorporates an overview of fibre Bragg grating technology and extends this to a brief discussion on its applications in structural health monitoring.

Chapter 3 introduces the concept of humidity sensing which covers various sensing techniques that are commonly used with a literature review on the fibre optic techniques for humidity detection reported to date.

Chapter 4 discusses the principles, fabrication and characterisation of the FBG-based sensor schemes for humidity detection.

Chapter 5 presents the results obtained from a series of experiments carried out using different types of concrete specimens to evaluate the effectiveness of the sensor developed, working in conjunction with civil engineers.

Chapter 6 concludes the thesis with the results obtained from the sensors developed in this work and discusses further developments and applications of the sensor scheme.

The thesis concludes with a list of peer review published material by the author, arising from the work in the thesis.

1.4. References

[1] K. C. Kao and G. A. Hockham, "Dielectric Fibre Surface Waveguides for Optical Frequencies", *IEEE Proceedings*, 113(1966), 1168-1163.

[2] K .T. V. Grattan and B. T. Meggitt, "*Optical Fiber Sensor Technology*", First Edition, Chapman and Hall, 1995.

[3] *Proceedings of 15th International Conference on Optical Fiber Sensors*, 6-10 May, 2002, Portland, USA

[4] *Proceedings of 16th International Conference on Optical Fiber Sensors*, 13-17 October, 2003, Nara, Japan.

[5] *Proceedings of 17th International Conference on Optical Fiber Sensors*, 23-27 May, 2005, Bruges, Belgium.

[6] K. O. Hill, "Photosensitivity in Optical Fiber Waveguides: From Discovery to Commercialization", *IEEE Journal on Selected Topics in Quantum Electronics*, 6(2000), 1186-1189.

[7] G. Meltz, W. W. Morey and W. H. Glenn, "Formation of Bragg Gratings in Optical Fibers by a Transverse Holographic Method", *Optics Letters*, 14(1989), 823-825.

[8] Othonos and K. Kalli, "*Fiber Bragg Gratings: Fundamentals and Applications in Telecommunication and Sensing*",Artech House, 1999.

[9] Y. J. Rao, "Recent Progress in Application of In-Fibre Bragg Grating Sensors", *Optics and Engineering*, 31(1999), 297-324.

[10] R. C. Tennyson, A. A. Mufti, S. Rizkalla, G. Tadros and B. Benmokrane, "Structural Health Monitoring of Innovative Bridges in Canada with Fiber Optic Sensors", *Smart Materials and Structures*, 10(2001), 560-573.

[11] E. Udd, S. Calvert and M. Kunzler, "Usage of Fibre Grating Sensors to Perform Critical Measurements of Civil Infrastructure", in *Proceedings of OFS 16*, Nara, Japan, 2003, 496-499.

[12] J. D. Doornink, B. M. Phares, Z. Zhou, J. Ou, T.W. Graver and Z. Xu, "Fiber Bragg Grating Sensing for Structural Health Monitoring of Civil Structures", *Proc. International Symposium on Advances and Trends in Fiber Optics and Applications*, 293(2004).

[13] Y. M. Gebremichael, W. Li, W. J. O. Boyle, B. T. Meggitt, K. T. V. Grattan, B. McKinley, G. F. Fernando, G. Kister, D. Winter, L. Canning and S. Luke, "Integration and Assessment of Fibre Bragg Grating Sensors in an All-fibre Reinforced Polymer Composites Road Bridge", *Sensor and Actuators A*, 118(2005), 78-85.

[14] P. M. Nellen, R. Bronnimann and U. Sennhauser, "Optical Fiber Bragg Grating for Structural Monitoring in Civil Engineering", in *Proceedings of 16th Congress of IABSE*, Lucerne, 2000.

[15] W. H. Chung, S. Y. Liu, B. O. Guan, T. L. Chan, T. H. T Chan and H. Y. Tan, "Structural Monitoring of Tsing Ma Bridge using Fiber Bragg Grating Sensors", in *Proceedings of Sixth Chinese Optoelectronics Symposium*, 2003, 144-146.

[16] http://www.jpbroomfield.co.uk/html/corrosion_topics-corrosion-of-steel-in-concrete.htm

[17] "Corrosion of Steel in Concrete: Durability of Reinforced Concrete Structures", *BRE Digest* 444 Part 1, BRE Press, 2000.

[18] G. Sergi and A. Dunster, "Corrosion of Steel in Concrete: A Review of the Effect of Humidity", *BRE Digest* 491, BRE Press, 2004.

[19] J. Hundt and J. Buschmann, "Moisture Measurement in Concrete", *Materials and Structures*, 4(1971), 253-259.

[20] J. G. Assenheim, "Moisture Measurement in the Concrete Industry", *Concrete Plant and Production*, 11(1993), 129-131.

[21] http://archives.cnn.com/2000/US/05/22/walkway.collapse/#r

Chapter 2:

Fibre Bragg Grating Based Sensors

2.1. Introduction

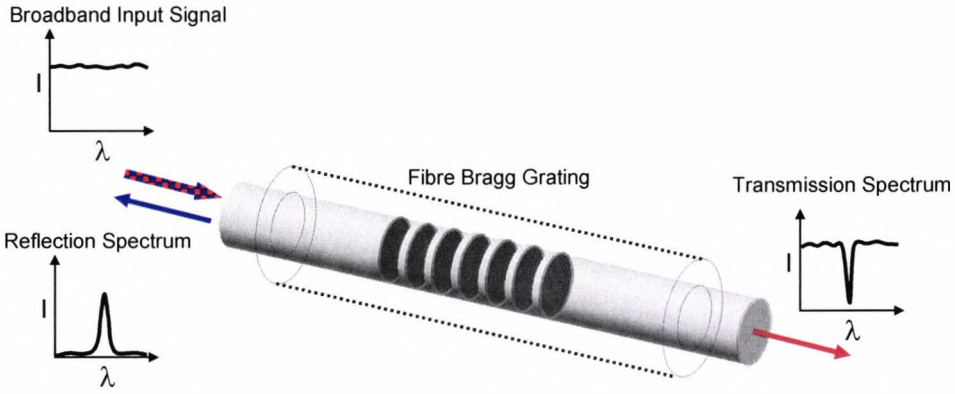

Figure 2-1: Illustration of a fibre Bragg grating.

A fibre Bragg grating (FBG), as shown in Figure 2.1, is a photoinduced in-fibre device formed by periodic refractive index modulation through the exposure of the fibre core to a UV interference pattern. This results in an intracore grating device which behaves as a wavelength selective filter with inherent sensitivity to temperature and strain. The invention of FBG has revolutionized the field of telecommunication and sensing and has led to numerous applications in various industries [1, 2]. Main usage of FBGs includes filtering devices in wavelength division multiplexing (WDM) optical communication systems, wavelength stabiliser in diode lasers, fibre lasers and physical sensors (strain, temperature, pressure, etc) in a range of applications.

As discussed in Chapter 1, the creation of FBG would not be possible without the photosensitivity of optical fibres and this was first discovered at the Communication Research Centre (CRC), Ottawa, Canada in 1978 while investigating the non-linear effect of a custom made silica optical fibre [3]. During the experiment, intense Argon ion laser radiation was launched into a germanium-doped silica fibre in a three-mirror-cavity fibre Raman laser configuration. After a prolonged exposure to the laser radiation, it was observed that the transmitted light decayed substantially, causing an increase in the intensity of the light reflected back from the fibre. Further experiments performed by Kenneth Hill [4], as shown schematically in Figure 2.2, confirmed that the phenomenon was due to the refractive index modulation of the fibre core as a result of the standing wave pattern created by the laser beam reflected back into the core of the fibre at the fibre end. The photoimprinted Bragg grating with a period equal to approximately half the wavelength of the laser source was found to be permanent and has a narrow-band frequency response which can be tuned by temperature or strain. This internally written Bragg grating which exhibits resonance at the writing laser wavelength is thus known as the "Hill grating" [5]. The creation of "Hill grating" hence marks the discovery of photosensitivity in optical fibres and the term photosensitivity has since been used to denote a permanent light-induced refractive index change [3].

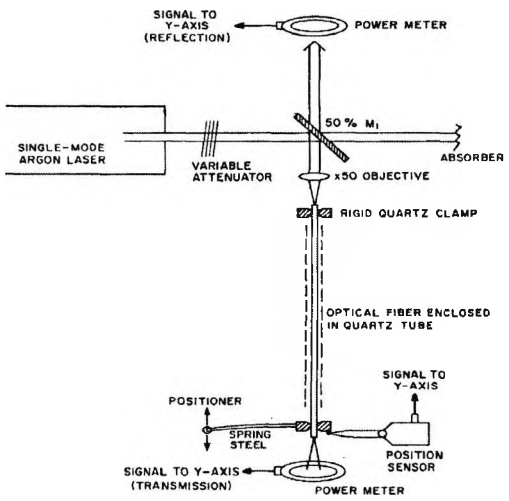

Figure 2-2: Schematic of the apparatus used by Hill *et al.* [4] to investigate the formation of Bragg grating in optical fibre.

Although photosensitivity has been observed in a wide variety of optical fibres with a range of dopants, the phenomenon was originally perceived to be associated with the germanium dopant in optical fibres. Such fibres result in the creation of the germanium oxygen vacancy point defects induced by the modified chemical vapour deposition (MVCD) technique used in the fibre preform fabrication. These point defects, known as germanium oxygen-deficient centres (GODCs), exhibit absorption bands between 240 – 250 nm and are linked to the photoinduced refractive index change mechanism in the optical fibre. There have been several hypotheses proposed to explain the photoinduced refractive index change and are all linked to the common element that is the GODCs as the main precursors for this mechanism; however the phenomenon of photosensitivity cannot be explained fully by any model. Detailed discussion on the phenomenon of photosensitivity and the mechanism of photoinduced refractive index change will not be covered in this thesis but a comprehensive review on this subject can be found in literature published by Othonos and Kalli [1].

The use of the "Hill grating" is limited by the operational wavelength which is close to that of the writing laser at visible wavelengths. This limitation however, was overcome about 10 years later using a transverse holographic technique reported by Meltz and his coworkers [6] at United Technologies Research Center (UTRC). The technique described allows gratings with resonance wavelengths in the infrared region to be written through the side of the fibre using the interference pattern created by two overlapping UV beams at 244 nm. Soon after, there was an upsurge in research activities on FBGs due to its potential applications, particularly in the fibre optic communication sector. To date, there have been numerous articles on all aspects of FBG-related research and many commercial devices and systems based on FBG technology which can be found in many different areas. This gives a clear indication of the research underpinning the FBG technology which remained strong, even after a discovery made more than 25 years ago.

In this chapter, the background to FBGs is introduced, covering several aspects which include the general properties of FBG, different classification of grating types, various inscription techniques and finally a brief overview on the use of FBGs as sensors in the built environment.

2.2. Properties of FBGs

This section aims to give a general overview of various properties of FBG. Although there exists a variety of both simple and complex grating structures (e.g. chirped gratings, blazed gratings, etc.) that fall under the general category of FBGs, discussion in this section is solely focused on the properties of a simple uniform grating which is employed in this research work.

2.2.1. Bragg Resonance Condition

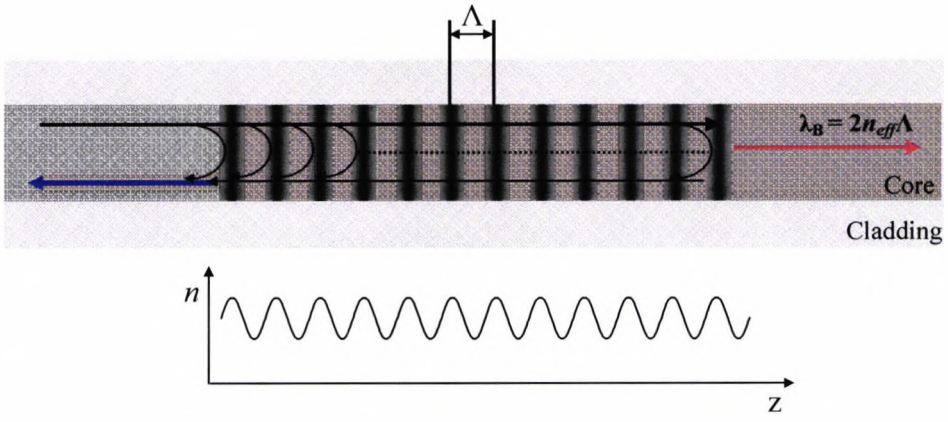

Figure 2-3 Schematic of a fibre Bragg grating and the refractive index modulation profile in the fibre core.

The diagram in figure 2-3 depicts the structure of a simple uniform FBG which consist of a periodic refractive index modulation along the core of a photosensitive optical fibre. Light propagating along the fibre core will be reflected by the series of grating planes that forms the structure of the FBG. At each of the grating planes, reflection of the incident light takes place. This results in series of reflections along the entire length of the grating. If the Bragg resonance condition is not fulfilled, the light reflected at each of these grating planes will be out of phase and eventually cancels out as it adds destructively. When the Bragg resonance condition is met, the reflected light at each grating plane which will be in-phase accumulates and adds

constructively to form a back-reflected peak with a centre wavelength that can be defined by the grating parameters.

The first-order Bragg resonance condition is given by [1],

$$\lambda_B = 2n_{eff}\Lambda \tag{2-1}$$

where λ_B is the centre wavelength of the incident light that is being reflected back by the FBG commonly known as the Bragg wavelength, n_{eff} is the effective refractive index value of the fibre core at the Bragg wavelength and Λ is the period of the grating structure.

The Bragg resonance condition is met by the fulfilment of the principles of energy and momentum conservation. To conserve the energy, the frequency of the incident light should be the same as the reflected light, giving

$$e_i(h\nu_i) = e_r(h\nu_r) \tag{2-2}$$

where e_x (x denotes i for incident and r for reflected) is the product of the Planck's constant, h, and the frequency of the light, ν_x.

For the conservation of momentum, the wavevector of the reflected wave, k_r, must be equal to the sum of the incident wavevector, k_i and the grating wavevector, K (with a magnitude of $2\pi/\Lambda$). This is given by

$$k_r = k_i + K \tag{2-3}$$

If the Bragg resonance condition is met, k_i and k_r in opposite directions but equal in magnitude, equation 2-3 becomes [1]

$$2\left(\frac{2\pi n_{eff}}{\lambda_B}\right) = \frac{2\pi}{\Lambda} \tag{2-4}$$

Equation 2-4 can be simplified to give the resulting first-order Bragg condition as given in equation 2-1.

2.2.2. Reflectivity of a Uniform Fibre Bragg Grating

FBG produced by the irradiation of the UV interference pattern gives a refractive index modulation profile of a sinusoidal nature and can be given by the following expression [1],

$$n(z) = n_0 + \Delta n \cos\left(\frac{2\pi z}{\Lambda}\right) \tag{2-5}$$

where n_0 is the average refractive index of the fibre core, Δn is the amplitude of the induce refractive index change with typical values ranging from 10^{-3}-10^{-5} and z is the distance along the fibre. An expression was derived by Lam and Garside [7] to describe the reflectivity (R) of a Bragg grating with a constant amplitude of modulation and period as a function of the grating length (l) and wavelength (λ) which is given by [1],

$$R(l,\lambda) = \frac{\Omega^2 \sinh^2(sl)}{\Delta k^2 \sinh^2(sl) + s^2 \cosh^2(sl)} \tag{2-6}$$

where Δk is the detuning wavevector equal to k-π/λ, k is the propagation constant equal to $2\pi n_o/\lambda$ and $s = (\Omega^2 - \Delta k^2)^{1/2}$ and Ω is the coupling coefficient for sinusoidal variation of the refractive index modulation along the fibre core and is given by [1],

$$\Omega = \frac{\pi \Delta n}{\lambda}\left(1 - \frac{1}{V^2}\right) \tag{2-7}$$

where $(1-1/V^2)$ represents the fraction of the fibre mode power confined in the fibre core and can be estimated using the normalised frequency [8],

$$V = \left(\frac{2\pi}{\lambda}\right) a\sqrt{n_{co}^{2} - n_{cl}^{2}} \qquad (2\text{-}8)$$

where a is the radius of the fibre core, n_{co} and n_{cl} represent the refractive indices of the core and cladding respectively.

At the Bragg resonance wavelength, the detuning wavevector is equal to zero and this results in a simplified expression for the reflectivity (R) showing its dependence on the amplitude of the induced refractive index change and the length of the grating.

$$R(l, \lambda) = \tanh^{2}(\Omega l) \qquad (2\text{-}9)$$

2.2.3. Strain and Temperature Sensitivities of FBGs

The FBG has an inherent sensitivity to strain and temperature. Its spectral characteristic changes when any of the grating parameters, as defined in equation 2-1 (i.e. refractive index and period of the grating structure), is subjected to strain and/or temperature perturbation. The influence of these two parameters which induce a change in the Bragg wavelength ($\Delta\lambda_B$) can be emphasised by differentiating equation 2-1 and is given by,

$$\Delta\lambda_B = 2n_{eff}\Delta\Lambda + 2\Lambda\Delta n_{eff} \qquad (2\text{-}10)$$

The change in Bragg wavelength as a function of the strain applied to the FBG is linked to 1) the physical deformation experienced by the optical fibre which consequently changes the grating period, and 2) the strain-optic effect that affects the effective refractive index of the FBG. Similarly, temperature-induced Bragg wavelength shift is contributed by 3) the thermal expansion of the optical fibre material and 4) the thermo-optic effect.

To describe the strain-induced Bragg wavelength shift, equation 2-10 can be modified to give [9],

$$\Delta\lambda_B = \lambda_B \left(\frac{\frac{\partial \Lambda}{\Lambda}}{\frac{\partial l}{l}} + \frac{\frac{\partial n_{eff}}{n_{eff}}}{\frac{\partial l}{l}} \right) \frac{\Delta l}{l} \tag{2-11}$$

where l is the length of the grating and $\frac{\partial \Lambda}{\Lambda} = \frac{\partial l}{l} = \frac{\Delta l}{l}$ represents the strain (ε) induced on the fibre, thus giving

$$\frac{\Delta\lambda_B}{\lambda_B} = \varepsilon + \frac{\Delta n_{eff}}{n_{eff}} \tag{2-12}$$

The right hand side of the above equation shows the contributing terms which result in the shift in Bragg wavelength and are represented by the physical deformation induced on the optical fibre (first term) and the change in refractive index value due to strain-optic effect (second term). The equation can be re-written as a more commonly used expression to determine the strain-related Bragg wavelength shift and is given by [10],

$$\frac{\Delta\lambda_B}{\lambda_B} = (1 - p_e)\varepsilon \tag{2-13}$$

where p_e is the strain-optic coefficient and is defined by

$$p_e = \frac{n_{eff}^2}{2}\left[p_{12} - v(p_{11} + p_{12})\right] \tag{2-14}$$

where p_{11} and p_{12} are the Pockel's coefficients (typical values for a germanosilicate optical fibre- p_{11}:0.131 and p_{12}:0.252) [1] and v is the Poisson's ratio (typical value:0.16) [1]. p_e is usually considered as a constant which can be calculated using the fibre parameters and has a typical value of ≈0.22 [11]. For operation at the 1550 nm wavelength region and at a constant temperature, the typical strain response of a FBG has a sensitivity of ≈1.2 pm per microstrain (με).

Similarly, to consider the thermal-induced Bragg wavelength shift, equation 2-10 can be modified to give

$$\Delta\lambda_B = \lambda_B\left(\frac{1}{\Lambda}\frac{\partial\Lambda}{\partial T} + \frac{1}{n_{eff}}\frac{\partial n_{eff}}{\partial T}\right)\Delta T \qquad (2\text{-}15)$$

where the term $\frac{1}{\Lambda}\frac{\partial\Lambda}{\partial T}$ represents the thermal expansion coefficient (α) of the optical fibre and the term $\frac{1}{n_{eff}}\frac{\partial n_{eff}}{\partial T}$ is the thermo-optic coefficient (ξ) with values of $0.55\text{x}10^{-6}$ (silica) and $8.6\text{x}10^{-6}$ (germania-doped , silica core fibre) respectively [1]. This gives a typical FBG thermal sensitivity of ≈13 pm/°C when operating at 1550 nm.

With these typical values of the optical fibres used to fabricate FBGs, it is clear that the thermo-optic effect is a far more dominant factor as compared to thermal expansion; therefore the thermal-induced Bragg wavelength shift is contributed mainly by the change in the refractive index value of the FBG (nearly 90% of the total contribution). However, when the FBG has an overlay of materials which possess different thermal expansion coefficients as is the case for silica optical fibre, this correlation is altered. Materials including metals and polymers have been considered by various researchers [12-16] to tailor the thermal response of the FBG for a range of sensing applications.

2.3. Classification of FBGs

The classification of FBGs is associated to the growth dynamic of the Bragg gratings during the inscription process and their spectral and thermal characteristics. Although this is complicated by various types of photosensitive fibres, the UV radiation bands and the characteristics (CW/pulse and power) of the laser sources, FBGs can be generally classified into 3 different types, namely, type I, type IIA and type II.

Type I FBGs are most commonly used in various optical communication and sensing applications. It can be fabricated in most photosensitive fibres using either CW or pulsed UV laser sources [1]. In a typical inscription process, the monotonic positive change in the refractive index due to UV radiation resulted in an increase of reflectivity at the Bragg wavelength. A fundamental trait of a type I FBG is the spectral characteristics which is complementary in both

transmission and reflection mode. Among the different classes of FBGs, the type I FBG exhibits the lowest thermal sustainability. For example, type I FBGs fabricated using the highly photosensitive Boron/Germanium fibre can be erased at temperature of ≈400°C, which increases to 500°C, if a type IIA is fabricated using the same fibre. However, the grating thermal sustainability is also highly dependent on the fibre composition. Comparing different fibre compositions, the temperature at which type I FBGs can be erased for Germanium-doped fibre is ≈750°C and a higher value of 900°C can be achieved using Antimony or Tin doped fibres [17].

Type IIA FBGs have similar spectral characteristics as the type I FBGs. The type IIA FBG is formed by further extending the UV exposure period used in the inscription process of the type I FBG. This causes the type I grating to be partially erased after prolonged exposure to the UV radiation before the formation of the type IIA grating. The formation of the grating is accompanied by a negative change in the refractive index of the fibre resulting in a blue shift in Bragg wavelength. A type IIA grating has a relatively broader bandwidth as compared to the type I grating and is more thermally stable at high temperatures [1].

Type II gratings are distinctly different from the two grating types discussed above. They are referred to damaged-written grating due to the inscription process (single intense laser pulse) used which causes physical damage in the fibre structure and results in a large refractive index change in small localised regions at the core and cladding boundary. The spectral characteristics are also very much different from that of the type I and IIA, in which the wavelengths longer than the Bragg wavelength pass through the type II grating and the shorter wavelengths are coupled into the fibre cladding [1]. Such a grating type is shown to exhibit very high temperature stability and no degradation in grating reflectivity is observed even when tested in an elevated temperature environment of 800°C over a period of 24 hours.

2.4. FBG Inscription Techniques

There are many techniques reported to date, for the inscription of Bragg gratings in optical fibres. These include the internal writing technique [5] used to produce the well-known "Hill grating" and a range of external writing techniques proposed by various researchers, for example, the

interferometric [6], point by point [18] and phase mask [19] methods. External writing techniques are much preferred due to the nature of the setup which allows gratings to be written through the side of the fibre and they are used to overcome the limitations of internally written gratings.

This section summarises the common external writing techniques reported. More comprehensive information on various inscription techniques to create regular or complex grating structures can be found in textbooks by Othonos and Kalli [1] or Kashyap [20].

2.4.1. Interferometric Techniques

2.4.1.1. Amplitude Splitting Interferometric Technique

The first interferometric technique for FBG fabrication as shown in figure 2-4 was demonstrated by Meltz *et al.* [6] in 1989. The set-up was based on an amplitude splitting interferometer which consists of a beam splitter and a set of mirrors. The incoming UV laser beam was divided and subsequently recombined to generate a two-beam interference pattern which was imprinted onto the core of a photosensitive fibre to create a permanent refractive index modulation thus forming the Bragg grating. Using this technique, the Bragg wavelength of the FBG can be selected by changing the period of the interference pattern which is identical to the period of the Bragg grating (Λ) and is given by [1]

$$\Lambda = \frac{\lambda_w}{2\sin\theta} \tag{2-16}$$

where λ_w is the wavelength of the writing laser and θ is the half angle of the intersecting beams.

Since the Bragg condition is only fulfilled when the resonance wavelength (λ_B) is equal to 2 times the product of effective refractive index and the period of the grating, the resonance wavelength can be selected by changing the angle at which the two beams intersect and is given by the following expression [1],

$$\lambda_B = \frac{n_{eff}\lambda_w}{\sin\theta} \tag{2-17}$$

where λ_B is the Bragg resonance wavelength and n_{eff} is the effective refractive index of the grating.

The amplitude splitting interferometric technique offers flexibility in terms of the Bragg wavelength selection. The fabrication set-up, however, is susceptible to mechanical vibration and requires precise alignment of the optical components. The interference fringe pattern produced is also prone to drift over a period of time due to the long optical path length.

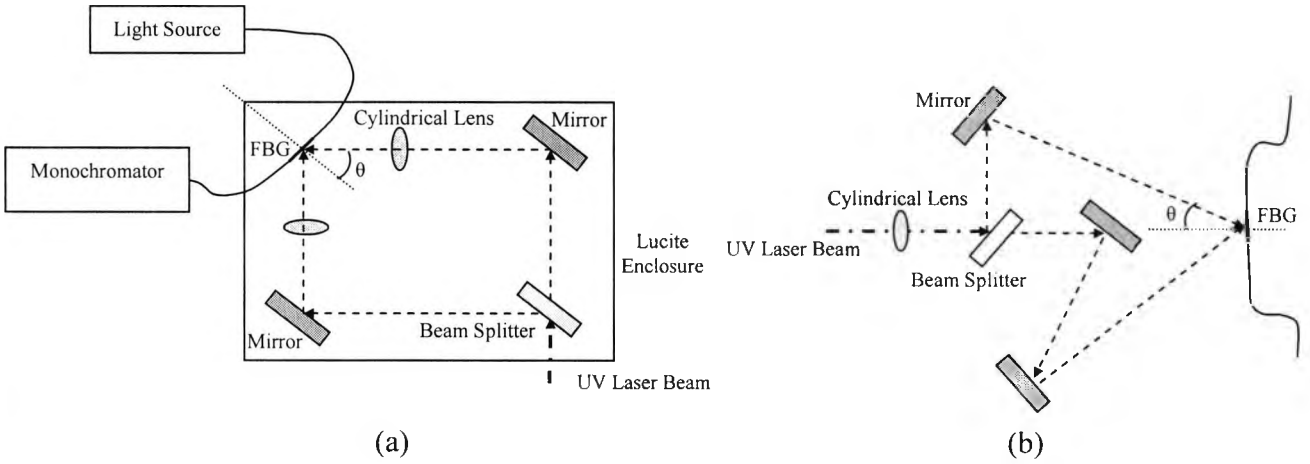

Figure 2-4: Schematic diagrams of amplitude splitting interferometric FBG inscription technique. (a) Set-up used by Meltz *et al.* [6] for the first demonstration of side written FBG. (b) Alternative configuration [1] with additional mirror to compensate for the imbalanced beam path in (a) due to the number of reflections, hence ensuring the two beams arriving at the fibre are identical.

2.4.1.2. Wavefront Splitting Interferometric Technique

The Lloyd mirror and prism interferometers are examples of wavefront splitting interferometers used for grating fabrication as shown schematically in figure 2-5 [1]. The Lloyd mirror interferometer configuration simply consists of a single mirror which is positioned orthogonally to the optical fibre. The incident laser beam is centred at the position where the mirror and fibre intersects. With the placement of the mirror, one half of the incident beam passing through the

cylindrical lens is guided directly to the fibre, with the other half reflected off the mirror surface. This causes the two halves of the beam to overlap, thus forming an interference pattern for grating inscription. With the mirror replaced by a prism, the fabrication set-up can be configured as a prism interferometer. In this set-up, the incident laser beam is expanded through refraction at the input face of the prism. The beam is spatially divided into two halves, with one projected directly onto the output face of the prism while the other is refracted towards the same output point through total internal reflection. This thus causes the two beams to interfere, creating fringe pattern for grating inscription.

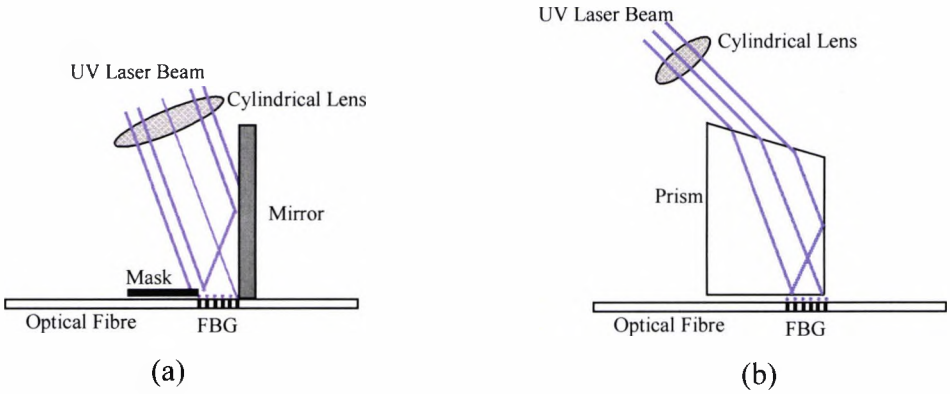

Figure 2-5: Illustration of wavefront splitting interferometic inscription technique. (a) Lloyd interferometer and (b) Prism interferometer.

Though not as popular in use as the amplitude splitting interferometric technique, the wavefront splitting interferometers requires only one optical component which eases the requirements for alignment and vibration isolation. The interference fringes produced by the two intersecting beams are more stable owing to the shorter distance which the beams are separated, thus are less susceptible to air current and temperature change. One of the main drawbacks of this technique is that the FBG produced has short grating length which is generally limited to half of the laser beam. With a laser beam width of a Gaussian profile, the interference of the folded beams gives a non-uniform intensity profile and together with the path length difference introduced by the reflection at the mirror, the quality of the resultant fringe pattern is degraded. Therefore, the coherence length of the laser source and the uniformity of the intensity profile should be considered when using this technique.

2.4.2. Phase Mask Technique

The phase mask writing technique for fibre Bragg grating fabrication was first reported by Hill and his co workers [19]. This technique was created to provide an effective and simple way of fabricating FBGs with higher tolerance against mechanical vibrations and coherence quality of the writing laser source. The set-up requires minimal optical components and is relatively easy to align. The fabrication process is highly repeatable, thus allows FBGs to be produced in volume.

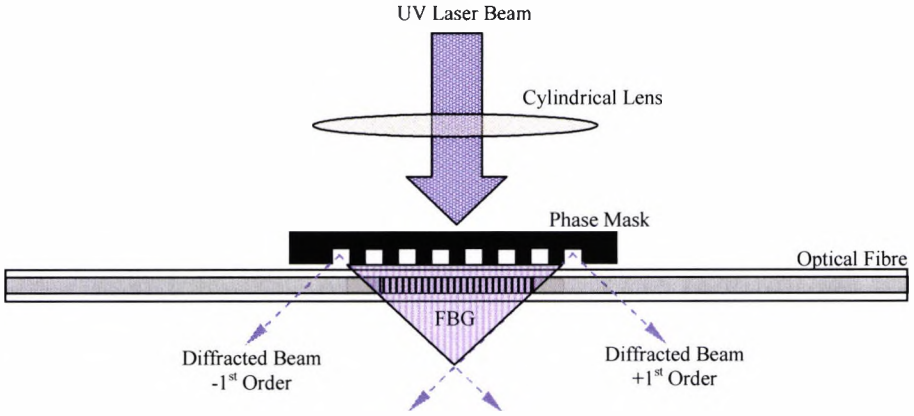

Figure 2-6: Schematic of phase mask technique.

The main feature of this technique is the diffractive optical element (Phase mask) used to modulate spatially and diffract the incident UV laser beam. The phase mask is a surface-relief grating etched onto a UV transparent silica substrate using photolithography techniques. The grating resembles a square-wave profile with a controlled mark-space ratio and etch depth. In order to effectively generate the interference fringes for FBGs inscription, the etch depth is controlled so as to suppress the diffraction of the incident laser beam into the zero order and maximises the light contained in the ±1 order [10]. In practice, the zero order can be suppressed to less than 5% of the total light intensity and around 35% diffracted to the ±1 orders which form the principle beams to produce the interference pattern. The fringe period, which corresponds to the period (Λ) of the FBG (thus the Bragg wavelength, λ_B), is half the period (Λ_{Mask}) of the phase mask [20]. The selection of the phase mask period to produce FBGs at a specific wavelength is independent of the wavelength of the UV laser, however, the etch depth required to suppress the zero order is a function of wavelength and optical dispersion of the silica substrate [10, 20].

The diagram in figure 2-6 shows the typical set-up of the phase mask writing technique. The photosensitive fibre is placed directly behind and in very close proximity to the phase mask. The FBG is created by exposing the fibre to the fringe pattern created from the interference of ±1 orders. Despite the numerous advantages, a drawback of using the phase mask for the direct inscription of the FBG is the lack of wavelength selectivity. Therefore, for applications which need FBGs with different Bragg wavelengths, multiple phase masks are required. Soon after the first demonstration of the phase mask technique, variants of the technique were discussed by several researchers [21-26]. These techniques were aimed to improve on the technique reported by Hill *et al.* [19]. For example, Armitage [21] proposed to insert a fused silica block in between the phase mask and the optical fibre for FBG fabrication. The diffracted UV beams enter the face of the silica block and are internally reflected off the side walls before emerging on the opposite face. This slight modification to the existing technique creates a non-contact far field method which allows gratings to be written in optical fibre whilst minimizing the risk of damaging the phase mask.

To improve on the wavelength selectivity, techniques involving pre-straining optical fibre before fabrication [22] and demagnification of the periodicity of the UV pattern through a simple lens system [23] have been proposed. Alternatively, the position of the optical fibre can be placed at an angle relative to the phase mask. Such a technique was demonstrated by Othonos and Lee [24] to tune the Bragg wavelength of FBG fabricated using a phase mask. In their experiment, one end of the fibre was placed against the mask and the other end away from the mask at various distances ranging from 0-500 μm. A tuning range of 2 nm was demonstrated, showing FBGs fabricated at different Bragg wavelength which can be derived using the general expression given by

$$\lambda_B = 2n\Lambda\sqrt{1+\frac{r^2}{l^2}} \qquad (2\text{-}19)$$

where r is the distance between one end of the fibre and the mask, l is the length of the phase grating [24].

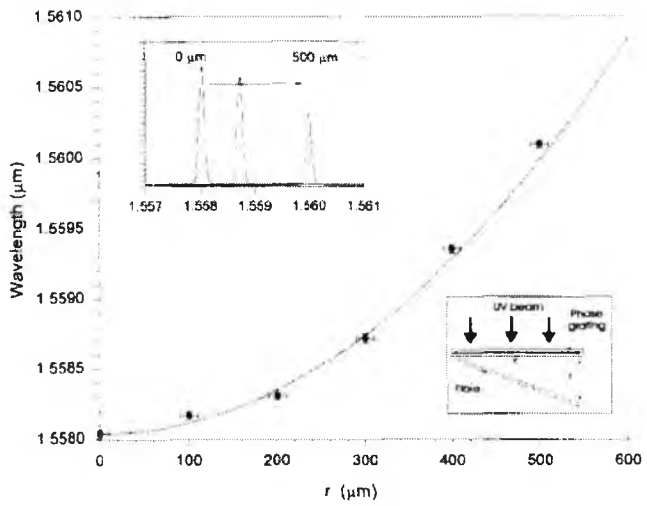

Figure 2-7: Tuning of the Bragg wavelength through placement of fibre relative to the phase mask position. [24]

The phase mask can be incorporated into various interferometer configurations as shown in figure 2-8. In these configurations, the phase mask functions as a beam splitting element, and is used together with a pair of steering mirrors to form a phase mask based interferometer for FBG fabrication [25, 26]. Similar to the technique discussed in Section 2.4.1.1, the ±1 order laser beams diffracted from the phase mask are recombined to produce interference fringes for grating inscription. The angle (θ_c) at which the two beams intersect determines the Bragg wavelength and is given by

$$\theta_c = \theta_p + 2\theta_m \qquad (2\text{-}20)$$

where θ_p is the angle of the diffracted order and θ_m is the angle of the steering mirrors.

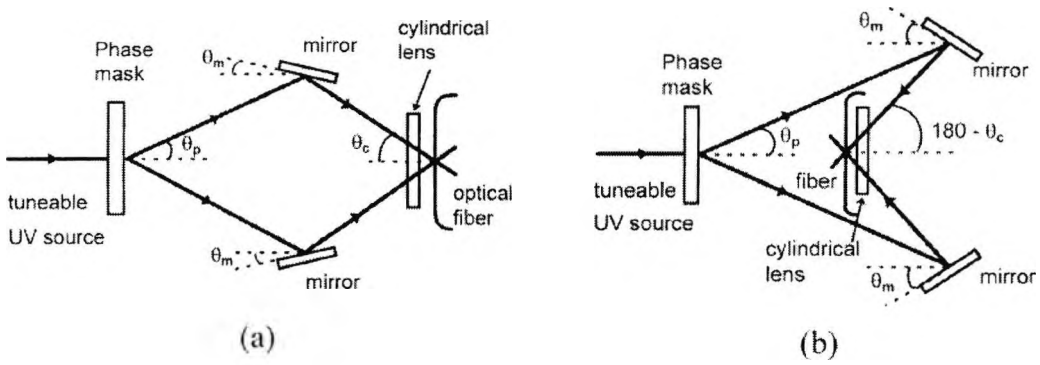

Figure 2-8: Set-up used for phase mask based interferometric inscription technique. [25]

Substituting equation (2-20) into (2-17) gives the relationship between the Bragg wavelength (λ_B), the angle of the diffracted order and steering mirrors and is given by

$$\lambda_B = \frac{n_{eff}\lambda_L}{\sin(\theta_p + 2\theta_m)} \qquad (2\text{-}21)$$

Though the technique demonstrated allows the Bragg wavelength to be tuned by changing the angle of the steering mirrors or the wavelength of the writing laser source, the main drawback of this technique is that the optical configuration needs to be adjusted in order to compensate for the change in the direction of the beam path (thus maintaining beam overlap) as a result of the change in θ_c which is dependent on both the wavelength of the laser and mirror angle. The variation in wavelength dependent θ_c, however, can be easily compensated by changing the distance between the phase mask and the mirror using a translation stage.

2.4.3. Point-by-point Writing

Fibre Bragg grating fabrication using the point-by-point writing technique can be realised by illuminating the fibre core with a highly focused KrF excimer laser beam. The periodic refractive index modulation profile along the fibre is formed by repeatedly exposing a single spot on the fibre core to the focused UV laser beam, each spaced out in a distance which corresponds to the

period (Λ) of the Bragg grating to form the alternating grating planes that form the grating structure. This technique was first discussed by Malo *et al.* [18], using pulses of 248 nm laser beam to demonstrate the fabrication of a third order FBG containing 225 index perturbation with a period (Λ) of 1.59 μm, resulting in a grating length of 360 μm. The flexibility of this inscription technique allows the period of the grating to be controlled, thus allowing FBGs of different Bragg wavelength to be fabricated. This technique however is only suitable for short gratings due to several factors which include the difficulty in controlling precise translation stage movement over a long distance, possible change in grating spacing due to thermal and strain effects induced on the fibre during the fabrication process [1, 20]. The point-by-point technique is a time consuming process and it also requires a high precision translation stage to allow fine control of the fibre movement.

2.5. Application of FBG Based Sensors in the Built Environment

The widespread research and development activities carried out across the world by various research institutions and commercial enterprises, coupled with the ever demanding need of the industries have pushed the FBG sensor technology into maturity over recent years. With the availability of commercial sensors and interrogation systems, there has been an increase of FBG-based sensing systems employed in various industries, for example, aerospace, marine, transportation, energy, oil and gas [27-29]. In particular, considerable attention has been drawn to the application of FBGs as sensors in the field of civil engineering where FBG-based technology has found a niche market in structural health monitoring (SHM) [30-41].

The structural integrity of civil structures is of paramount importance. Degradation as a result of various processes such as corrosion, fatigue, overloading, may lead to the failure of these structures and often with potential disastrous consequences. Hence, engineers require effective tools to help monitor the health status of civil structures in order to take preventative measures or carry out structural repairs.

A structure is only tested for deterioration and damages when the signs of degradation are evident [31]. Routine visual inspection as part of the maintenance procedure is not effective in picking

out these deficiencies, particularly those that develop within the structure. Therefore, a structural health monitoring system offers a very attractive scheme which allows engineers to collect vital information that helps to assess the condition of a civil structure.

The early generation of SHM systems employs conventional electronic/electrical-based sensors with impeding limitations [31]. They are generally bulky and not durable enough to be embedded into a structure for *in-situ* measurements. These sensors are designed to operate as point sensors which restrict the desirable multiplexing feature of an SHM system. The long lead lines required to cover the usually large civil structures could also cause a problem for the electrical signals due to noise pickup and electro-magnetic field (EMF) interference. In view of this, fibre optic sensors (FOSs) have been considered as a potential alternative in SHM systems. Advantages of the FOS include, small size, immunity to EMF interference, light weight, operation in harsh environments, etc. FBG sensors, in particular, are considered as one of the most promising sensor types due to the added advantages over other classes of FOSs (for example, intensity-based sensors) such as the ease of multiplexing capability and wavelength encoded optical signal. FBG sensors are commonly employed as strain sensors to detect local damages in structures for example, bridges [32], which can manifest crack, fatigue, stiffness loss, etc, where strain is considered as an alternative parameter to monitor these effects. In the section below, several examples are given to highlight the growing acceptance of the FBG-based sensors in civil engineering applications. The use of FBG sensors has been considered in various structures [32-40] such as bridges, buildings, dams and tunnels.

Bridges are by far the most common example of a civil structure in which FBG sensors are installed to provide information for structural performance assessment. The evaluation of FBG-based systems for SHM purposes in bridge structures has been carried out across the world covering North America [34-36], Europe [37,38] and Asia [33,39].

The Intelligent Sensing for Innovative Structures (ISIS) research initiative in Canada, established in early 1990s, has resulted in a total of 16 bridges being fitted with a combination of FBG sensors, strain and thermal gauges [35]. Among these bridges, the Beddington Trail Bridge in Alberta is one of the first to have its carbon fibre composite cables embedded in the concrete girders fitted with FBG sensors [34, 35]. The objective of the study was to monitor the long term

tendon/concrete bonding and relaxation characteristics of three different types of pre-stressed tendons used in the construction. Installation of the sensors was carried out in 1993 and most were found to have survived when measurements were made in 1999.

The Taylor Bridge in Manitoba is another project under the ISIS initiative. It is considered to be one of the world's largest highway bridges reinforced by fibre reinforced plastic (FRP). The bridge is 165.1m long with a total of 40 pre-stressed girders, 4 of which consist of carbon fibre reinforced polymer (CFRP) tendons. CFRP was also used to reinforce the girders and a slab of the bridge deck. A total of 63 FBG sensors, together with electronic strain gauges (60% of the installed strain gauges malfunction due to excessive moisture) were installed at different locations on the structure to monitor the strain induced on the reinforcement. The effectiveness of these FBG systems installed was demonstrated by the strain change experienced by one of the sensors mounted on a CFRP tendon when a truck and a trailer were driven past in opposite direction. The loading directions of the two vehicles can be identified by the two peaks in the strain response as shown in figure 2-9.

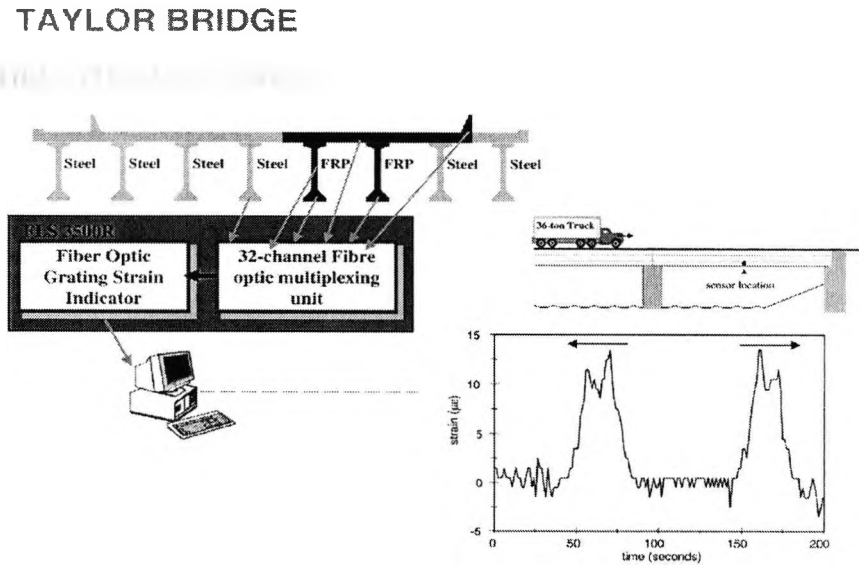

Figure 2-9: Illustration of the FBG-based SHM system installed on Taylor Bridge. Insert: Measurements taken from a FBG sensor mounted on the CFRP tendon, showing the strain change caused by passing vehicles. [35]

In Winterthur, Switzerland, a stay cable bridge (Stork Bridge) built in 1996 was installed with a FBG monitoring system in an effort to evaluate the advantages of CFRP cables incorporated in the suspension scheme [37]. Arrays of FBG sensors, each consisting of 7 sensors, were fitted near the cable anchor. Sensors were mounted on load wires as well as prestrained wires to detect signs of debonding between the sensing element and the wire. Sensors were also fitted on dummy wires to measure cable temperature for measurement compensation purposes. The strain measurements in figure 2-10 show the results obtain over a three years period. Data obtained were also plotted together with measurements from electronic strain gauges, showing a good agreement between the two different technologies employed.

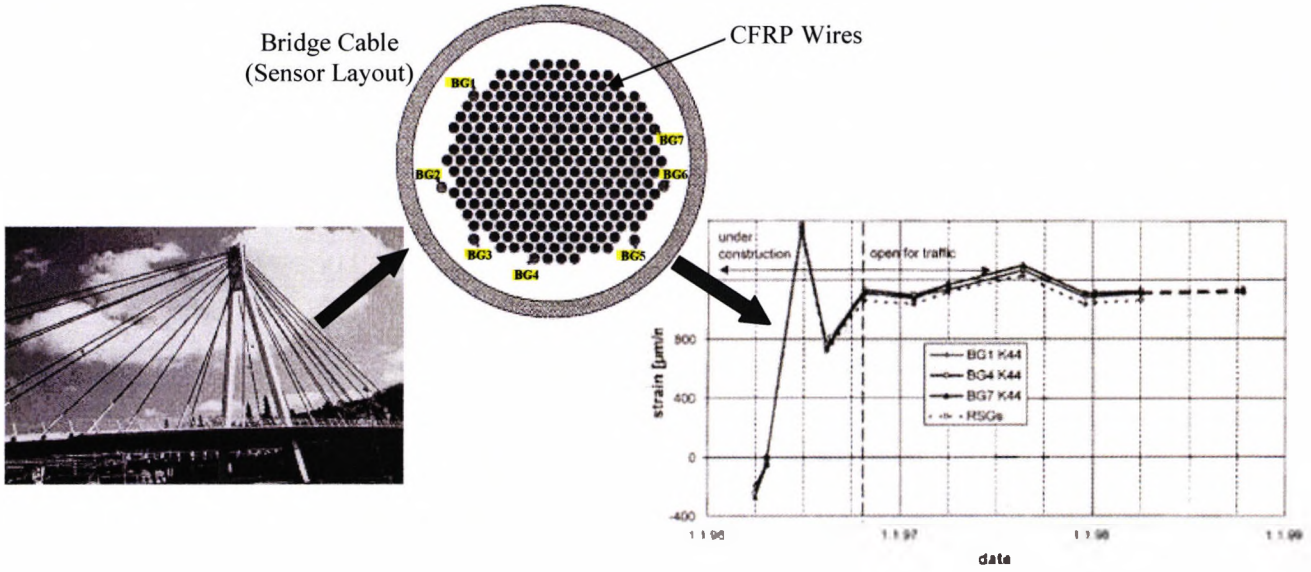

Figure 2-10: Picture of Stork Bridge and the strain measurements obtained from the sensor array mounted on the cables. [37]

The Horsetail Falls Bridge in Oregon, USA, as shown in Figure 2-11, is an historic concrete bridge originally built to support lightweight traffic [36]. It is situated in a tourist area and has been subjected to a load (mainly tour buses) which is not originally designed to cope. Hence, a project was commissioned by the Oregon Department of Transportation in 1998 to strengthen the structure whilst preserving the appearance of the bridge. The bridge underwent a composite wrap procedure as a means to strengthen the structure. In order to monitor the shear and tensile strain, the structure was installed with 28 FBG sensors in both the concrete beam as well as the composite wrap at key locations. Extensive static tests carried out over a period of 5 years to

monitor the integrity have shown that the outfitted structure performed well after the strengthening procedure. When used with a high speed sensor interrogation unit, the sensing system can be employed to perform dynamic measurements which show to be effective in bridge traffic monitoring.

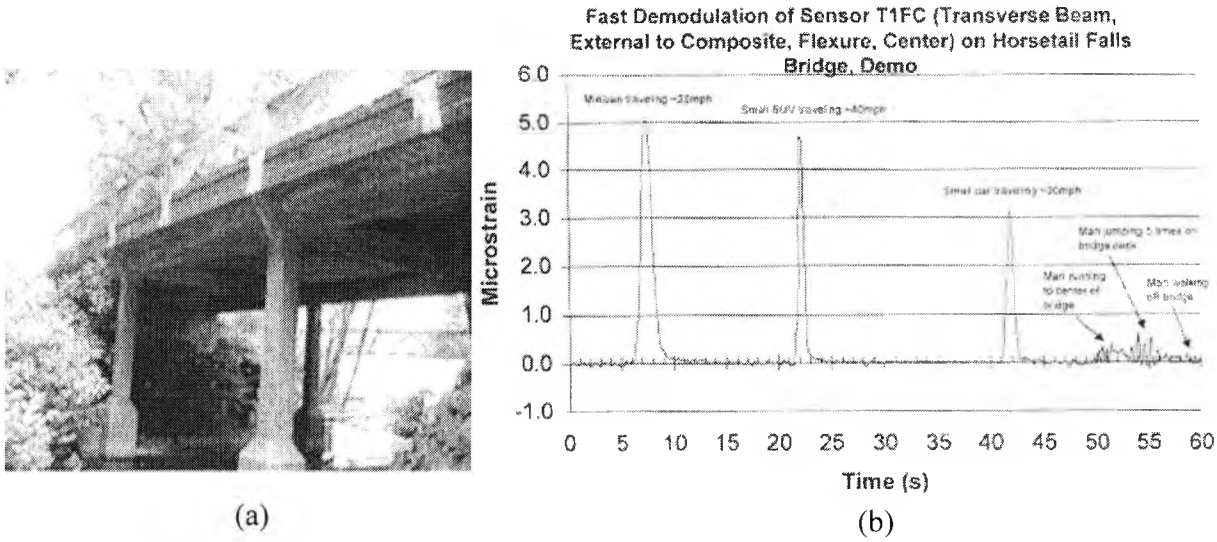

Figure 2-11: (a) Picture of Horsetail Falls bridge. (b) Dynamic measurements of the bridge traffic using FBG sensor. [36]

In Japan, an FBG-based SHM system has also been demonstrated in a 12-story steel building to evaluate the performance of the structure [40]. Low-yielding steel panel dampers were used in the structure to act as an energy absorber to suppress the vibration from the building caused by earthquakes. In order to obtain relevant information for the evaluation, a series of FBGs used in the SHM system as shown in figure 2-12 was configured through the use of various mechanical designs to function as strain, temperature and displacement sensors. To test the effectiveness of system, these sensors were installed in the steel structure as shown in figure 2-13. The displacement sensors, in particular, were mounted diagonally across the dampers which were welded to the steel beam column joint to detect any deformation caused by the bending motion as a result of vibration.

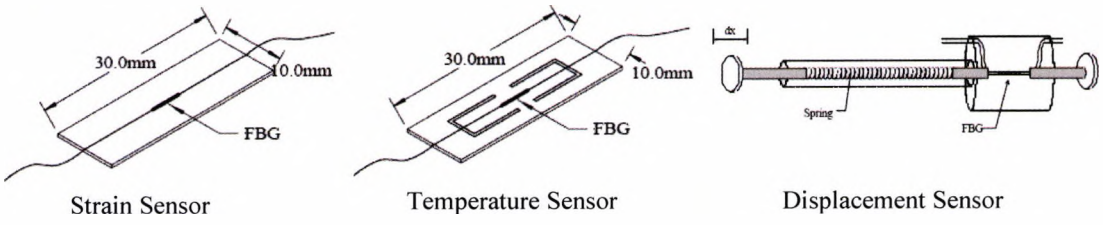

Figure 2-12: Various configurations to implement FBG-based strain, temperature and displacement sensors for SHM system installed in a steel building. [40]

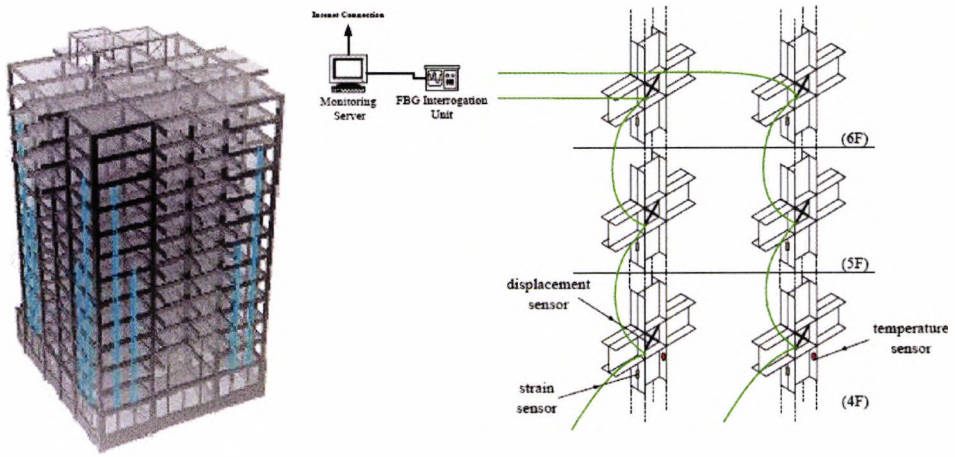

Figure 2-13: Illustration of the 12-story steel building structure and the layout of the SHM system installed onto the building structure. [40]

The discussions above are based on a few of the numerous examples available in order to highlight the utilisation of FBG sensors in built environment. These mainly emphasise the use of FBGs as strain sensors to detect possible damages in the civil structure as a result of physical loading which can be manifested by deformation, crack formation, fatigue, overloading, etc. However, for chemical-related sensing which is an important aspect particularly for concrete-based structures, very little work has been done to explore the possibility of developing FBG-based sensors to monitor parameters (for example, pH level, salt content, moisture level) which can offer structural health information from a chemical perspective.

So far, only FBG-based sensors designed for corrosion detection have been demonstrated by Lo and Xiao [41] and is shown in Figure 2-14. The sensing element was constructed using a prestressed FBG which is partially coated with copper. The fabrication technique used essentially creates two different sensors using a single FBG for simultaneous corrosion and temperature measurements. The sensing principle is based on the change in strain level as a result of the change in coating thickness of the copper layer caused by corrosion, this consequently releases the residual strain of the prestressed FBG and hence causing the Bragg wavelength to shift. However such a sensor technique cannot differentiate the impact caused by specific corrosive ions and thus is unable to provide detailed information in relation to the mitigation of dominating corrosive ions.

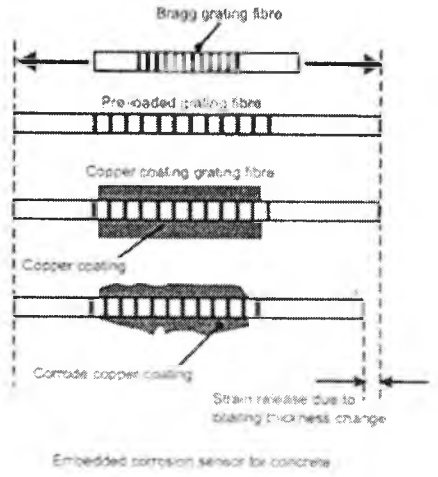

Figure 2-14: Design of the corrosion sensor for concrete application. [41]

2.6. Summary

The discovery of photosensitivity in optical fibre has revolutionised the field of optical communications and sensing as this phenomenon, first observed nearly 3 decades ago, has led to the creation of FBGs which have been successfully employed in a range of optical devices and applications. The general properties of a uniform FBG which is formed by periodic refractive index modulation along the fibre core have been discussed in this chapter. FBGs can be fabricated using a range of methods, with the phase mask method being the most common due to

the simplicity of the inscription technique. A key trait of a FBG is its inherent sensitivity to strain and temperature; the two main parameters that can perturb the properties of the FBG, causing its spectral characteristics to change. As such, it has been used in various applications predominantly as physical sensors to monitor strain and temperature.

Structural health monitoring is one area where FBGs have found a niche market, and thus is the focus of this thesis. Their use allows civil engineers to obtain information pertaining to the condition of a civil structure through a series of sensing elements mounted at key locations, forming a sensor network which can be easily implemented using the FBG technology. The sensor is effective in providing structural health information by detecting physical loading in the form of strain applied to the FBG which can manifest as deformation, crack formation, fatigue, overloading, etc. However, this approach may be more effective, particular for the case of concrete-based structures, if the sensor network includes FBGs that are configured to function as chemical sensors to monitor parameters such as moisture level, pH or salt content. These measurements may potentially allow civil engineers to conduct a more comprehensive analysis on the structure and may also serve as an early warning before the onset of physical degradation.

Research work on the development of FBG-based chemical sensors for SHM applications is relatively limited and has only been demonstrated in the form of a corrosion sensor to date. Hence, there is a gap in this area in which the work reported herein is set to address. In the following chapters, the discussions are focused on the development and evaluation of FBG-based sensors for the detection of humidity/moisture - an important factor for chemical processes in concrete since water is the transport medium of all corrosive ions in concrete and participates in nearly all chemical reactions.

2.7. References

[1] A. Othonos and K. Kalli, "Fiber Bragg Gratings: Fundamentals and Applications in Telecommunication and Sensing", *Artech House*, 1999.

[2] Y. J. Rao, "Recent Progress in Application of In-Fibre Bragg Grating Sensors", *Optics and Engineering*, 31(1999), 297-324.

[3] K. O. Hill, "Photosensitivity in Optical Fiber Waveguides: From Discovery to Commercialization", *IEEE Journal on Selected Topics in Quantum Electronics*, 6(2000), 1186-1189.

[4] K. O. Hill, B. Malo, F. Bilodeau and D. C. Johnson, "Photosensitivity in Optical Fibres", *Annual Reviews Material Science*, 23(1993), 125-157.

[5] K. O. Hill, Y. Fuji, D. C. Johnson and B. S. Kawasaki, "Photosensitivity in Optical Fiber Waveguides: Application to Reflection Filter Fabrication", *Applied Physics Letter*, 32(1978), 647-649.

[6] G. Meltz, W. W. Morey and W. H. Glenn, "Formation of Bragg Gratings in Optical Fibers by a Transverse Holographic Method", *Optics Letters*, 14(1989), 823-825.

[7] D. K. W. Lam and B. K. Garside, "Characterization of Single-Mode Optical Fiber Filters", *Applied Optics*, 20(1981), 440-445.

[8] J. C. Palais, "Fiber Optic Communications", 2nd edition, Prentice Hall, 1988.

[9] W. He, H. Cheng, J. Mei and D. Jiang, " Direct Measurement of Strain-Optic Effect in Fiber Bragg Gratings", in *Proceedings of OFS 15*, Portland, USA, 2002, 171-174.

[10] K. O. Hill and G. Meltz, "Fiber Bragg Grating Technology", *Journal of Lightwave Technology*, 15(1997), 1263-1276.

[11] A. D. Kersey, M. A. Davis, H. J. Patrick, M. LeBlanc, K. P. Koo, C. G. Askin, M.A. Putnam and E. J. Friebele, "Fiber Grating Sensors", *Journal of Lightwave Technology*, 15(1997), 1442-1463.

[12] S. Gupta, T. Mizunami, T. Yamao and T. Shimomura, "Fiber Bragg Grating Cryogenic Temperature Sensors", *Applied Optics*, 35(1996), 5202-5205.

[13] T. Mizunami, H. Tatehata and H. Kawashima, "High Sensitivity Cryogenic Fibre-Bragg-Grating Temperature Sensors Using Teflon Substrates", *Measurement Science and Technology*, 12(2001), 914-917.

[14] G. Lin, L. Wang, C. Yang, M. Shih and T. J. Chuang, "Thermal Performance of Metal-Clad Fiber Bragg Grating Sensors", *IEEE Photonics Technology Letters*, 10(1998), 406-408.

[15] J. Paul, L Zhao, B. Ngoi and Z. Fang, "Bragg Grating Temperature Sensors: Modelling the Effect of Adhesion of Polymeric Coating", *Sensor Review*, 24(2004), 364-369.

[16] C. Lupi, F. Felli, L. Ippoliti, M. A. Caponero, M. Ciotti, V. Nardelli and A. Paolozzi, "Metal Coating of Fibre Bragg Grating Sensors at Cryogenic Temperature", *Smart Materials and Structures*, 14(2005), N71-N76.

[17] S. Pal, "Characterisation and High-Temperature Sensing Potential of Fibre Bragg Gratings in Specialised Optical Fibres", PhD Thesis, City University, 2004.

[18] B. Malo, K. O. Hill, F. Bilodeau, D. C. Johnson and J. Albert, " Point-By-point Fabrication of Micro-Bragg Grating in Photosensitive Fibre using Single Excimer Pulse Refractive Index Modification Techniques", *Electronics Letters*, 29(1993), 1668-1669.

[19] K. O. Hill, B. Malo, F. Bilodeau, D. C. Johnson and J. Albert, " Bragg Grating Fabrication in Monomode Photosensitive Optical Fiber by UV Exposure Through a Phase Mask", *Applied Physics Letters*, 62(1993), 1035-1037.

[20] R. Kashyap, "Fiber Bragg Gratings", *Academic Press*, New York, 1999.

[21] J. R. Armitage, "Fibre Bragg Reflectors Written at 262nm using a Frequency Quadrupled Diode Pumped Nd^{3+}:YLF Laser", *Electronics Letters*, 29(1993), 1181-1183.

[22] Q. Zhang, D. A. Brown, L. Reinhart, T. F. Morse, J. Q. Wang and G. Xiao, "Tuning Bragg Wavelength by Writing Grating on Prestrained Fibers", *IEEE Photonics Technology Letters*, 6(1994), 839-841.

[23] J. D. Prohaska, E. Snitzer, S. Rishton and V. Boegli, "Magnification of Mask Fabricated Fibre Bragg Grating", *Electronics Letters*, 29(1993), 1614-1615.

[24] A. Othonos and X. Lee, "Novel and Improved Methods of Writing Bragg Gratings with Phase Masks", *IEEE Photonics Letters*, 7(1995), 1183-1185.

[25] M. L. Dockney, S. W. James and R. P. Tatam, "Fibre Bragg Gratings Fabricated using a Wavelength Tuneable Laser Source and a Phase Mask Based Interferometer", *Measurement Science and Technology*, 7(1996), 445-448.

[26] R. Kashyap, "Assessment of Tuning the Wavelength of Chirped and Unchirped Fibre Bragg Grating with Single Phase Mask", *Electronics Letters*, 34(1998), 2025-2027.

[27] http://www. micronoptics.com

[28] http://www.fos-s.com

[29] http://www.smartec.ch

[30] K. T. Lau, "Fibre-Optic Sensors and Smart Composites for Concrete Applications", *Magazine of Concrete Research*, 55(2003), 19-34.

[31] H. Li, D. Li and G. Song, "Recent Applications of Fiber Optic Sensors to Health Monitoring in Civil Engineering", *Engineering Structures*, 26(2004), 1647-1657.

[32] J.D. Doornink, B.M. Phares, Z. Zhou, J. Ou, T.W. Graver and Z. Xu, "Fiber Bragg Grating Sensing for Structural Health Monitoring of Civil Structures", in *Proceedings of International Symposium on Advances and Trends in Fiber Optics and Applications*, Chongqing, China, 2004, 293.

[33] T. Graver, D. Inaudi and J. Doornink, "Growing Market Acceptance for Fiber-Optic Solutions in Civil Structures", in *Proceedings of Optics East*, Philadelphia, USA, 2004.

[34] R. Maaskant, T. Alavie, R. M. Measures, G. Tadros, S. H. Rizkalla and A. Guha-Thakurta, "Fiber-Optic Bragg Grating for Bridge Monitoring", *Cement and Concrete Composites*, 19(1997), 21-33.

[35] R. C. Tennyson, A. A. Mufti, S. Rizkalla, G. Tadros and B. Benmokrane, "Structural Health Monitoring of Innovative Bridges in Canada with Fiber Optic Sensors", *Smart Materials and Structures*, 10(2001), 560-573.

[36] E. Udd, S. Calvert and M. Kunzler, "Usage of Fibre Grating Sensors to Perform Critical Measurements of Civil Infrastructure", *in Proceedings of OFS 16*, Nara, Japan, 2003, 496-499.

[37] P. M. Nellen, R. Bronnimann and U. Sennhauser, "Optical Fiber Bragg Grating for Structural Monitoring in Civil Engineering", in *Proceedings of 16th Congress of IABSE*, Lucerne, 2000.

[38] Y.M. Gebremichael, W. Li, W.J.O. Boyle, B.T. Meggitt, K.T.V. Grattan, B. McKinley, G.F. Fernando, G. Kister, D. Winter, L. Canning and S. Luke, "Integration and Assessment of Fibre Bragg Grating Sensors in an All-fibre Reinforced Polymer Composites Road Bridge", *Sensor and Actuators A*, 118(2005), 78-85.

[39] W. H. Chung, S. Y. Liu, B. O. Guan, T. L. Chan, T. H. T Chan and H. Y. Tan, "Structural Monitoring of Tsing Ma Bridge using Fiber Bragg Grating Sensors", in *Proceedings of Sixth Chinese Optoelectronics Symposium*, 2003, 144-146.

[40] H. Iwaki, H. Yamakawa, K. Shiba and A. Mita, " Structural Health Monitoring System using FBG-Based Sensors for a Damage Tolerant Building", in *Proceeding 3rd International Workshop on Structural Health Monitoring*, Standford University 2001.

[41] Y. Lo and F. Xiao, "Measurement of Corrosion and Temperature Using a Single-Pitch Bragg Grating fiber Sensor", *Journal of Intelligent Material Systems and Structures*, 9(1998), 800-807.

Chapter 3:

Humidity Sensing: An Overview

3.1. Introduction

Humidity is a general term which is defined as the amount of water vapour present in the air [1] - it is water in the form of gaseous state and is present everywhere in the atmosphere. Like temperature, strain or pressure, for example, humidity constitutes one of the most commonly required physical quantities in the field of measurements. It has shown significant importance in a diverse range of applications, as illustrated in Figure 3-1, where air conditioning for human comfort and combating bacteria growth to process control to maintaining product quality [2] are just some of the many examples to highlight the vast demand for humidity monitoring in important applications. The requirements for humidity monitoring may vary according to the application and hence there exist various terms associated with, and techniques employed to perform humidity measurements. In this Chapter, a brief overview on the basic concept and definitions associated with humidity measurements is given. Fibre-optic based sensing techniques for humidity sensing are discussed, including a review of the various methods employed to-date.

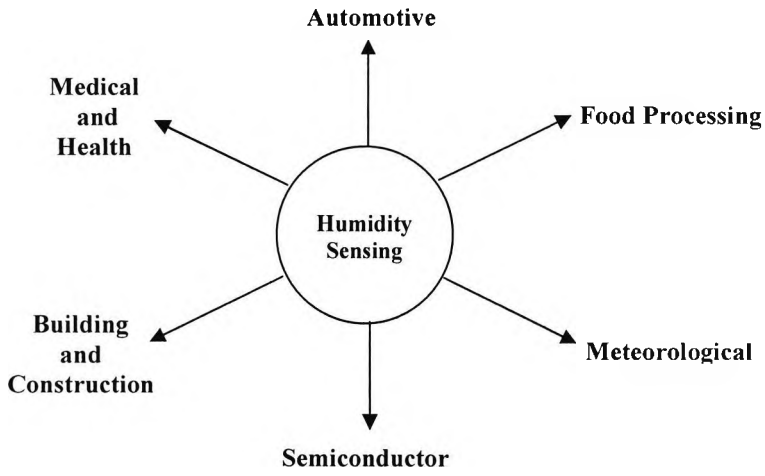

Figure 3-1: An example of applications of humidity sensors in various industries.

3.2. Brief Overview and Definitions of Humidity

The term humidity, as discussed earlier, refers to presence of water in gaseous form but it is often used to refer to expressions which are related to water vapour characteristics and in the field of measurement, there are various terms associated with such water vapour measurements. In addition, the term *moisture* is frequently interchanged with *humidity* even though the actual definition of *moisture* refers to the water in liquid form that may be present in solid materials [3].

Since humidity is a measure of water in gaseous state present in the environment, water vapour found in a gas mixture behaves in accordance with the gas laws and the amount of pressure it exerts equates to the partial pressure of the water vapour components in the gas mixture, as defined by Dalton's law [3]. In the atmosphere, the total air pressure is the sum of the partial vapour pressure of individual components that form the air mixture. Using Dalton's law,

$$P_{Total} = P_{nitrogen} + P_{oxygen} + P_{water\ vapour} + P_{other\ gases} \qquad (3\text{-}1)$$

where P_{Total} is the total pressure exerted by air, P_s stands for the partial pressure where s represents the individual components in an air mixture.

When air is fully saturated with water, the pressure exerted by the water vapour present is defined as the saturation water vapour pressure (P_{ws}). As shown in Figure 3-2, this value varies as a function of temperature and it increases as the temperature rises.

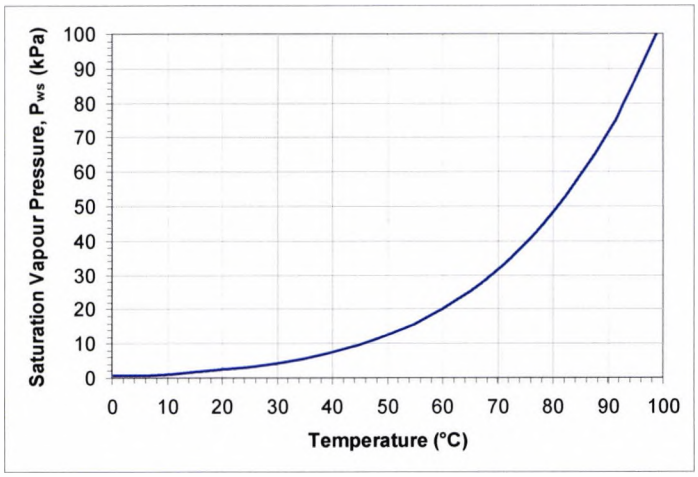

Figure 3-2: Saturation water vapour pressure as a function of temperature.

A common way to relate the amount of water vapour present in the environment is to take the ratio of the actual water vapour pressure and the saturation water vapour pressure at a specific temperature. The resultant term, known as the *relative humidity* (RH), simply represents the ratio of the amount of water vapour present in the atmosphere to the maximum amount the atmosphere can hold and is often expressed as a percentage using the following equation,

$$\text{Relative Humidity (RH)} = {}^{P_w}\!/_{P_{ws}} \times 100\% \qquad (3\text{-}2)$$

where P_w is the partial pressure of the water vapour and P_{ws} is the saturation water vapour pressure.

If air is cooled down sufficiently; to a point where it becomes saturated with water molecules (RH=100%) and condensation occurs as a result, the temperature at which this occurs is known as the *dew point*. In a similar way to relative humidity, the dew point temperature is another term frequently used to express the amount of water vapour present in the atmosphere. It is much

preferred in some applications, for example, in meteorology, as it provides a better "absolute" measurement of water vapour content than RH measurements, which may fluctuate with temperature.

The dew point temperature or RH can be calculated by using the dry and wet bulb temperature method [3]. The name was derived from the technique employed which involves using regular bulb thermometers to perform temperature measurements. The dry bulb temperature is simply the temperature of the air, whereas the wet bulb temperature is the temperature achieved as a result of water evaporation and latent heat transfer. The process of obtaining the wet bulb temperature involves covering the thermometer bulb with a damp wick and passing unsaturated air over to allow heat transfer from the wet surface to the surrounding atmosphere as evaporation takes place. As the temperature of the wet surface drops below the ambient temperature, heat flows from warm air to cool surface causing a drop in the surrounding temperature. This process results in a lower vapour pressure of water, thus decreasing the rate of evaporation. The temperature eventually equilibrates to a point where the rate of heat transfer from the air to wet surface equals the rate at which the heat at the surface is lost through evaporation. This stabilised temperature is known as the wet bulb temperature and is used together with the dry bulb temperature to determine either the dew point temperature or relative humidity.

Thus relative humidity, dew point and wet bulb temperature are just some of the common terms used in humidity measurements but other parameters which include humidity ratio or moisture content expressed as a dimensionless quantity and absolute humidity expressed in g/m^3 can also be used. The choice of measurement and the expression of humidity are dependent on the applications and requirements. Relative humidity, however, remains the most commonly used term in general humidity/moisture measurements.

3.3. Various Techniques for Humidity Detection

From the simplest way of exploiting the expansion and contraction of materials such as human hair to the most sophisticated techniques, such as using a miniaturised electronic chip, a variety of methods has been explored to obtain meaningful humidity measurements. These methods are

employed either by probing the fundamental properties of water vapour or using various transduction methods which are capable of giving humidity-related measurements. This section gives a brief review of general techniques of this type used for the detection of humidity, covering different approaches such as mechanical, optical and electronic methods. A separate part, section 3.4, will follow to discuss in detail the various fibre-optic based techniques that have been reported for humidity sensing.

3.3.1. Mechanical Hygrometer

The mechanism of a typical mechanical hygrometer, as shown in Figure 3-3, is based on one of the oldest techniques that rely on the use of materials which expand and contract in proportion to the humidity change. Common materials used include synthetic fibres and human hair. The hygrometer is formed by linking the material to strain gauges or other similar mechanical devices to measure the displacement caused by the change in humidity. Calibration is required to relate the displacement to the relative humidity level in the environment. Such a method is inexpensive and easy to implement. However, it has inherent non-linearity and hysterisis issues which need to be compensated when the measurements are performed. The response of the device tends to be slow, thus making it unsuitable for most of those applications where environmental conditions change rapidly.

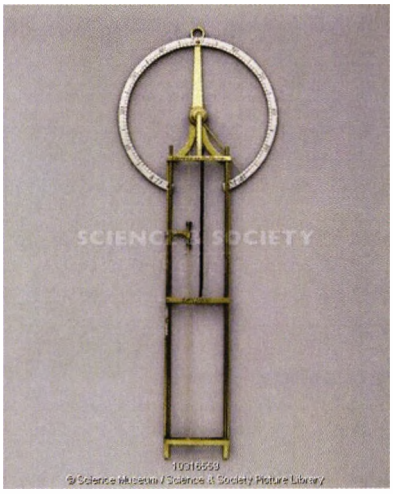

Figure 3-3: Picture of a mechanical hygrometer. The device incorporates a human hair which stretches as it absorbs moisture, thus changing the length that can be calibrated to provide humidity measurements. Source: http://www.scienceandsociety.co.uk

3.3.2. Chilled Mirror Hygrometer

The chilled mirror hygrometer, also known as the optical condensation hygrometer, is a device based on an optical technique for the determination of the dew point temperature. It is known to be the technique which provides the most accurate and reliable measurements. Unlike the mechanical hygrometer, this device performs fundamental measurements which are often used as a calibration standard. As illustrated in Figure 3-4, a conventional chilled mirror hygrometer contains a temperature-controlled reflective condensation mirror and an optoelectronic module which monitors the optical signal reflected from the surface of the mirror. In the 'dry' condition, where the mirror temperature is higher than the dew point, the maximum signal is reflected into the detector of the optoelectronic module. When the temperature drops below the dew point, the signal intensity is reduced due to the scattering of light as a result of water droplets forming on the mirror surface.

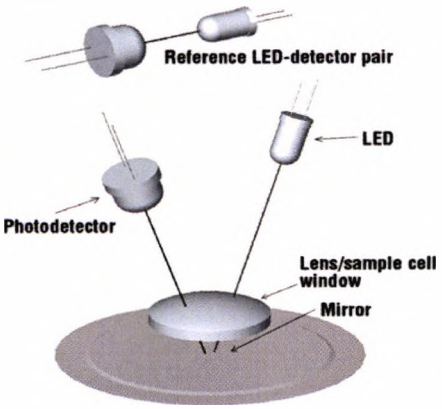

Figure 3-4: Schematic of a chilled mirror hygrometer. Source:http://www.sensorsmag.com

The chilled mirror hygrometer can be used to provide highly accurate measurements. However, this method is expensive and requires regular maintenance due to its susceptibility to surface contamination. The requirements for control electronics and their close proximity to the location where measurements are carried out also place an operational limitation on the device.

3.3.3. Wet and Dry Bulb Psychrometer

A simple and relativity low cost method which has been popular for humidity measurements is the wet and dry bulb psychrometer. It consists of two thermometers (e.g., electric or glass), one of which is covered with a damp wick to determine the wet bulb temperature and the other to measure the temperature of the sampled gas (dry bulb temperature). Examples of such measuring device are the sling psychrometer which operates by whirling the device through the air to obtain the temperature readings and the Assman psychrometer, a similar device with a fan attached to the unit to provide air flow.

Humidity is determined through fundamental measurements by monitoring the so-called "wet-bulb depression" which is the difference between the dry and wet bulb temperatures. Conversion charts are used to relate the wet bulb depression value and the dry bulb temperature and thus to enable relative humidity to be calculated.

This measurement device is the least expensive one which can also be used to provide a calibration standard. However, it is not suitable for operation in small enclosed areas (where the moisture from the wet bulb significantly changes the water vapour content in the environment) and precautions are necessary to minimise measurement errors caused by contamination on the wick covering the thermometer, inconsistency in the wetting of the wick and the inaccuracy of the thermometers used. In comparison with the other fundamental methods discussed previously, the chill mirror hygrometer is still the preferred method due to the ease of operation, albeit at a higher cost.

3.3.4. Infrared (IR) Optical Absorption Hygrometer

The general operation principle of the IR hygrometer is based on a dual-wavelength absorption technique that uses a primary wavelength at which strong optical radiation absorption is observed and a secondary/reference wavelength where the absorption is negligible. Humidity measurements are then taken in the form of transmission ratios at these two chosen wavelengths. This technique allows the direct measurement of water absorption which eliminates any optical or

electronic related drift in the readings and also interference caused by contaminants such as particles and other gaseous species in the test environment.

As this technique uses specific wavelengths that allow selective measurements to be taken, the choice of the absorption wavelengths is application-specific and requires careful consideration to avoid cross-sensitivities to any other gaseous species likely to be present in the environment. The inherent optical absorption characteristics of water have therefore been considered as alternative approach for humidity measurements. Ultraviolet (UV) based absorption methods have also been explored and an instrument using such an approach exists in the form of Lyman-Alpha hygrometer [3]. However, this method/instrument is not commonly used due to its complexity in design and high cost. The IR absorption hygrometer is a non-contact instrument and is generally unaffected by contaminants. The sensitivity of the instrument is dependent on the absorption path length and is thus governed by the Beer-Lambert Law [4] where the transmission of the IR radiation through the absorbing gas is inversely proportional to the exponential function of gas concentration and the path length. This instrument has negligible drift and can generally operate over a wide humidity range. The cost of the instrument is also higher than that of the chilled mirror hygrometer and the instrument itself requires periodic calibration.

3.3.5. Miniaturised Electronic Humidity Sensors

This section covers sensors using any form of electrical/electronic based transduction technique for the purpose of humidity detection. The development of these miniaturised electronic humidity sensors has been driven by various industries which have a demand for low cost, reliable and compact sensors. Transduction techniques that have been reported to create these miniaturised sensors include capacitive, resistive and gravimetric methods. An extensive review on these sensors and their performance has been conducted recently by Lee and Lee [5]. A similar review was carried out by Chen and Lu [6] with an emphasis on the wide range of sensing materials employed by the different humidity sensor types.

Amongst the various humidity sensors discussed, the capacitive and resistive-based humidity sensors are the most commonly used, with capacitive based sensors dominating and making up

nearly 75% of the commercial humidity sensor market [7]. Capacitive-based humidity sensors operate on the basis of dielectric changes of a thin hygroscopic film upon exposure to moisture. The design of the sensor typically consists of two interdigitated electrodes (IDE) coated with a humidity sensitive dielectric layer, as shown in figure 3-5.

A similar design configuration is employed in the resistive humidity sensors. The resistive-based sensors rely on the transduction mechanism involving the change in conductivity caused by the absorption of moisture in a hydroscopic material such as conductive polymers. Generally, both sensor types, which are classified as secondary measurement devices, are inexpensive and have low power consumption. They can both operate over a wide humidity range with good repeatability but suffer from temperature dependency and cross-sensitivities to some chemical species.

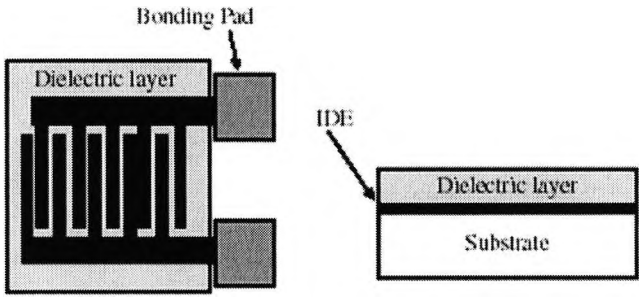

Figure 3-5: Schematic of a capacitive humidity sensor with interdigitated electrodes (IDE) sandwiched between a moisture sensitive dielectric layer and a substrate. [5]

3.4. Review on Fibre Optic Sensors for Humidity Detection

The discussions in the preceding sections have highlighted the vast range of options available for measuring humidity. Standard methods that relate the fundamental properties of water vapour to various transduction schemes that rely on electrical, optical and mechanical approaches to provide humidity induced measurements have been presented. Applications that utilise these techniques can be found in various situations, each with the need to address different key requirements such as precision, cost, ease of operation and maintenance, background interference, operation environment and remote operation, for example.

All the techniques discussed so far have their own particular advantages and disadvantages and none of them can fulfil majority of the requirements discussed above. Therefore, the selection of an appropriate method which has the optimum characteristics for a specific application is usually made, compromising these key requirements. Devices that employ standard methods such as the chilled mirror dew point sensors or wet and dry bulb psychrometers are classified as fundamental instruments which offer good accuracy. However, these devices require careful operation and routine maintenance to ensure the accuracy of the measurements. They are also awkward to implement in environments where online and remote monitoring is required. Secondary humidity measuring devices such as the electronic-based (capacitive/resistive) humidity sensors are considered to be robust, low cost, easy to operate and to maintain. As such, they are more popular in most industrial applications and constitute a large percentage of the commercialised humidity sensor market. These sensors however, are generally not suitable to be employed in an environment of a potentially hazardous or explosive nature and also in situations where requirements such as immunity to electromagnetic interference, multi sensor operation, *in-situ* and remote monitoring are, for example, required.

With the advent of optical fibre technology, a considerable amount of research has been focused on fibre-optic (FO) based techniques for humidity sensing. In a similar way to their electronic counterparts, FO humidity sensors are secondary devices but show additional features like small size, immunity to electromagnetic interference, multiplexing and remote sensing capabilities, of which the counterpart electronic sensors lack. However, the limitations of the operating range and accuracy of the FO-based humidity sensors are some of the drawbacks which researchers are striving to address to date. Nevertheless, these sensors have found useful applications in various areas where electronic sensors were found to be inappropriate, thereby showing the real potential of FO-based sensors. Thus, this forms the main motivation that has driven the research activities on the development of a range of FO humidity sensors over the last 20 years.

There are numerous published technical papers covering both potential sensing materials and FO techniques suitable for humidity sensing, with the two main subjects which define the format of most discussions reported. Various FO based humidity sensing techniques reported so far, with designs covering both extrinsic and intrinsic sensor types, can be further classified according to

the techniques commonly employed in optical fibre sensing [8, 9]. Generally, these techniques include direct spectroscopic, evanescent wave, in-fibre grating and interferometric methods.

The literature reviewed in this thesis is by no means exhaustive but it is sufficiently representative of the major techniques and research effort internationally, thus focusing mainly on the sensing techniques reported from the early 1980s until the present.

3.4.1. Direct Spectroscopic-Based Sensors

The spectroscopic method has been a 'workhorse' technique widely used in chemical analysis. This method examines the optical signal and relates absorption or fluorescence-based measurements to the concentration of the target analyte. Hence it is not surprising that it is a popular choice of method for many FO chemical based sensors. Generally, as shown in Figure 3-6, the design of the sensors can simply comprise optical fibres with a sample cell for direct spectroscopic measurements or be configured as fibre optrodes where a chemical selective layer, comprising chemical reagents in suitable immobilising matrices, is deposited onto the optical fibre [9, 10]. Most spectroscopic-based configurations for humidity sensing are based on the optrode design where moisture sensitive reagents are attached to the tip of the sensing fibre, usually with the aid of a polymeric material to form the supporting matrix.

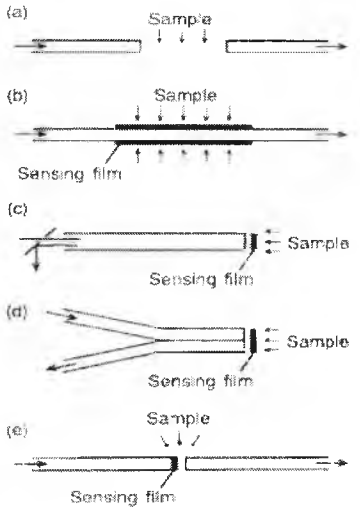

Figure 3-6: Various configurations for spectroscopic fibre-optic sensors. [16]

3.4.1.1. Absorption-Based Sensors

A variety of potential materials and chemical reagents have been reported in light of their humidity-dependent optical absorption properties. Examples include reagents such as the Cobalt Chloride ($CoCl_2$) [11-14], Cobalt Oxide (Co_3O_4) [15], Rhodamine B [16] Crystal Violet [17,18],

and more recently, materials such as eletrochromic polymers [19] and Bacteriorhodopsin (BR) doped biochromic film [20].

In these approaches, measurements were made by monitoring the intensity variation as a result of absorption due to the interaction between the chemical reagents involved and moisture. A light source, of selected wavelength which corresponds to the absorption bands of the chemical reagents, is required.

Examples of such sensors include those from Zhou *et al.* [11] who have demonstrated an in-line absorption based humidity sensor using a porous optical fibre segment doped with $CoCl_2$, an inorganic salt compound which exhibits strong absorption on the band between 550-750nm. As it hydrates, the colour of the salt compound changes from blue to pink and the absorption peak undergoes a hypsochromic shift. The use of the absorption characteristics of the compound contained in a variety of materials such as gelatine and cellulose has also been discussed by various authors [12, 13]. To create a sensing element from these materials, a 0.5cm long borosilicate glass fibre, with a typical diameter ranging from 150μm-300μm was pre-treated to create a porous structure before being immersed into a aqueous $CoCl_2$ solution, followed by being dried at room temperature. As the sensing element is porous, some of the light launched into the fibre will be absorbed by the reagent and some will be scattered out of the structure. Hence the scattering loss was taken into consideration when the humidity-dependent absorption measurements were made. Sensor operation up to a limit of 50%RH was observed and the operating range was found to be dependent on the concentration of the $CoCl_2$ solution used for the fibre treatment. The sensor configuration discussed shows good reversibility and has a response time of 2-3 minutes.

Tao *et al.* [14] have recently demonstrated an active fibre core optical sensor (AFCOS) for humidity detection using a similar in-line absorption sensing concept. The porous sensing element was created using the sol-gel technique. Instead of pre-treating a segment of porous silica fibre with chemical reagent, the sensing element was mould-cast using a sol solution premixed with $CoCl_2$, shown in Figure 3-7. This method offers more flexibility and it can be easily tailored to meet specific sensor requirement by controlling the dimension, composition and porosity of the sol gel silica structure. The demonstrated sensor consists of a 0.2cm long $CoCl_2$ doped sol-gel

silica fibre (diameter: 390μm) with both ends attached to optical fibres of similar diameter. The optical signal at 632nm, propagating through the active fibre core, was monitored to obtain information on the humidity level. The sensor described was reported to exhibit good response and is able to detect humidity level down to 2%RH. However, the upper operating limit for the current sensor design is <10%RH, which can be tailored by adjusting the dopant concentration.

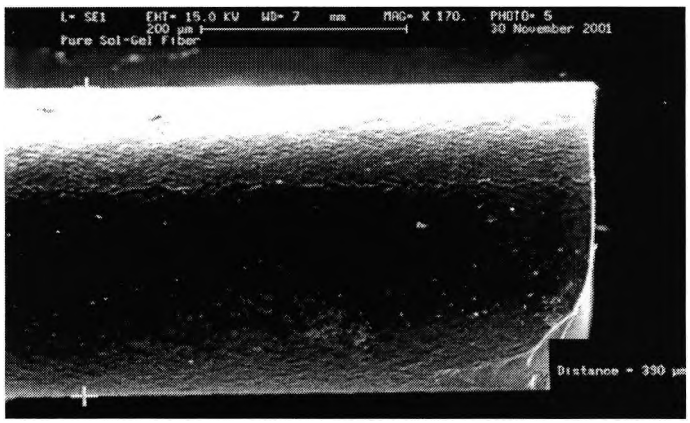

Figure 3-7: SEM picture of the porous sol-gel silica fibre, showing the interconnected porous structure on the surface of the fibre. [14]

Otsuki *et al.* [16] have discussed an air gap design, shown in Figure 3-8, utilising in-line absorption configuration. The sensor demonstrated was formed with an air gap between two sections of a large core fibre positioned on the same axis. One end of the fibre was dip-coated with a dye solution containing Rhodamine B (RB) and hydroxypropyl cellulose (HPC). To measure the optical signal as a function of humidity, light was coupled into the sensor from one end of the fibre, passing through the dye-doped film and collected by the other fibre. The sensor discussed is able to operate between 0-95%RH and has a response time of approximately 2 minutes.

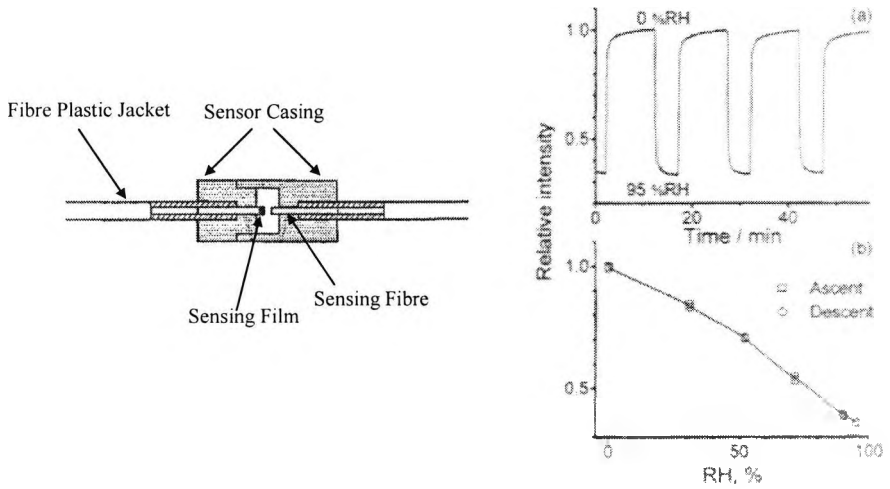

Figure 3-8: Sensing characteristics of a fibre-optic humidity sensor using the air-gap configuration [16].

3.4.1.2. Fluorescence-Based Sensors

A humidity sensitive optrode membrane fabricated using a dye-doped (Rhodamine 6G) gelatine film has been discussed by Choi *et al.* [21]. The sensing membrane, which can be readily adapted for FO sensing, exhibits strong fluorescence at 568nm when excited at 536nm. A hypsochromic shift was observed with a resultant decrease in the emission intensity at 568nm when the humidity level was increased from 0-100%RH.

The use of the fluorescence quenching mechanism for humidity detection has been explored by Posch and Wolfbeis [22]. The perylene-based sensor, implemented by attaching the sensing film at the end of a fibre bundle which forms the common arm of a bifurcated FO light guide, was evaluated over the range from 0-100%RH and the sensor response was found to be non-linear and exhibited cross-sensitivity to oxygen.

A similar approach using a quenching mechanism was demonstrated by Raichur and Pedersen [23]. The sensor, designed for applications in drying and baking processes, employs a highly fluorescent film based on aluminium/morin complex immobilised in polyvinyl pyrrolidone (PVP). The quenching of the fluorescence emission from the metal ion-organic complex, which arises due to the interaction between the aluminium ions and moisture, exhibits a linear response that

follows the Stern-Volmer equation. The sensor showed good humidity response when assessed at elevated temperatures, up to 90°C. However, prolonged testing showed a 20% decrease in output signal which could be attributed to the choice of polymer matrix used.

Luminescence lifetime-based methods [24-27] can also be considered to overcome some of the issues encountered by the intensity-based method such as the re-absorption of the fluorescence signal, scattering, light intensity variations and the concentration of the luminescence compounds used. The use of luminescence lifetime based system using ruthenium-based complex immobilised in Nafion© membrane for the measurement of water content in organic solutions and humidity in the air has been discussed by Glenn *et al.*[25]. This sensor was able to respond to the change of water in both the liquid and gaseous phases but the operational lifetime of the sensing component is only about 4 days and it requires a regeneration procedure to restore its functionality. A more robust and stable sensing system, using the same ruthenium complex immobilised in a PTFE disk, was recently demonstrated by Bedoya and his co-workers [27]. Phase-sensitive detection for humidity measurements was employed using a modified commercial lifetime-based instrument. The optrode fabricated has an operational range of 4-100%RH and displays good performance in terms of response time, repeatability and stability.

3.4.2. Evanescent Wave Sensors

Light travelling through a step index optical fibre is guided within the medium as a result of total internal reflection (TIR) if the critical angle criterion is fulfilled [28]. At each point of TIR, the interference between the incident and reflected signals, shown in Figure 3-9, at the core/cladding interface generates a standing wave which extends beyond the core of the optical fibre and penetrates into the cladding region.

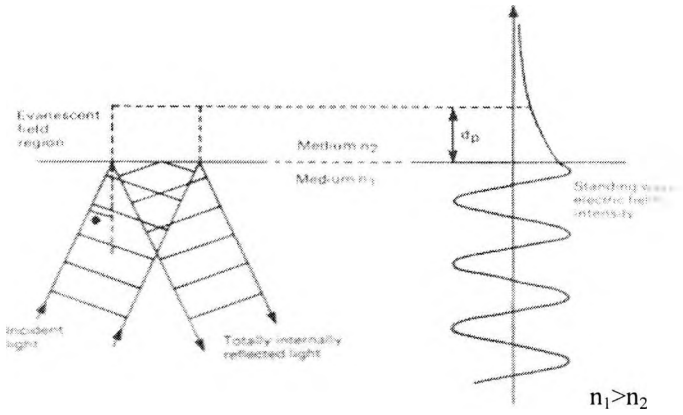

Figure 3-9: Evanescent field generated at the interface of two optically transparent media. [29]

This creates an evanescent field with an amplitude that decays exponentially with distance away from the core/cladding interface and follows the form,

$$E(z) = E_0 \exp(-z/d_p) \tag{3-3}$$

where the penetration depth (d_p) is defined as the depth at which the amplitude of the evanescent field, E, has decayed to 1/e of the initial value E_0 at the core/cladding interface and this is given by,

$$d_p = \frac{\lambda}{2 \cdot \pi \cdot n_{core}\left[Sin^2\theta - (n_{clad}/n_{core})^2\right]^{1/2}} \tag{3-4}$$

where λ is the wavelength of the propagating signal in the optical fibre, θ is the angle of incidence normal at the interface, n_{core} and n_{clad} are the refractive indices of the fibre core and cladding respectively.

The evanescent wave (EW) sensing method allows the optical fibre to be used as an intrinsic sensor where the field generated at the interface interacts with the target analyte surrounding the fibre, thus giving information as a result of optical absorption, refractive index change or scattering [30].

Various optical fibre configurations can be used for evanescent wave sensing. A common approach is to use a plastic clad optical fibre with a section of the cladding removed, in order to gain access to the evanescent field. The structure of the de-clad fibre can also be modified by heating and bending it to form a U-bent fibre, causing the evanescent field to extend further away from the interface, hence enhancing the interaction between light and the target analyte. Other methods to gain access to the evanescent field include side polishing of optical fibres cast in a polymer block to expose the fibre core or heating and stretching the optical fibre to form a fibre taper.

Chemical reagents or selected matrices can be coated onto a de-clad optical fibre, forming a common design configuration for EW absorption- or fluorescence-based sensors. Comparing these to the sensors discussed in the previous section, the use of such a configuration gives flexibility in terms of the interaction length, time response and distributed sensing capability [31]. However, the required optical path length to achieve a similar sensitivity as is achieved for example in the direct absorption method either by using a direct sample cell or configuration based on active fibre core [11,14], is much longer due to the small path length interaction at every reflection point along the fibre [14, 30].

3.4.2.1. Optical Absorption

The majority of the EW methods reported are based on the absorption principle, which involves the use of chemical reagents immobilised in suitable organic or inorganic matrices. One of the earliest EW absorption based humidity sensors was demonstrated by Russell and Fletcher [32] in 1985 using a 600μm optical fibre with 12cm of $CoCl_2$/gelatine sensing film. Ballantine and Wohltjen [33] then proposed a similar sensor the following year, using a 9cm long glass capillary waveguide coated with $CoCl_2$/poly(vinylpyrrolidone) (PVP) film. In both sensors discussed, the general operating range is limited and they could only respond to a humidity level higher than 50%RH.

Using the same chemical reagent and organic film combination ($CoCl_2$/gelatine), Kharaz and Jones [34] later demonstrated a quasi-distributed FO humidity sensing network consisting of 4

sensors using a 200μm hard clad silica fibre with each positioned about 20m apart. Measurements were obtained using an optical time domain reflectometry (OTDR) technique, shown in Figure 3-10, utilising dual pulsed laser diodes emitting at 670nm and 850nm. An operating range of 20%RH-80%RH was demonstrated using the sensor network and the performance was reported to be stable for a temperature range from 25°C-50°C.

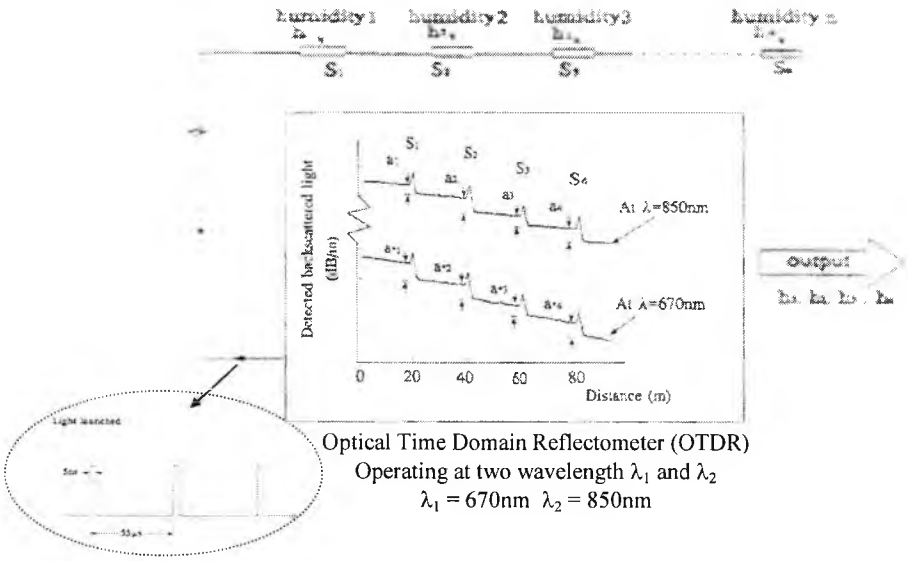

Figure 3-10: Optical responses of distributed fibre optic sensing system using optical time domain reflectometer (OTDR). [34]

Kharaz *et al.* [35] extended their research work by investigating the influence of the immobilising matrices on the sensors performance. This was carried out by comparing various immobilising materials, such as hydroxyethylcellulose (HEC) and gelatine, together with $CoCl_2$. A U-bent fibre configuration, shown in Figure 3-11, was used during the evaluation to enhance the interaction of the evanescent field with the sensing film.

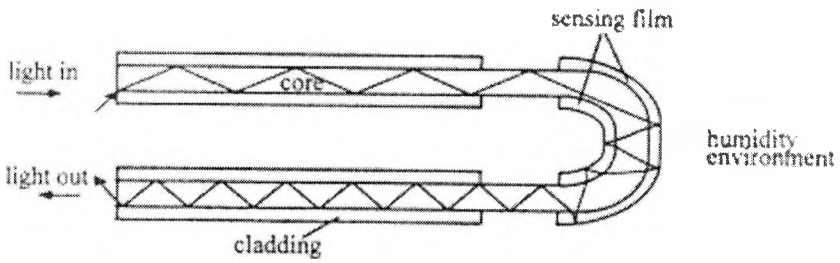

Figure 3-11: U-bent evanescent wave sensor configuration using cladding as the active sensing region. [35]

From the studies performed using films of similar reagent/immobilising material ratio, gelatine film was found to be insensitive below 40%RH, whereas HEC was able to respond to the 30-96%RH range, hence clearly showing the influence of the film constituent on the operating range of the sensor. This observation was substantiated by the work discussed by Jindal *et al.* [36]. In their research, a U-bent humidity sensor using $CoCl_2$/polyvinyl alcohol (PVA) film was reported to be sensitive to a humidity range from 3%RH-90%RH. Further detailed work to optimise the performance of the $CoCl_2$/PVA sensor was then undertaken by Khijwania *et al.* [37], in which the effects of film thickness, bend radius and fibre core diameter were investigated.

In addition to $CoCl_2$, which from the literature seems to be a common choice of reagent used in the EW absorption-based humidity sensors discussed so far, other reagent/immobilising matrix combinations deposited on U-bent sensors have also been reported by various authors [38-40]. These include Rhodamine B/Hydroxypropyl (HPC) film, Phenol Red/ Polymethylmethacrylate (PMMA) film and Magnesium oxide sol-gel film, with a reported operating range of 0-95%RH, 20-80%RH and 5-85%RH respectively.

3.4.2.2. Refractive Index Change

Refractive index (RI) change is another approach used for EW sensing method. An example of humidity sensing based on this approach was demonstrated by Muto *et al.* [41] using a plastic optical fibre (POF) as shown in Figure 3-12. The fibre core of the POF (diameter: 1mm) was made from PMMA with a refractive index of 1.489 at 680nm. Hence to render the fibre responsive to humidity, a polymer blend of HEC/Polyvinylidenefluoride (PVDF) was deposited on the fibre core, forming a cladding layer (thickness: 0.5-1μm). The humidity sensitive cladding layer has a refractive index value of 1.492 when in dry state, creating a lossy waveguide which reduces the intensity of the light propagating through the fibre. As the cladding layer hydrates, the refractive index value falls below that of the core, reducing the intensity loss, thus forming the basis for humidity detection. The sensor responded well to a humidity range of 20-80%RH, with negligible temperature dependence. The time response to a step humidity change of 50%RH was reported to be less than 5 seconds.

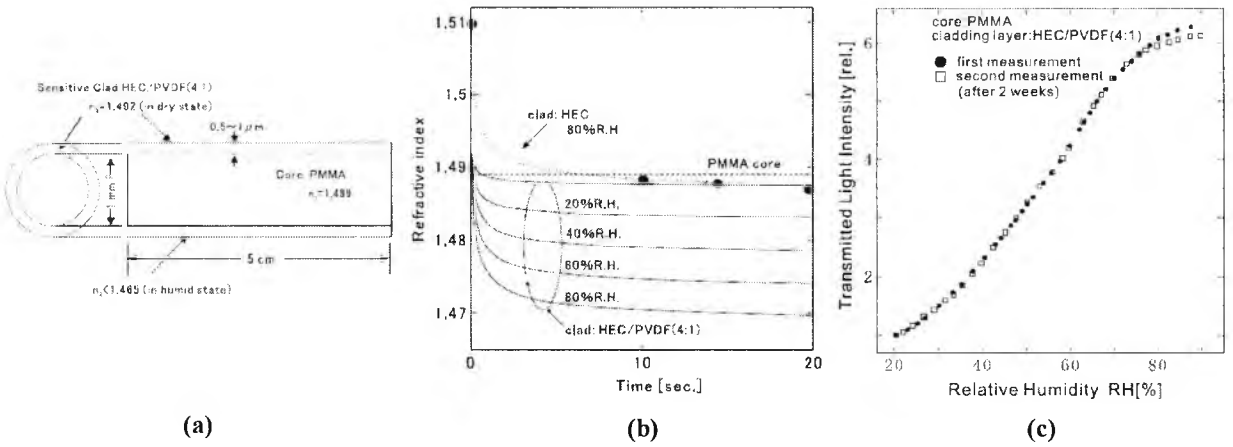

Figure 3-12: Evanescent wave POF humidity sensor using PMMA core and HEC/PVDF film. (a) Sensor configuration, (b) Refractive index change of HEC/PVDF film at various humidity conditions. (c) Sensor characteristics. [41]

Extensive studies were carried out by Arregui *et al.* [42] using hydrogels, a class of polymeric material known for its excellent water absorption properties, as potential material for the sensing approach is discussed in this section. The evaluation was performed using de-clad optical fibres coated with poly-hydroxyethyl metharyclate (poly-HEMA), poly-acrylamide, poly-N-vinyl pyrrolidinone (poly-N-VP) and agarose gel, taking into account of the effect of pore size for the selected materials on the sensitivity and time response of the sensor. Among the materials tested, the sensor with agarose gel gives the best overall performance, achieving an operating range of 10-90%RH. It was also reported to exhibit a better response time and stability than rest of the materials evaluated.

The use of a tapered fibre with agarose gel for humidity sensing based on refractive index change has been demonstrated by Bariain *et al.* [43]. The sensor consists of a tapered single-mode telecommunication grade fibre with a waist size of 25μm, coated with agarose gel of a similar mix concentration to that described by Arregui *et al.* [42] and a comparison was made between the two different sensor types using the same material. The tapered sensor was reported to have a similar operating range and time response to the sensor using a de-clad fibre. However, the dynamic range of the optical intensity measurements taken in a similar test was found to be much higher than that for the tapered fibre sensor. Based on the same approach, humidity sensors with

nanostructured films deposited onto tapered fibres using the ionic self-assembled monolayer (ISAM) deposition technique have been discussed recently [44, 45] and are shown in Figure 3-13. The ISAM deposition technique proposed allows the sensitivity of the sensor to be optimised by controlling the thickness of the coating film and a faster time response (than for the previous sensors discussed) was also possible due to the thin sensing film used.

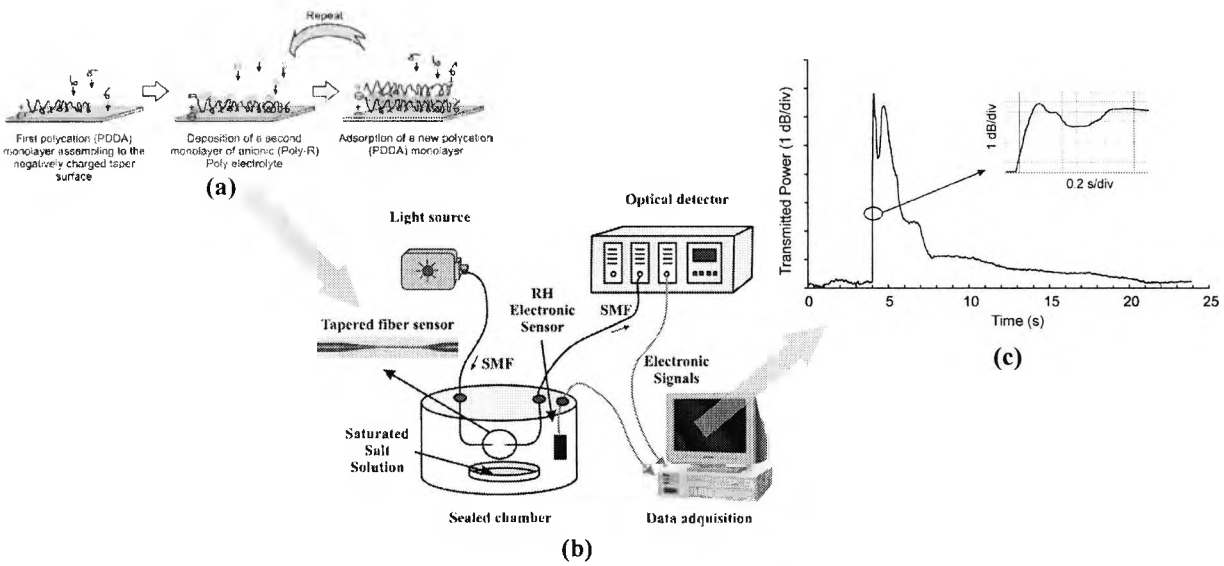

Figure 3-13: Tapered optical fibre humidity sensor with ISAM overlay. (a) Schematic of ISAM deposition process. (b) Experimental set-up for sensor characterisation. (c) Sensor response to a short abrupt change of humidity simulated by human breath. [45]

Using a side polished optical fibre with a humidity-sensitive overlay is another scheme for humidity sensing. To expose the evanescent field and create such a sensor, the flat surface parallel to the fibre axis was polished back to remove the cladding. Side polishing can be realised by first immobilising the optical fibre in a rigid material, forming a rectangular block with fibre extending out from the two end faces of the block orthogonal to the fibre axis. The advantage of using this scheme is that the sensing element can be fabricated using inexpensive components and a variety of coating materials can be deposited onto the flat surface of the fibre block. However, the fabrication procedure is very time consuming and depending on the design of the fibre block and the exposed interaction length can be limited.

Gaston *et al.* [46, 47] proposed a humidity sensor based on a single mode, side polished fibre with a PVA overlay. The fibre block, with an exposed interaction length of about 2-3mm, was

covered by a PVA layer with thickness in the order of 100μm. The humidity response was examined using two different laser sources emitting at 1550nm and 1310nm respectively. Both wavelengths showed a different sensing characteristic, with 1550nm giving an operating range of ~50-90%RH (dynamic range: 2.2dB) and 1310nm of ~70-85%RH (dynamic range: 8.2dB).

A sensor designed for low humidity detection and based on side polished fibre using a Titanium Oxide (TiO_2) overlay was demonstrated by Alvarez-Herrero *et al.* [48] and is shown in Figure 3-14. The nanostructure overlay was deposited over the polished fibre block by using the electron beam evaporation method. The humidity-induced optical response of the sensor was monitored in the form of a wideband optical spectrum consisting of resonance bands which satisfied the phase matching conditions. The resonances found at specific wavelengths occur when the refractive index of the fibre guided mode is equal to that of the highest order mode of the overlay, thus resulting in coupling of the optical signal from the fibre to the overlay. Depending on the refractive index value of the overlay, the wavelength of the resonance shifts accordingly to fulfil the phase matching condition. This forms the basis of the sensing scheme, created by monitoring the wavelength shift of the resonance bands. The sensor demonstrated shows a linear wavelength shift from 0-15%RH, with a sensitivity of ~0.5nm/%RH. As the RH level increases beyond 20%RH, the sensitivity of the sensor decreases (~0.03nm/%RH for 30-80%RH), showing a smaller wavelength change.

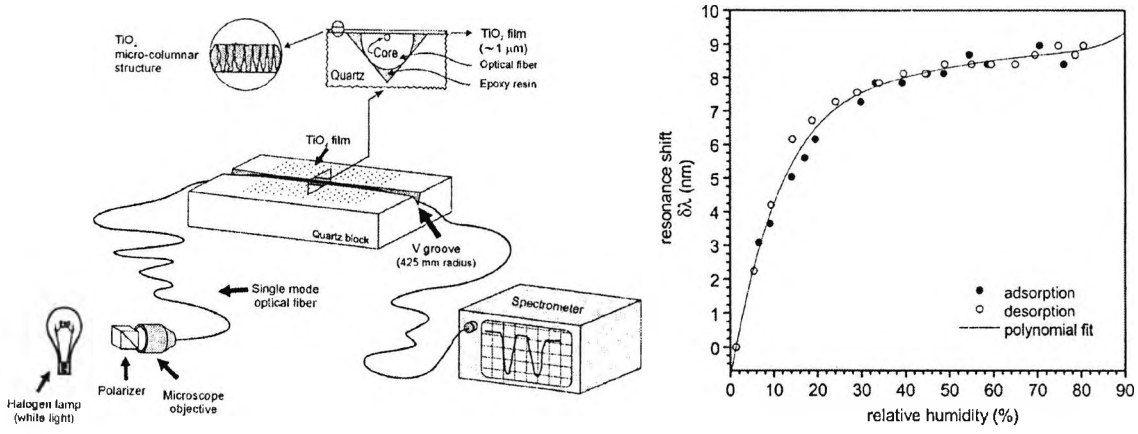

Figure 3-14: (a) Experimental set-up for monitoring humidity-induced resonance band shift of a side-polished optical fibre with TiO_2 overlay. (b) Sensor response to humidity measured using resonance at 633nm (Temperature: 26.1°C ± 0.6°C). [48]

3.4.2.3. Light Scattering

EW sensors based on the light scattering phenomenon can be realised by having a porous material acting as the cladding in the optical fibre structure. This porous cladding layer scatters the evanescent wave that extends from the fibre core, thereby causing a reduction in the intensity of the optical signal propagating along the fibre. As the cladding layer absorbs water molecules, the scattering phenomenon is more evident, resulting in a further decrease in the transmitted optical power.

The use of the EW light scattering technique for humidity sensing was demonstrated by Ogawa *et al.* [49] using a silica core fibre with a porous SiO_2 cladding. A sensor with an interaction length of 40mm was evaluated using an LED emitting at 850nm. The sensor was demonstrated both as a point sensor (optical transmission power measurements at 850nm) and a distributed sensing system, formed by cascading three similar sensors along the same fibre and interrogated using the OTDR technique. The sensor evaluated was found to respond well to humidity change from 20-95%RH, with a small temperature variation dependence of 0.1dB (Test temperature range: 20-100°C).

A similar scattering approach for humidity sensing was discussed by Xu *et al.* [50]. In their work, a U-bent configured EW humidity sensor was implemented using sol-gel technology, thus providing a flexible means of synthesizing custom coating solution to create the porous sol-gel silica film. A light source of a similar emitting wavelength at NIR as employed by Ogawa *et al.* [49], was used during the evaluation, in order to minimise the influence of the Rayleigh scattering effect which dominates at the shorter wavelength range.

3.4.3. In-Fibre Grating Sensors

The in-fibre grating sensor represents a class of intrinsic FO sensors that has gained widespread popularity in recent years. It has been used in numerous applications in various industries due to its inherent sensitivity to temperature, strain and refractive index change [51-53]. The grating

structure within the fibre sensor is created by UV-induced periodic refractive index modulation of the fibre core and can be generally classified into two main categories depending on the grating period, namely the fibre Bragg grating (FBG) and long period grating (LPG).

Detailed description and operation of FBG has been discussed in the previous chapter. LPGs have grating structure with a period typically ranging from 100μm-1000μm. In contrast to the FBG, the forward propagating core mode is coupled into the co-propagating cladding modes. These cladding modes attenuate rapidly as it propagate along the fibre, resulting in a series of attenuation bands centred at several discrete wavelengths. Each of the attenuation bands corresponds to the coupling of the core mode into different cladding modes. The wavelength at which the phase matched coupling occurs is given by the equation [53]

$$\lambda = \left[n_{eff}(\lambda) - n^{i}_{clad}(\lambda)\right]\Lambda \qquad (3\text{-}5)$$

where $n_{eff}(\lambda)$ is the effective refractive index of the core mode, $n^{i}_{clad}(\lambda)$ is the refractive index of the ith cladding mode and Λ is the grating period.

In a similar way to the FBG, the spectral response of the LPG is affected by strain and temperature. In addition to that, the coupling between the core and the cladding modes causes the evanescent field to extend outside the cladding which consequently renders the LPG sensitive to any changes in the medium surrounding the device. A detailed description of the LPG and its application can be found in review papers by James and Tatam [53].

LPG-based sensors are commonly used in chemical sensing. The LPG can be employed as a general refractive index sensor and used in conjunction with chemical selective materials to create a species-specific chemical sensor. This thus forms a very attractive refractive index based chemical sensing mechanism which has been employed in the detection of a variety of chemical species [53]. The FBG-based sensors, on the other hand, are on the whole used predominantly for the monitoring of physical parameters such a temperature, strain or pressure. To use an FBG as a chemical sensor, a common approach is to select a material selectively sensitive to the chemical measurand and capable of inducing mechanical deformation as it interacts. This is done to

produce a secondary strain-induced measurement using the FBG sensor as a result of physical or chemical interactions. The selection of the sensing materials for a FBG chemical sensor is therefore more stringent than LPG as it should not only be responsive to the selected chemical species but also be able to expand in order to induce strain on the FBG. Applications of FBGs in chemical sensing reported so far are largely limited to hydrogen gas detection [54], salinity measurement [55] and moisture sensing [56-58].

The concept of in-fibre grating devices for humidity sensing is fairly new. To date, there are only a few literature reports on the subject, which date back to the year 2001. Humidity sensing using a FBG was first reported by researchers from EPFL, Switzerland [56-57] where studies were carried out to investigate the influence of humidity on commercial polyimide-recoated FBGs. The findings from the investigations concluded that an FBG with polyimide coating was able to respond linearly over a wide humidity range. The sensor was reported to respond well to a humidity range of 10%-90%RH and display good repeatability. Due to its inherent sensitivity to temperature, a compensation scheme was required to extract humidity measurements from the sensor readings. The same sensing scheme proposed for humidity sensing was further explored by various groups and has been demonstrated in several interesting applications which include soil moisture monitoring [59-60] and moisture detection in concrete [61-62].

The use of LPGs for humidity sensing was first reported by Luo *et al.* [63] from Luna Innovations, USA. In the sensor design discussed and shown in Figure 3-15, carboxymethylcellulose (CMC) hydrogel was covalently attached to cladding of a LPG to form the humidity sensor. The sensor demonstrated was found to operate well over a humidity range from 0-95%, with a non-linear response dependency with humidity change. The sensor was observed to be unstable when it was fully saturated at conditions approaching 100%RH and temperature compensation was also required to obtain accurate humidity measurements. The sensor developed by Luna Innovations was evaluated on several separate occasions, as a moisture ingress sensor in aircraft lap joints [64] and as a monitoring device for the moisture detection in building envelopes [65]. In both evaluations, promising results were obtained, thus showing the potential of in-fibre grating-based humidity sensor in commercial/industrial based applications.

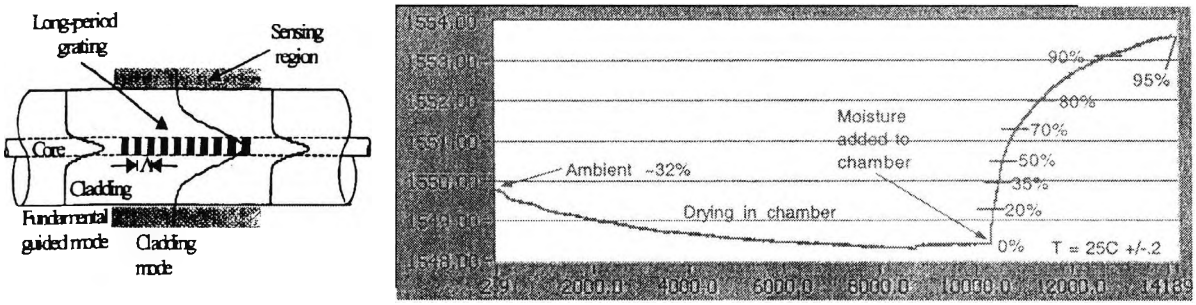

(a) (b)

Figure 3-15: (a) Schematic of a LPG sensor. (b) Sensing characteristics of a CMC-coated LPG humidity sensor. [63]

A similar LPG-based humidity sensing scheme was demonstrated by Tan *et al.* [66] using a gelatine-coated LPG and Konstantaki *et al.* [67] proposed a LPG humidity sensor utilising polyethylene oxide (PEO)/$CoCl_2$ hybrid overlay as the moisture sensitive coating. In both sensors, however, the operating humidity range was found to be limited.

3.4.4. Interferometric Sensors

Light interferometry is a powerful and versatile tool that has been applied in optical fibre sensing to yield high performance FO sensors. In addition to the advantages attributed to the use of fibre optics, FO interferometric sensors generally provide geometric versatility in terms of sensor design and a high level of measurement sensitivity [68]. The sensing mechanism relies on the perturbation of the phase properties of the light signal travelling in the optical fibre introduced by an external environment. The detection of the phase change is realised by mixing the signal of interest with a reference signal, consequently converting the phase difference between the two signals into an optical intensity change. Various interferometer configurations such as the Mach-Zehnder, Michelson, Sagnac and Fabry-Perot can be used to perform the detection. The operation of FO based sensors utilising these configurations and its applications have been discussed in some detail by several authors including Edd [69, 70], Dandridge [68] and Mitchell [71].

One of the earliest FO interferometric humidity sensors was demonstrated by Mitschke [72] in 1989. The proposed sensor design consists of a thin film Fabry-Perot interferometer formed at the tip of the optical fibre as shown in figure 3-16. The interference between the optical signals

reflected by the mirror at both ends of the cavity gives rise to a spectral response which gives a maximum intensity output (resonances) at specific wavelengths. These multiple resonances are separated by the free spectral range (λ_{FSR}) which is given by

$$\lambda_{FSR} = c/2nd \tag{3-6}$$

where c is the speed of light, n is the refractive index of the cavity and d is the cavity length.

As shown in Figure 3-16, the Fabry-Perot cavity in the proposed design was created by a layer of TiO_2 sandwiched in between two partially reflecting mirrors, with the thickness of the cavity optimised to match the operation at the wavelength of the input diode laser source. As the refractive index of the cavity material has a dependence on humidity, the resonance was therefore shifted in response to humidity change and can be conveniently detected by performing intensity measurement at a fixed wavelength. The sensor demonstrated suffers from cross sensitivity to temperature which can be corrected using a suitable compensation scheme. Nevertheless, it showed a good response between 0-80%RH and a response time of less than a minute.

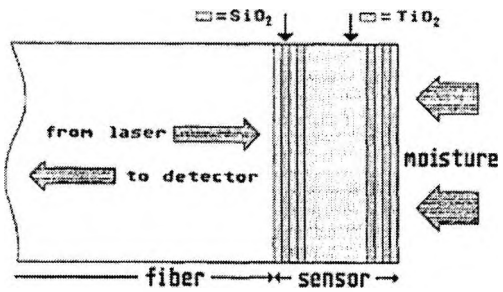

Figure 3-16: FO Fabry-Perot interferometric humidity sensor. [72]

Similar Fabry-Perot interferometric humidity sensors with a submicron cavity length were reported by Arregui *et al.* [73-74] and Yu *et al.* [75]. A typical multilayer thin film interferometric cavity was formed by stacking bilayers of alternating cationic and anionic polymers at the fibre tip. This was achieved by using the ISAM technique which gives good control over the cavity length as well as the material composition of each coating layer. Sensors

with a cavity length (or the number of bilayers) optimised at a specific operating wavelength were shown to be able to operate over a wide humidity range. A very fast response time, in the order of less than a few seconds, was reported and the sensor has been recommended as a possible diagnostic tool to monitor human breathing [76].

Kronenberg et al. [77] explored the use of a low coherence interferomertric system arranged in tandem configuration for humidity detection. The system consists of two Michelson interferometers - 1) an interrogation system to perform the measurements and 2) a bi-fibre optic sensor based on Michelson configuration formed by a reference uncoated fibre and a hydrogel-coated fibre. In a similar way to the FBG sensing mechanism described in the preceding section, the fibre sensor relies on humidity-induced swelling to stretch the fibres which in turn creates an interferometric sensor with an unbalanced path length.

3.5. Summary

In this chapter, the subject of humidity has been discussed with an emphasis on the variety of methods available to perform measurements of this important industrial parameter. Fundamental and secondary methods involving mechanical, optical, temperature and electronic based techniques were discussed briefly, covering the key operating principles, as well as the advantages and disadvantages of each method.

None of these methods, however, can offer an 'ideal' solution to address the various and specific requirements arising from the diversity of potential applications seen in industry today. For the case of moisture detection in concrete structures, in particular, the method employed should fulfil requirements such as meeting the demands of cost, size, remote monitoring and multiplexing capability for multipoint measurements for civil engineering structures. For example, employing fundamental methods such as the highly accurate chilled mirror hygrometer are impossible where the need is to embed the sensor into a concrete structure and secondary devices such as the low cost miniaturised electronic sensors may not be suitable for multiplexing and remote sensing, or sufficiently rugged for long term use. In addition to these requirements, the moisture sensor designed for use to monitor the slow varying process within the concrete structures should meet

the specifications (based on the discussions with the civil engineers involved in this project) in order to obtain meaningful data which can be related to corrosion. Hence the minimum specification for the performance of the sensor should show:

1) Relative Humidity Response Range	40%RH to 90%RH (±10%RH)
2) Response Time	<60 mins
3) Physical Dimension (Active Sensor Size)	<10 mm
4) Multiplexing Capability	

Fibre-optic sensing technology provides an alternative to the conventional sensing methods available as it offers several advantages over their electronic counterparts which make it potentially more feasible as an approach for moisture detection in concrete structures. An extensive literature review was given in the later part of the chapter which discussed the various optical sensing techniques employed for humidity detection. The survey covered various extrinsic and intrinsic methods reported over the years, many of which discussed are mainly on the sensing characteristics obtained in a controlled laboratory environment. Among the wide variety of methods reported, the FBG-based sensor offers the most promising approach in to address the requirements of the application in question. This method thus provides a solid basis for the optical fibre humidity sensor development in this work, which is discussed in detail in the following chapters.

3.6. References

[1] Collins Cobuild Advanced Learner's English Dictionary, Fourth Edition, *Harper Collins Publishers*, 2003.

[2] H. Arai, T. Seiyama, "Humidity Sensors", in *Sensors: A Comprehensive Survey: Volume 3-Chemical and Biosensors*, Part II W. GÖpel, J. Hesse, J. N. Zemel (eds), VCH, 1992

[3] P.R. Wiederhold, "Water Vapor Measurements", *Marcel Dekker*, 1997.

[4] H. H. Willard, L. L. Merritt, J. A. Dean and F. A. Settle, "Instrumental Methods of Analysis", Seventh Edition, *Wasworth Publishing Company*, 1988.

[5] C. Y. Lee and G. B. Lee, "Humidity Sensors: A Review", *Sensor Letters*, 3(2005), 1-14.

[6] Z. Chen and C. Lu, "Humidity Sensors: A Review of Materials and Mechanisms", *Sensor Letters*, 3(2005), 274-295.

[7] Z. M. Rittersma, "Recent Achievements in Miniaturised Humidity Sensors-A Review of Transduction Techniques", *Sensors and Actuators A*, 96(2002), 196-210.

[8] K. T. V. Grattan and T. Sun, "Fibre optic sensor technology: an overview", *Sensors and Actuators A*, 82 (2000), 40-61.

[9] K. T. V. Grattan and B. T. Meggitt (eds), "Optical Fiber Sensor Technology Volume 4: Chemical and Environmental Sensing", *Kluwer Academic Publishers*, 1999.

[10] G. Gauglitz, "Opto-Chemical and Opto-Immuno Sensors", in *Sensors Update* volume 1, H. Baltes, W. Gopel, J. Hesse (eds), VCH, 1996.

[11] Q. Zhou. M. R. Shahriari, D. Kritz and G. H. Sigel, Jr, "Porous Fiber-Optic Sensor for High-Sensitivity Humidity Measurements", *Analytical Chemistry*, 60 (1988), 2317-2320.

[12] S. Otsuki, K. Adachi, "Humidity Dependence of Visible Absorption Spectrum of Gelatin Films Containing Cobalt Chloride", *Journal of Applied Polymer Science*, 45 (1993) 1557-1564.

[13] F. Boltinghouse and K. Abel, "Development of an Optical Relative Humidty Sensor. Cobalt Chloride Optical Absorbency Sensor Study", *Analytical Chemistry*, 61(1989), 1863-1866.

[14] S. Tao, C. B. Winstead, R. Jindal and J. P. Singh, "Optical-Fiber Sensor Using Tailored Porous Sol-Gel Fiber Core", *IEEE Sensors Journal*, 4(2003), 322-328.

[15] M. Ando, T. Kobayashi and M. Harutu, "Humidity-Sensitive Optical Absorption of CO_3O_4 Film", *Sensors and Actuators B*, 32(1996), 157-160.

[16] S. Otsuki, K. Adachi and T. Taguchi, "A Novel Fiber-Optic Gas Sensing Arrangement Based on an Air Gap Design and an Application to Optical Detection of Humidity", *Analytical Sciences*, 14(1998), 633-635.

[17] Y. Sadaoka, M. Matsuguchi, Y. Sakai and Y. Murata, "Optical Humidity Sensing Characteristic of Nafion-dyes Composite Thin Film", *Sensors and Actuators B*, 7(1992), 443-446.

[18] T. E. Brook, M. N. Taib and R. Narayanaswamy, "Extending the Range of a Fibre-Optic Relative Humidity Sensor", *Sensors and Actuators B*, 38-39(1997), 272-276.

[19] B. Kondratowicz, R. Narayanaswamy and K. C. Persaud, "An Investigation into the Use of Electrochromic Polymers in Optical Fibre Gas Sensors", *Sensors and Actuators B*, 74(2001), 138-144.

[20] J. P. Sharkany, S. O. Korposh, Z. I. Batori-Tarci, I. I. Trikur and J. J. Ramsden, "Bacteriorhodopsin-based Biochromic Films for Chemical Sensors", *Sensors and Actuators B*, 107(2005), 77-81.

[21] M. M. F. Choi and O. L. Tse, "Humidity-Sensitive Optode Membrane Based on a Fluorescent Dye Immobilised in Gelatin Film", *Analytica Chimica Acta*, 378 (1999), 127-134.

[22] H. E. Posch, O.S. Wolfbeis, "Fibre-Optic Humidity Sensor Based on Fluorescence Quenching", *Sensors and Actuators*, 15 (1988), 77-83

[23] A. Raichur and H. Pedersen, "Fiber Optic Moisture Sensor for Baking and Drying Process Control", Proc. Food Processing Automation IV, *AM. Soc. Agric. Eng.*, (1995), 180-189.

[24] D. B. Papkovsky, G. V. Ponomarev, S. F. Chernov, A.N. Ovchinnikov and I. N. Kurochkin., "Luminescence lifetime-based sensor for relative air humidity", *Sensors and Actuators B*, 22(1994), 57-61.

[25] S. J. Glenn, B. M. Cullum, R. B. Nair, D. A. Nivens, C. J. Murphy and S. M. Angel, "Lifetime-based Fiber-Optic Water Sensor Using a Luminescent Complex in a Lithium-treated Nafion Membrane", *Analytical Chimica Acta*, 448 (2001), 1-8.

[26] J. M. Costa-Fernandez, M. E. Diaz-Garcia and A. Sanz-Medel, "A Critical Comparision of Different to Develop Room Temperature Phosphorescence Sensing Phases of Air Moisture" *Sensors and Actuators B*, 35-39 (1997), 103-109.

[27] M. Bedoya, M. T. Diez, M. C. Moreno-Bondi and G. Orellana, "Humidity Sensing with a Luminescent Ru(II) Complex and Phase- Sensitive Detection", *Sensors and Actuators B*, 113(2006), 573-581.

[28] J. C. Palais, "Fiber Optic Communications", Chapter 5, fifth edition, *Prentice Hall*, 2005.

[29] J. P. Dakin and B. Culshaw, "Optical Fiber Sensors: Principles and Components", *Artech House*, 1988.

[30] G. Steward, "Fiber Optic Sensors in Environmental Monitoring", in *Optical Fiber Sensor Technology Volume 4: Chemical and Environmental Sensing*, K.T.V. Grattan and B.T. Meggitt (eds), Kluwer Academic Publishers, 1999.

[31] B. D. MacCraith, "Optical Fiber Chemical Systems and Devices", *in Optical Fiber Sensor Technology Volume 4: Chemical and Environmental Sensing*, K.T.V. Grattan and B.T. Meggitt (eds), Kluwer Academic Publishers, 1999.

[32] A. P. Russell and K S. Fletcher, "Optical Sensor for the Determination of Moisture", *Analytica Chimica Acta*, 170(1985), 209-216.

[33] D. S. Ballantine and H. Wohltjen, "Optical Waveguide Humidity Detector", *Analytical Chemistry*, 58, 13 (1986), 2883-2885.

[34] A. Kharaz and B. Jones, "A Distributed Fibre Optic Sensing System for Humidity Measurement", *Measurement and Control*, 28(1995), 101-103.

[35] A. Kharaz, B. E. Jones, K. F. Hale, L. Roche and K. Bromley, "Optical Fibre Relative Humidity Sensor Using a Spectrally Absorptive Material", ", in *SPIE Proceedings of International Conference on Optical Fiber Sensors*, Venice, Italy, 4185(2000), 370-373.

[36] R. Jindai, S. Tao, J. P. Singh and P. S. Gaikwad, "High Dynamic Range Fiber Optic Relative Humidity", *Optical Engineering*, 41, 5(2002), 1093-1093.

[37] S. K. Khijwania, K. L. Srinivasan and J. P. Singh, "Performance Optimised Fiber Sensor for Humidity Measurement", *Optical Engineering*, 44, 3 (2005), 034401-1 – 034401-7.

[38] S. Otsuki, K. Adachi and T. Taguchi, "A Novel Fiber Optic Gas Sensing Configuration Using Extremely Crived Optical Fibers and an Attempt for Optical Humidity Detection", *Sensors and Actuators B*, 53(1998), 91-96.

[39] B. D. Gupta and Ratnanjali, "A Novel Probe for a Fiber Optic Humidity Sensor", *Sensors and Actuators B*, 80(2001), 132-135.

[40] S. K. Shukla, G. K. Parachar, A. P. Mishra, P. Misra, B. C. Yadav, R. K. Shukla, L. M. Bali and G. C. Dubey, "Nano-like magnesium Oxide Films and its Signifigance in Optical Fiber Humidity Sensor", *Sensors and Actuators B*, 98(2004), 5-11.

[41] S. Muto, O. Suzuki, T. Amano and M. Morisawa, "A Plastic Optical Fibre Sensor for Real-time Humidity Monitoring", *Measurement Science and Technology*, 14 (2003), 746-750.

[42] F. J. Arregui, Z. Ciaurriz, M. Oneca and I. R. Matias, "An Experimental Study about Hydrogels for the Fabrication of Optical Fiber Humidity Sensors", *Sensors and Actuators B*, (2003)

[43] C. Bariain, I. R. Matias, F. J. Arregui and M. Lopez-Amo, "Optical Fiber Humidity Sensor based on a Tapered Fiber Coated with Agarose Gel", *Sensors and Actuators B*, 69 (2000), 127-131.

[44] J. M. Corres, J. Bravo and I. R. Matias, "Nonadiabatic Tapered Single-Mode Fiber Coated with Humidity Sensitive Nanofilms", *IEEE Photonics Technology Letters*, 18, 8 (2006), 935-937.

[45] J. M. Corres, J. Bravo and I. R. Matias, "Sensitivity Optimisation of Tapered Optical Fiber Humidity Sensors by Means of Tuning the Thickness of Nanostructured Sensitive Coatings", *Sensors and Actuators B*, (2006).

[46] A. Gaston, I. Lozano, F. Perez, F. Auza and J. Sevilla, "Evanescent Wave Optical-Fiber Sensing (Temperature, Relative Humidity and pH Sensors)", *IEEE Sensors Journal*, 3, 6, (2003), 806-811.

[47] A. Gaston, F. Perez and J. Sevilla, "Optical Fiber relative Humidity Sensor with Polyvinyl Alcohol Film", *Applied Optics*, 43, 21 (2004), 4127-4132.

[48] A. Alvarez-Herrero, H. Guerrero and D. Levy, "High-Sensitivity Sensor of a Low Relative Humidity Based on Overlay on Side-Polished Fibers", *IEEE Sensors Journal*, 4, 1 (2004), 52-56.

[49] K. Ogawa, S. Tsuchiya and H. Kawakami, "Humidity Sensing Effects of Optical Fibers with Microporous SiO_2 Cladding", *Electronics Letters*, 24, 1 (1988), 42-43

[50] L. Xu, J. C. Fanguy, K. Soni and S. Tao, "Optical Fiber Humidity Sensor Based on Evaenscent Wave Scattering", *Optics Letters*, 29, 11 (2004), 1191-1193.

[51] A. Othonos, "Fiber Bragg Gratings", *Review of Scientific Instruments*, 68 (1997), 4309-4341.

[52] Y.J. Rao, "Recent Progress in Applications of In-Fibre Bragg Grating Sensors", *Optics and Lasers in Engineering,* 31 (1999), 297-324.

[53] S.W. James and R. P. Tatam, "Optical Fibre Long-Period Grating Sensors: Characteristics and Application", *Measurement Science and Technology*, 14(2003), R49-R61.

[54] B. Sutapun, M. Tabib-Azar and A. Kazemi, "Pd-coated elastooptic fiber optic Bragg grating sensors for multiplexed hydrogen sensing", *Sensors and Actuators B*, 60 (1999), 27-34.

[55] J. Cong, X. Zhang, K. Chen and J. Xu, "Fiber Optic Bragg Grating Sensor Based on Hydrogels for Measuring Salinity",*Sensors and Actuators B*, 87 (2002), 487-490.

[56] P. Giaccari, H. G. Limberger, P. Kronenberg, "Influence of Humidity and Temperature on Polyimide-Coated Fiber Bragg Gratings", in *Proceedings OSA Trends in Optics and Photonics Series: Bragg Gratings, Photosensitivity, and Poling in Glass Waveguides*, Washington, DC, USA, 61 (2001), BFB2.

[57] P. Kronenberg, P. K. Rastogi, P. Giaccari, H. G. Limberger, "Relative Humidity Sensor With Optical Fiber Bragg Grating", *Optics Letters*, 27 (2002), 1385-1387.

[58] T. L. Yeo, T. Sun, K. T. V. Grattan, D. Parry, R. Lade and B. D. Powell, "Characterisation of a Polymer-coated Fibre Bragg Grating Sensor for Relative Humidity Sensing", *Sensors and Actuators B*, 110(2005), 148-156.

[59] M. Laylor, S. Calvert, T. Taylor, W. Schulz, R. Lumsden, E. Udd, "Fiber optic grating moisture and humidity sensors", in *Proceedings Smart Structures And Materials: Smart Sensor Technology & Measurement System*, San Diego, CA, USA, 4694 (2002), 210-217.

[60] W. Kunzler, S. Calvert, M. Laylor, "Measuring Humidity & Moisture with Fiber Optic Sensors", in *Proceedings Sixth Pacific Northwest Fiber Optic Sensor Workshop*, Oregon, USA, 5278 (2003), 86-93.

[61] T. L. Yeo, D. Eckstein, B. McKinley, L. F. Boswell, T. Sun, K. T. V. Grattan, "Demonstration of a Fibre Optic Sensing Technique for the Measurement of Moisture Absorption in Concrete", *Smart Material and Structures*, 15(2006), N40-N45.

[62] T. L. Yeo, M. A. C. Cox, L. F. Boswell, T. Sun, K. T. V. Grattan, "Optical Fiber Sensor for Monitoring Ingress of Moisture in Concrete Structure", *Review of Scientific Instruments*, 77(2006), 055108-1 – 055108-7.

[63] S. Luo, Y. Liu, A. Sucheta, M. Evans and R. van Tassell, "Applications of LPG Fiber Optical Sensors for Relative Humidity and Chemical Warfare Agents Monitoring", in *Proceedings Advanced Sensor Systems and Applications*, 4920 (2002), 193-204.

[64] K.R. Cooper, Y. Ma, J.P. Wikswo and R.G. Kelly, " Simultaneous monitoring of the corrosion activity and moisture inside aircraft lap joints", *Corrosion Engineering, Science and Technology*, 39 (2004), 339-345.

[65] W. M. Healy, S. Luo, M. Evans, A. Sucheta and Y. Liu, "Development of an Optical Fiber-based Moisture Sensor for Building Envelopes", in *Proceedings 24th AIVC Conference and BETEC Conference on Ventilation, Humidity Control and Energy*, (2003), 277-282.

[66] S. Tao, C. B. Winstead, R. Jindal and J. P. Singh, "Optical Fiber Sensor Using Tailored Porous Sol-Gel Fiber Core", *IEEE Sensors Journal*, 4, 3(2004), 322-328.

[67] M. Konstantaki, S. Pissadaki, S. Pispas, N. Madamopoulous and N. A. Vainos, "Optical Fiber Long Period Grating Humidity Sensor with PEO/$CoCl_2$ Coating", *Applied Optics*, 45(2006), 4567-4571.

[68] A. Dandridge, "Fiber Optic Sensors Based on the Mach-Zehnder and Michelson Interferometers", in *Fiber Optic Sensors: An Introduction for Engineers and Scientists*, E. Udd (Ed), John Wiley & Sons, 1991.

[69] E. Udd, "An Overview of Fiber-Optic Sensors", *Review of Scientific Instruments*, 66 (1995), 4015-4030.

[70] E. Udd, "Fiber Optic Sensors Based on the Sagnac Interferometer and Passive Ring Resonator", in *Fiber Optic Sensors: An Introduction for Engineers and Scientists*, E. Udd (Ed), John Wiley & Sons, 1991.

[71] G.L. Mitchell, "Intensity-Based and Fabry-Perot Interferometer Sensors", in *Fiber Optic Sensors: An Introduction for Engineers and Scientists*, E. Udd (Ed), John Wiley & Sons, 1991.

[72] F. Mitschke, "Fiber Optic Sensor for Humidity", *Optics Letters,* 14, 7 (1989), 967-969.

[73] F. J. Arregui, Y. Liu, I. R. Matias and R. O. Claus, "Optical Fiber Humidity Sensor using a Nano Fabry-perot cavity Formed by the Ionic Self-Assembly Method", *Sensors and Actuators B*, 59 (1999), 54-59.

[74] F. J. Arregui, K. L. Cooper, Y. Liu, I. R. Matias and R. O. Claus, "Optical Fiber Humidity Sensor with a Fast response Time using the Ionic Self- Assembly Method", *IEIEC Transaction on Electronics*, E83C, 3 (2000), 360-365

[75] H. Yu, L. Yao, L. Wang, W. Hu, D. Jiang, "Fiber Optic Humidity Sensor Based on Self-Assembled Polyelectrolyte Multilayers", *Journal of Wuhan of Technology Materials*, 16, 3 (2001), 65-69.

[76] Q. Chen, R. O. Claus, W. B. Spillman, F. J. Arregui, I. R. Matias and K. L. Cooper, "Optical Fiber Sensors for Breathing Diagnostic", in *Proceedings OFS 15*, Portland, Oregon, USA, 1(2002), 273- 276.

[77] P. Kronenberg, B. Culshaw and G. Pierce, "Development of a Novel Fiber Optic Sensor for Humidity Monitoring", in *Proceedings SPIE Conference on Sensory Phenomena and Measurement Instrumentation for Smart Structures and Materials*, (1999), 480-485.

Chapter 4:

FBG-Based Humidity Sensors: Principle, Development and Characterisation

4.1. Introduction

The emphasis of this chapter is on reporting the work carried out on the development and characterisation of polymer-coated FBG humidity sensors for structural health monitoring. The fibre-optic sensor system designed is based on the swelling of the moisture sensitive polymer layer, coated on an FBG, which was inscribed in a photosensitive optical fibre. Following the review of a range of methods discussed in the previous Chapters, this approach is developed to address specific issues arising from concrete health monitoring. The sensor basically behaves as a FBG-based strain sensor which relies on the secondary strain effect induced on the sensing element as a result of material expansion through the absorption of water molecules.

This chapter begins with a review of the basic principles of the sensing scheme employed in this work. A theoretical study on the strain related effects induced on the FBG which underpins the

analysis of the experimental data obtained during the course of this research will also be discussed. Key milestones during the development of the sensor, including material selection, sensor fabrication procedure and assembly are discussed in detail in this Chapter.

The final part of this chapter focuses on the characterisation of the polymer-coated FBG humidity sensors. Experimental results obtained from a series of investigations will be presented together with a detailed analysis in terms of the humidity and temperature responses, effect of coating thickness, time response and hysteresis effect of the basic characteristics of the sensors developed.

4.2. Principle of Operation

The operation of the FBG-based humidity sensor is based on the swelling of a moisture sensitive polymer coated on the sensing element. As discussed in chapter 2, an FBG is inherently sensitive to strain and temperature. The expansion of the coating layer, as a result of moisture absorption, induces a secondary strain effect on the polymer-coated FBG, causing the optical fibre to stretch. Therefore, any strain or temperature change applied to the sensing element perturbs the effective refractive index and the period of the FBG, consequently causing the Bragg wavelength to shift.

This shift in Bragg wavelength due to strain and thermal effects is given by

$$\frac{\Delta\lambda_B}{\lambda_B} = (1 - P_e)\varepsilon + \left[(1 - P_e)\alpha + \xi\right]\Delta T \qquad (4\text{-}1)$$

where P_e is the photoelastic constant of the fibre (typical value for silica fiber is 0.22 [1]), ε is the strain induced on the fibre, α is the thermal expansion coefficient of the FBG and ξ is the fibre thermo-optic coefficient ($\approx 8.6 \times 10^{-6}$ for Germanium-doped silica core fibre [2]).

For a bare fibre, the thermal related wavelength shift is mainly determined by the thermo-optic effect as the coefficient is nearly 15 times the value of the thermal expansion coefficient of silica. Thus, the thermally induced strain is relatively very small. For a polymer-coated FBG, however, on the assumption that the thermal expansion coefficient of the polymeric material is higher than

that of silica, the resultant thermal strain induced on the FBG due to the coefficient mismatch will have a significant contribution to the wavelength shift.

Equation (4-1) can be simplified, taking into account the strain effect induced (moisture/thermal) due to the polymer coating on the FBG. The shift in the Bragg wavelength for a polymer-coated FBG is therefore given by

$$\frac{\Delta\lambda_B}{\lambda_B} = (1-P_e)\alpha_{RH}\cdot\Delta RH + \left[(1-P_e)\alpha_T + \xi\right]\Delta T \qquad (4\text{-}2a)$$

where α_{RH} and α_T are the coefficient of moisture expansion (CME) and the coefficient of thermal expansion (CTE) of the polymer-coated FBG.

$$\frac{\Delta\lambda_B}{\lambda_B} = (1-P_e)\varepsilon_{RH} + (1-P_e)\varepsilon_T + \xi\cdot\Delta T \qquad (4\text{-}2b)$$

The above equation relates the shift in the Bragg wavelength of a polymer-coated FBG to three main components. This comprises of the two strain effects induced on the FBG due to 1) moisture absorption (ε_{RH}), 2) temperature change (ε_T) and the thermo-optic effect.

4.2.1. Strain Model on Polymer-Coated FBG

In order to determine the amount of strain induced on a polymer-coated FBG, as shown in Figure 4.1 (a), due to moisture absorption or temperature change, the sensing element is considered as a composite bar comprising of materials with different expansion coefficients. This section discusses the effective strain induced on a polymer-coated FBG using a method described by Case et al. [3] to determine the temperature-induced stress developed in a composite bar. Since thermal expansion of a material is analogous to moisture-induced expansion, this method can be adapted to approximate the effective strain induced on the polymer-coated FBG.

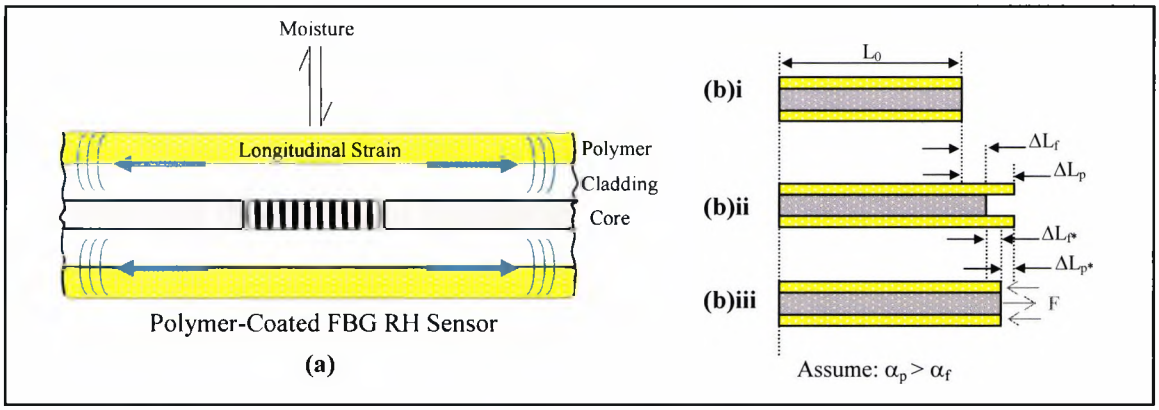

Figure 4-1: (a) Schematic of a polymer-coated FBG sensor. (b) Illustration of stress development on a composite bar. [3]

A composite bar consisting of a rod (silica optical fibre) and a circular tube (polymer tube) with a different expansion coefficient of α_f and α_P respectively is considered. Assuming that these two materials are bonded together as shown in figure 4-1(b), the internal stresses build up when the composite bar is experiencing either a change in temperature or moisture levels.

If these two materials are allowed to expand freely without any constraint, the change in length for these materials would be

$$\Delta L = \alpha_{(x)} \cdot \Delta x \cdot L_0 \qquad (4\text{-}3)$$

where ΔL is the change in length, $\alpha_{(x)}$ is the coefficient of moisture expansion (CME) or the coefficient of thermal expansion (CTE), Δx is the change in temperature or moisture level and L_0 is the initial length of the composite bar.

This would give rise to a difference in length between the two materials, which is

$$\Delta L = (\alpha_{p(x)} - \alpha_{f(x)}) \cdot \Delta x \cdot L_0 \qquad (4\text{-}4)$$

However, since the materials were bonded together, the change in length experienced when the bar is allowed to expand freely will be eliminated by an equal compression and expansion force (F) exerted on the polymer coating and the optical fibre respectively.

Hooke's law [4] of elasticity states that the amount by which a material body is deformed (the strain) is linearly related to the force causing the deformation (the stress). This relationship can be expressed by the equation

$$\sigma = E\varepsilon \tag{4-5a}$$

$$F/A = E \cdot \Delta L/L \tag{4-5b}$$

where σ and ε are the longitudinal stress and strain developed on the material and E is a the modulus of elasticity, also known as Young's Modulus.

If A_f and A_p are the cross sectional areas, and E_f and E_p are the values of the Young's modulus of the optical fibre material and of the polymer layer respectively, the expansion of optical fibre and the contraction of the polymer layer due to force, F, can be given by

$$\Delta L_{f^*} = (F \cdot L_0)/(A_f \cdot E_f) \tag{4-6a}$$

$$\Delta L_{p^*} = (F \cdot L_0)/(A_p \cdot E_p) \tag{4-6b}$$

The difference in length, as depicted in figure 4-1(b)ii, is hence eliminated by a force F which is pulling the optical fibre and compressing the polymer coating. Therefore,

$$(\alpha_{p(x)} - \alpha_{f(x)}) \cdot \Delta x \cdot L_0 = \Delta L_{f^*} + \Delta L_{p^*} \tag{4-7}$$

by substituting (4-6a) and (4-6b) into (4-7),

$$(\alpha_{p(x)} - \alpha_{f(x)}) \cdot \Delta x \cdot L_0 = (F \cdot L_0)/(A_f \cdot E_f) + (F \cdot L_0)/(A_p \cdot E_p) \tag{4-8}$$

and by rearranging equation (4-8), the amount of force (F) acting on the composite bar due to the expansion and contraction of materials can be determined,

$$F = \frac{(A_p \cdot E_p) \cdot (A_f \cdot E_f)}{(A_p \cdot E_p) + (A_f \cdot E_f)} \cdot (\alpha_{p(x)} - \alpha_{f(x)}) \cdot \Delta x \cdot L_0 \qquad (4\text{-}9)$$

Since the stress (σ) is equal to F/A and according to Hooke's Law ($\sigma = E.\varepsilon$), the strain acting on the optical fibre ($\varepsilon_{f(x)}$), as a result of a change in temperature/moisture levels experienced by the polymer-coated FBG, can be determined by using the following equation,

$$\varepsilon_{f(x)} = \frac{(A_p \cdot E_p)}{(A_p \cdot E_p) + (A_f \cdot E_f)} \cdot (\alpha_{p(x)} - \alpha_{f(x)}) \cdot \Delta x \qquad (4\text{-}10)$$

From the above relationship, it can be shown that the effective strain induced on the FBG is dependent on the cross-sectional area of the polymer coating: thus, the sensitivity of the sensing element can be tuned by changing the coating thickness of the sensor. However, factors such as response time of the sensor will also be affected by the coating thickness. These factors pertaining to the performance of the FBG sensor will be discussed further in this chapter.

4.3. Moisture Sensitive Coatings

Different materials possess different moisture swelling properties and therefore, the choice of the polymeric material plays a crucial role in the performance of the FBG-based moisture sensor. The detection of moisture using the FBG strain sensor depends on how effective the swelling of the material stretches the optical fibre. Some materials may give a linear response in terms of Bragg wavelength shift while some may not. It may also be desirable to use a material that has a high moisture swelling property but the strength of the material should also be considered to ensure a detectable strain can be induced on the fibre as it hydrates and swells. Therefore, there should be a compromise between these factors when selecting a suitable material for an optimised FBG-based humidity sensor.

The selection criteria of the 'ideal' coating material for the sensor are further complicated by the fact that there are numerous polymeric materials which have a certain affinity for moisture. Although the list of potential candidates is long, some of these potential materials are either

produced commercially for a specific application other than moisture sensing or specially designed and synthesized in research laboratories which are not easily available.

Hence, the selection of a suitable and practical coating material that may be applied in the laboratory is narrowed down in light of the following criteria:

- A knowledge of the critical performance parameters of polymers previously evaluated as a potential sensing material for humidity sensing, using various detection schemes (electronic/optical), from published data in the literature.
- Selected materials should be readily available and do not require advanced, specialised chemical knowledge and facilities to synthesise, process and handle them, recognizing the capabilities of the laboratory.
- Potential materials should be compatible with a simple and effective method of deposition, to allow for flexibility in the design of the sensor.

Based on the above points, two materials were chosen for evaluation – these being polyimide (PI) and polyvinyl alcohol (PVA), two contrasting polymeric materials (in terms of their properties). The use of these two materials as potential sensing materials has been discussed previously by several authors [5-13] for humidity sensing using different optical and electrical transduction methods. However, the focus here is to address issues in relation to a novel application in concrete structural monitoring, imposing as it does additional and demanding constraints upon the sensor design and thus the material choice. The properties of the two materials chosen are reviewed below.

4.3.1. Polyimide

Polyimide (PI) was developed by Dupont and made commercially available in the early 1960s [14]. It is known to possess excellent material properties which include good mechanical strength, good thermal and chemical stability and low dielectric constant, etc. Polyimide has applications in various industries such as electronic, aerospace and automotive sectors [15]. For example, PI can be moulded into load bearing parts, such as the chassis, struts or brackets, for use in automotive or aircraft structures. The excellent electrical and thermal properties of polyimide also

makes it an ideal replacement for glass or ceramics for used in high temperature resistant electrical connectors, switches and housing, etc. Due to its compatibility with microelectronic fabrication processes, the electronic industry has seen an increase in the use of polyimide coatings for microelectronic devices as PI solutions can be easily spun on wafers, exposed and etched with existing equipment. It can also be used as a masking material for multilayer resist processing, interlayer dielectrics, passivation and as a thermal-mechanical buffer.

Polyimide contains an aromatic ring and has the general structure shown in figure 4-2 [15]. A general method to synthesize this material involves a two-step polycondensation reaction process of aromatic dianhydride with aromatic diamines in a suitable solvent such as N-methyl-2-pyrrolidone (NMP) to form polyamic acid. Thermal treatment is then required to convert the polyamic acid into polymide and to remove the remaining solvent and water which was produced as a by-product from the imidisation process.

Different combinations of precursors [14] will result in different polymer chain structures, causing the material properties to vary. Commercially available polyimide samples are usually of aromatic heterocyclic type and depending on the source of supply, sold under different trade names, Kapton(Dupont), IP-2080(Dow), Matrimid 5218 (Ciba-Geigy), Ultem(General Electric) and LARC-TPI(Mitsu-Toatsu Chemicals) are just a few examples of commercial grade polyimide precursor solutions.

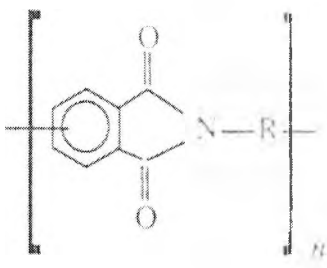

Figure 4-2: General structure of aromatic polyimide. [15]

Polyimide film has the tendency of absorbing moisture from the humid ambient environment, which can alter its mechanical and electrical properties. It is commonly used as a sensing material in electronic-based RH sensors, for example, in an electronic capacitive-based humidity sensor [5].

Gerlach and Sager [6] proposed a novel concept for a miniaturized electronic RH sensor based on the swelling of the polyimide film. The film coated on a silicon membrane forms part of the piezoresistive Wheatstone bridge circuitry, employed to monitor the bending stress caused by the deformation of the polyimide film as a result of moisture absorption. Although the moisture swelling capability of PI is not as high as other polymers such as hydrogel, the volume expansion of which was found to be reproducible and to vary linearly with humidity [16].

Unlike the coefficient of thermal expansion (CTE), the details of the coefficient of moisture expansion (CME) of a material is usually not readily available, even from the manufacturers. In an application where the moisture-induced swelling mechanism is used as a form of transduction method, the availability of such information will aid the design of the sensor. A method using an X-ray curvature measuring technique (see figure 4-3) was developed by Sager *et al.* [16] to determine the coefficient of moisture expansion of the commercial grade polyimide films used in their sensor design. This method involves using a bimorph system (analogous to a temperature bimetallic strip) created by using a silicon wafer coated with a polyimide layer. To determine the CME of the material, the moisture-induced bending or the curvature of the bimorph structure was measured at both lower humidity level and near 100%RH condition. The CME of the polyimide film measured was found to be in the range of about 60-90ppm/%RH and is dependent on the curing temperature and the material type.

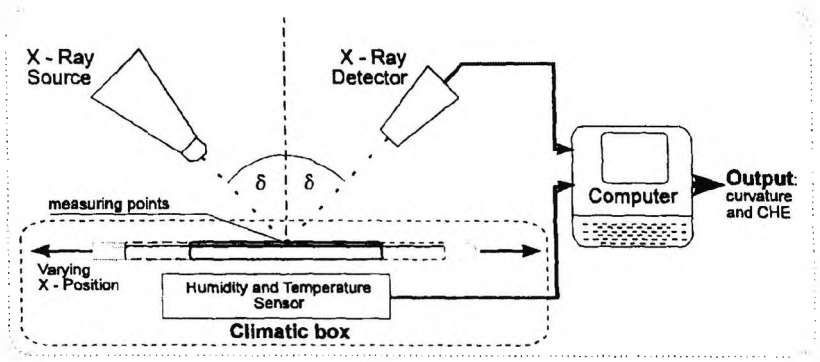

Figure 4-3: X-ray curvature system set-up for determining the coefficient of moisture expansion of polyimide. [16]

The effort led by Gerlach and his co-workers [16-18] has also provided valuable insight into the moisture-related swelling processes in polyimide films. Investigations were carried out using polyimide with different chemical structures to study the moisture intake and expansion behaviour of these materials. These moisture-dependent swelling properties of polyimide films have complex dependencies (see figure 4-4) on various factors which include the polymer type, deposition and curing conditions. In addition to that, the characteristics of the material itself, i.e. stiffness, degree of imidisation, shrinkage behaviour, etc, will also influence the moisture-dependent swelling behaviour. The information obtained therefore help in the better selection of polyimide material and its corresponding process conditions to tailor the material properties for specific applications.

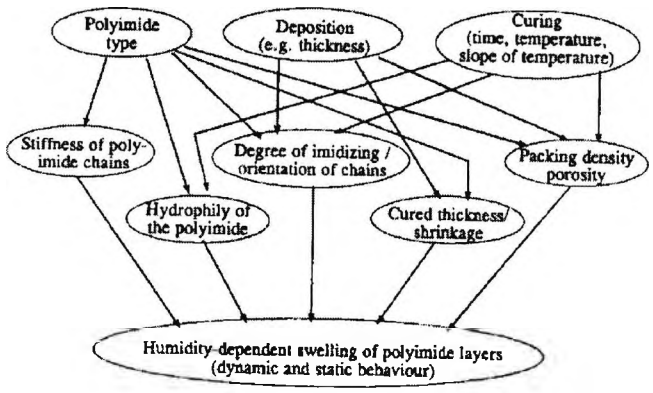

Figure 4-4: Various factors influencing the moisture swelling behaviour of polyimide. [16]

4.3.2. Polyvinyl Alcohol

Polyvinyl Alcohol (PVOH/PVA) is a water soluble polymer which can be synthesized by saponification of polyvinyl acetate. It has a range of applications in industries as diversified as textile, paper, food and pharmaceutical [19-21]. Examples of these applications include textile warp sizing, paper sizing and binding agent, adhesive, food packaging, emulsifying and thickening agent in cosmetics.

The general chemical structure for PVA, with the assumption of a high degree of hydrolysis, is shown in figure 4-5. For a lower degree of hydrolysis, the acetate block is included in the

polymer chain to represent a partially hydrolyzed PVA as shown in figure 4-5(b). There are different grades of PVA with properties that can be tailored for specific application. Grades of PVA can be classified according to its degree of hydrolysis and polymerisation. Comprehensive information on PVA can be found in literature compiled by C.A. Finch [21], which discussed in detail, the synthesis of the material, its chemical and physical properties and also its applications in various industries.

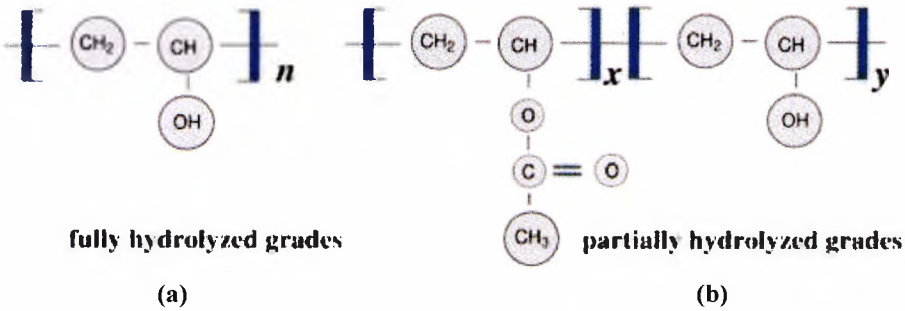

Figure 4-5: Chemical structure of polyvinyl alcohol. [19]

The production of PVA involves two main processes, 1) polymerisation of vinyl acetate monomers to form polyvinyl acetate (PVAc) and 2) Hydrolysis (saponification) of PVAc to replace the acetate group (CH_2COOH) with hydroxyl group (OH). The percentage of the PVAc blocks against the PVA blocks in the polymer chain represents the degree of hydrolysis (DH). An increase in the DH will enhance the tensile strength, the water resistance, the solvent resistance and the adhesion to hydrophilic surfaces. A decrease in DH will however improve the water sensitivity, solubility and flexibility of the material. It will also improve the adhesion to hydrophobic surfaces. The degree of polymerisation (DP) is associated with the molecular weight of the polymer chain. A high degree of polymerisation will result in enhanced tensile strength, adhesive strength, water resistance and an increase in the viscosity of the aqueous solution. On the contrary, low DP increases the solubility and water sensitivity of the polymer and decreases the material strength and viscosity of the aqueous solution. For partially hydrolysed (low DH), there are more acetal groups in the polymer chain and due to the spatial disturbances caused by this group, it restricts the close packing of the molecules, thus reduces the crystallinity and viscosity.

Fully and partially hydrolysed PVA will result in hydrophobic and hydrophilic films respectively. The influence of the degree of hydrolysis and polymerisation on properties of PVA are summarised in figure 4-6.

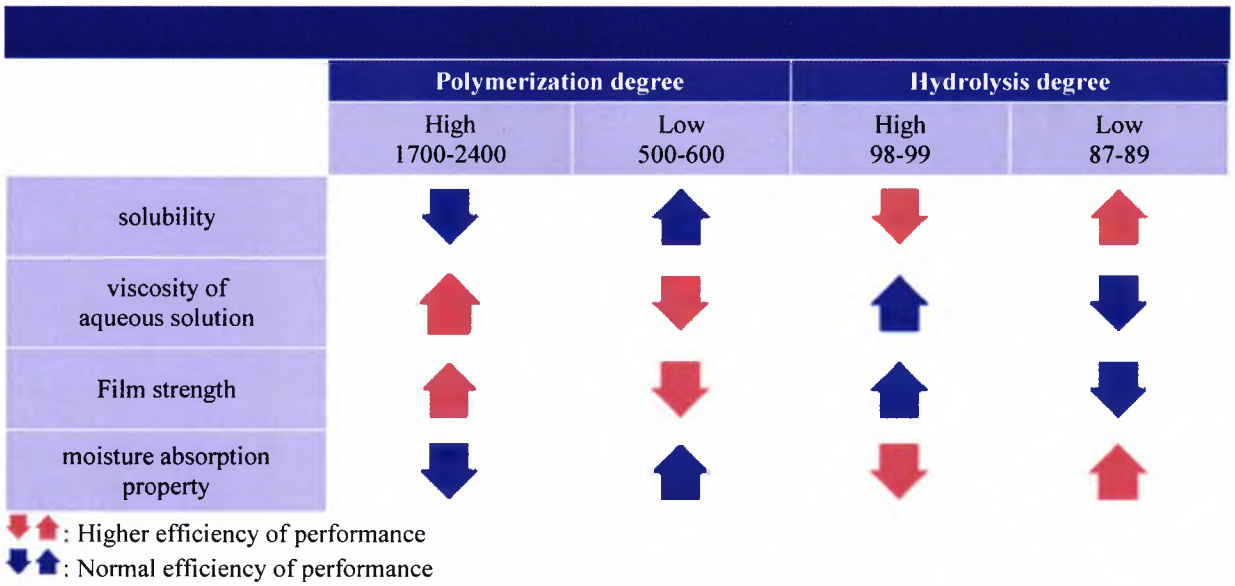

Figure 4-6: Characteristics of polyvinyl alcohol. [20]

A key characteristic of PVA is its affinity to water. As such, it has been considered by various researchers as a potential material for humidity detection and an evaluation of the PVA film using various electronic and optical based detection schemes has been reported for many years [8-13].

Penza and Anisimkin [8] have reported the use of a PVA-coated surface acoustic wave (SAW) device as a humidity sensor. The humidity detection was carried out by monitoring the change in the SAW characteristics, such as phase or frequency of the acoustic signal as it travels along the propagation path. The phase response of the sensor with a 1μm film was recorded as a function of the relative humidity. A non-linear response was observed, with the trend becoming slightly linear when the sensing temperature was varied from 20°C to 60°C. Low hysteresis was observed when the sensor was subjected to a humidity change between 10%RH to 90%RH, with humidity level both rising and falling. The hysteresis effect was found to be more prominent at higher RH level which suggests the formation of clusters of the absorbed water molecules in the PVA film. On the whole, the PVA SAW sensor exhibits good repeatability and reversibility with excellent

water resistance at room temperature. The sensor was found to be sensitive to ethanol and methanol vapours but has negligible sensitivity towards gases such as NH_3, NO_2, CO and H_2.

The use of PVA in conductometric/impedance type humidity sensors has been discussed by Wang et al. [9] and Yang et al. [10]. A layer of PVA film which exhibits high impedance was coated onto an alumina substrate with interdigitated electrodes. The sensor works on the basis of conductivity change of the device as the PVA film absorbs water where an increase in the moisture content in the sensing film results in an increase in conductivity, thus reducing the impedance value of the device. Again, the sensors reported exhibit a non-linear humidity response. The performance of such a sensor using pure PVA film is not very satisfactory and techniques such as using plasma treatment or mixing PVA with electrolyte were suggested [10] to enhance the performance of the sensor.

Instead of using the PVA film as a primary sensing element in a sensor configuration, it can also be used purely as a moisture absorbent matrix to immobilise a humidity sensitive chemical reagent for incorporation with an optical-based absorption technique. Singh and his co-workers [11, 12] have implemented an optical humidity sensor using a de-clad optical fibre coated with a $CoCl_2$-doped PVA film. This approach is based on the evanescent-wave absorption technique frequently used in fibre optic chemical sensing, together with using a common chemical salt which changes its optical absorption properties and also its colour, from blue to pink, as it hydrates. The PVA film merely acts as a chemical specific absorbing medium to support the chemical reaction between the moisture absorbed and the reagent. This intensity-based optical sensor is reported to exhibit a good degree of reversibility, repeatability and a good dynamic range.

A similar optical sensing scheme using PVA film was investigated by Gaston et al [13]. The variant of this scheme lies in the use of an undoped PVA film coated onto a de-clad communication grade singlemode optical fibre. The proposed scheme was based on the change of the refractive index value of the PVA coating which perturbs the light propagation conditions of the optical fibre. The detection of humidity simply involves monitoring the optical signal attenuation which varies as a function of the drift in refractive index value when the PVA coating absorbs moisture. The reported sensor is able to respond to humidity change with a good

sensitivity and response time. However, the detection range of the sensor is limited to 50%RH - 90%RH.

4.4. Sensor Fabrication

4.4.1. Inscription of FBG in Photosensitive Optical Fibre

All the FBGs used in this research work were fabricated using the fabrication facility at City University. Figure 4-7 shows the schematic of the set-up using the phase mask inscription technique and a picture of the FBG fabrication facility at City University. The set-up consists of a KrF excimer laser source (Braggstar 500, Tuilaser AG) to provide the UV radiation at 248nm. A plano-cylindrical lens (focal length: 200mm) was placed in the beam path to converge the elliptically-shaped laser beam into a thin line with a width of ~0.5mm and length of ~6.5mm. The laser beam is then projected through the phase mask to create the interference fringe pattern which is subsequently imprinted onto the optical fibre to modulate its core refractive index.

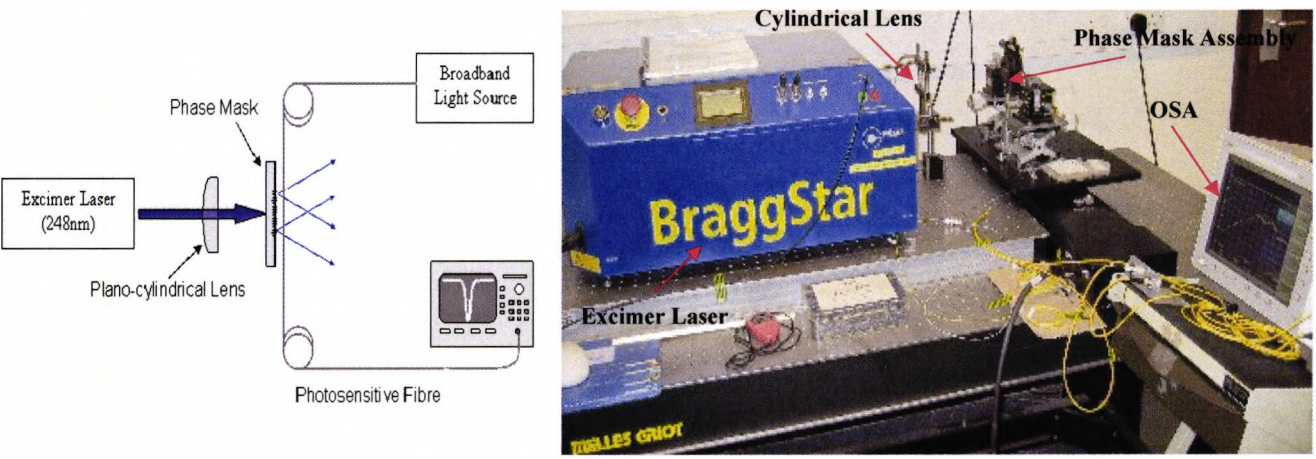

Figure 4-7: (a) Basic configuration of the phase mask writing set-up. (b) Photo of the FBG writing facility at City University.

During the fabrication process, the photosensitive fibre spliced to FC/PC connectors were connected to a broadband optical light source (Opto-Link Cooperation Limited, OLS15 CSF) at one end and to an optical spectrum analyser (Agilent 86140A) at the other to monitor the spectral

profile of the FBG. Figure 4-8 shows a typical spectral profile of a FBG with a transmission dip at a position corresponding to the Bragg wavelength. The Bragg wavelength can also be monitored (peak of the reflection spectrum) through an alternative configuration using a 2x1 fibre optic coupler.

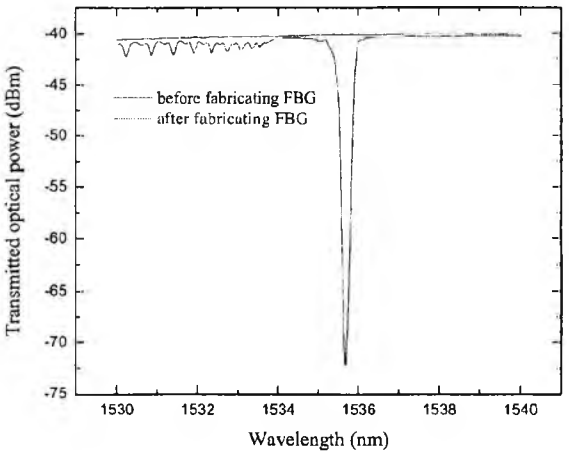

Figure 4-8: Typical transmission spectrum of a FBG written in a photosensitive fibre. [23]

4.4.1.1. Boron/Germanium Codoped Fibre Bragg Grating

All the fibre Bragg gratings, employed during the course of this research, were fabricated using commercially available Boron/Germanium (B/Ge) codoped photosensitive fibres purchased from FibreCore Ltd (PS1250/1500). The B/Ge codoped fibre was found to be the most photosensitive among the various types of optical fibres reported [22] and requires the shortest exposure time to achieve reflectivity saturation [2].

The thermal decay characteristics of FBGs written in B/Ge fibre have been investigated in some detail by several research groups [23-26]. These investigations provide essential knowledge on the potential for degradation, and hence the operational lifetime of the FBGs when used in elevated temperatures. Such information is vital to ensure effective operation of the FBG-based devices in various, specific applications.

The decay mechanism relates the thermally induced decay of the refractive index modulation (Δn_{mod}) [23, 25, 26] and the effective refractive index (Δn_{eff}) [23, 24] to the reduction in the grating peak reflectivity and the shift in the Bragg wavelength. The plots in figure 4-9 show the

thermal decay characteristics of type I FBGs written in B/Ge photosensitive fibre reported by Pal *et al.* [23]. The normalised integrated coupling coefficient[1] (η) and the Bragg wavelength were plotted against time to show the decay characteristics of the FBGs when subjected to 'burn-in' temperatures of 100°C, 200°C, 300°C and 400°C respectively. Theoretical curves based on 'power law' models [23, 27] were seen to match well with the experimental data obtained and were plotted to predict the grating lifetime at different temperatures. The information presented is useful for this work, in particular, where an annealing process is required to stabilise the performance of the FBGs prior to the polymer coating procedure, which requires thermal curing at high temperatures.

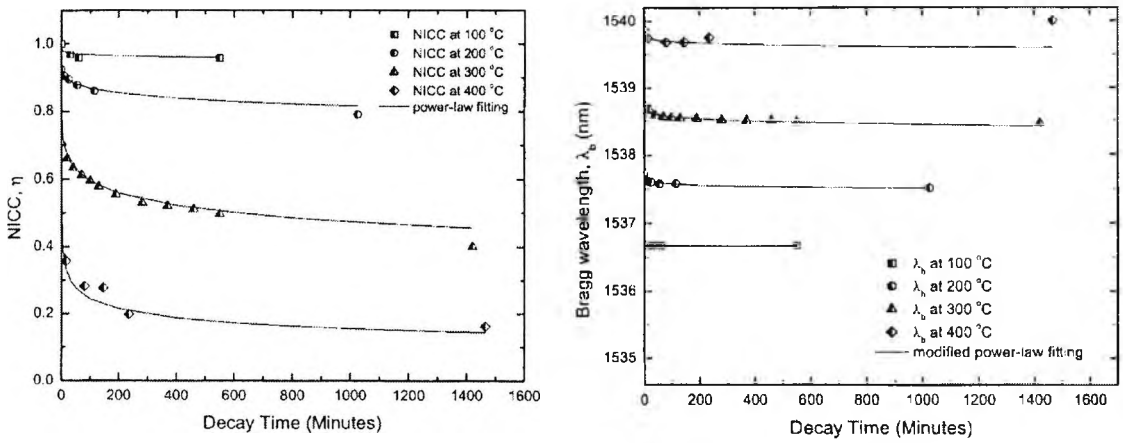

Figure 4-9: Thermal decay characteristics of type I B/Ge FBGs at various temperatures. [23]

Extensive studies on the sensing characteristics of FBGs fabricated into various types of photosensitive optical fibres, including B/Ge fibres, were carried out and reported by colleagues [28, 29] at City University. The work has been focused mainly on the photosensitivity, thermal sustainability and stability for high temperature sensing applications. Prior to the investigations on the fibre photosensitivity and FBG thermal characteristics, Pal [28] performed a detailed calibration of the FBG fabrication facility at City University using B/Ge fibres to establish fabrication parameters such as the laser energy and exposure duration to achieve reflectivity saturation. Typical exposure period to achieve reflectivity saturation, using a laser setting of

[1] Integrated coupling coefficient (ICC) is a term used in the power law thermal decay model [27] to determine the degradation of the peak reflectivity. ICC = $\tanh^{-1}(1-T_{min})$ where T_{min} is the transmission dip of the FBG at Bragg wavelength. NICC represents the ICC normalised to value of ICC at the beginning of the thermal test at time = t_{intial}.

12mJ at 200Hz, is about 60 seconds. The results obtained are shown in figure 4-10 and have been used as a reference by the research group for all subsequent fabrications of FBGs in B/Ge fibre.

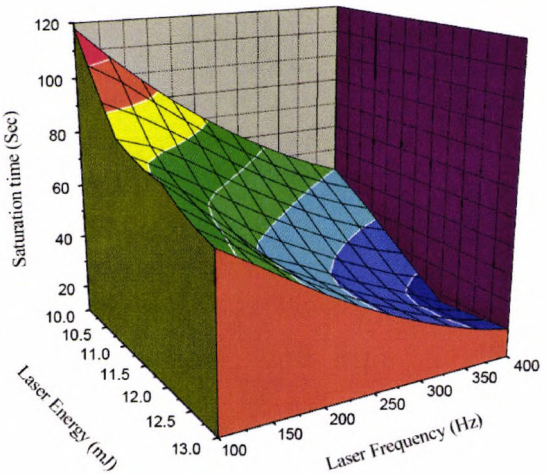

Figure 4-10: A 3-D plot describing the exposure time requirement to achieve reflectivity saturation at different laser energy and frequency settings. [28]

4.4.2. Coating Deposition

Dip coating is by far the simplest and most effective method that can be implemented for coating or depositing polymers in aqueous form. It is inexpensive to set up and can be used to coat objects of any shape and size. The dip coating process also reduces the amount of coating solution required and the thickness of the coated layer deposited on the sample can be easily manipulated by adjusting the withdrawal speed. However, the main disadvantage of this method is its susceptibility to cross-contamination when a multiple-layer coating process is required. Therefore, care should be taken to minimise contamination when multiple dip coating is implemented.

Two major steps are involved to use this approach to fabricate the sensing element and render it moisture sensitive. In addition to the writing of the FBGs using a UV laser, a polymer layer needs to be deposited onto the surface of the silica optical fibre. This is realised using the aforementioned coating technique which allows optical fibres to be coated with a polymeric layer by using a purpose built set-up in the laboratory.

The diagram shown in figure 4-11 depicts the set-up used to dip coat materials onto the optical fibre. The dip-coating system consists of a pulley mechanism integrated with a stepper motor. The withdrawal speed of the fibre was achieved through a stepper motor controller consisting of a motor driver board and a function generator. The sample (fibre) holder was made of a flat rectangular acrylic block attached to a rigid plastic rod. The vertical movement was achieved by pulling the sampler holder using the stepper motor via a piece of nylon string attached to the rod end of the sample holder and hoisted over the pulley system. The rod movement was stabilised by moving the sample holder through a hollowed out acrylic cylinder with a matching internal diameter. In addition, to prevent the "twisting" parasitic lateral movements occurring while the rod is in vertical motion, a screw was mounted on the cylinder and positioned in contact with the groove milled along the length of the rod.

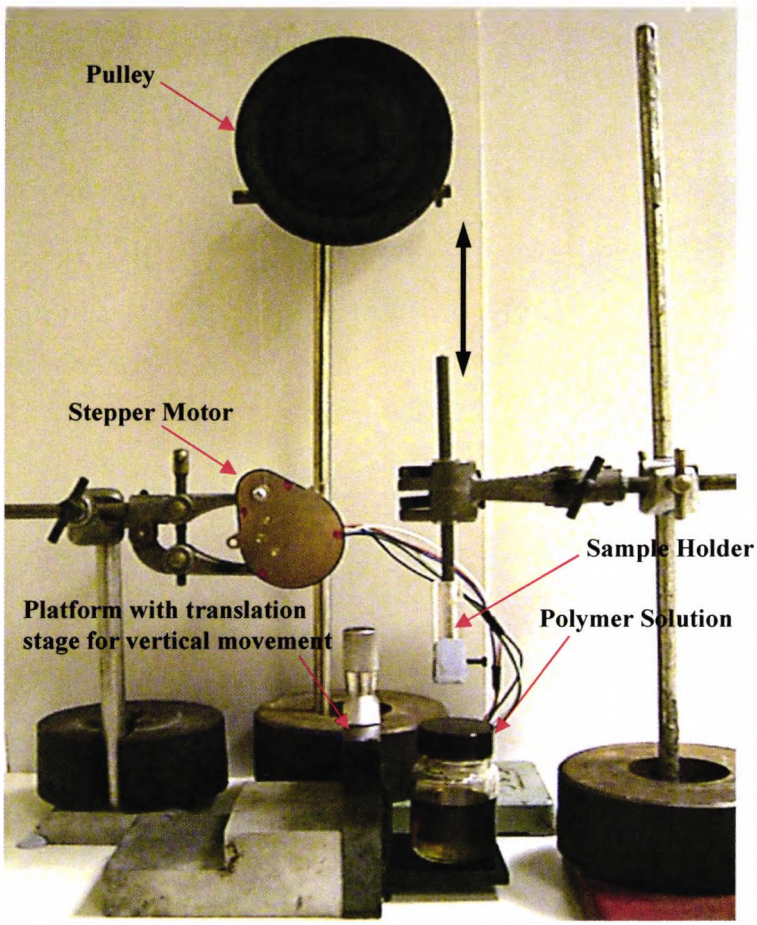

Figure 4-11: Dip coating system set-up.

4.4.2.1. Adhesion at Silica/Polymer Interface

In order to detect the moisture-induced expansion of the coating material, resulting in an imposed strain on the FBG, a strong bond at the silica/polymer interface is required to ensure effective strain transfer. A weak bond or incomplete adhesion between the two materials might result in slippage and erroneous readings which will affect the measurements taken using the FBG sensors.

A preliminary investigation, undertaken prior to the evaluation of FBGs using the selected materials, indicates that the bond formed between the polymer film and silica substrate is weak. This brief investigation was carried out by recreating the polymer/silica interface by coating a PI film on a microscope glass slide. In an attempt to remove any grease or dirt residue on the surface, the glass slide was first cleaned using isopropyl-alcohol. The coated samples were then thermally cured before being subjected to two simple visual assessments to test for adhesion quality.

A "dry" test was performed in an attempt to lift the polymer film off the glass slide by using a pair of tweezers. A considerable force was required to dislodge the polymer film off the glass slide. A "wet" test was carried out by soaking the glass slide in a beaker filled with water for at least 24 hours prior to a similar procedure used in the "dry" test. It was observed visually that the polymer film was lifted off the glass slide easily with a slight push on the film edge using the tweezers. In some cases, the polymer films were simply dislodged from the glass slide after a prolong soak in water.

These visual inspections made from the tests, though not exhaustive and particularly detailed, were sufficient to highlight the possible adhesion issues likely to be encountered during the course of this work. Although an exact cause of this weak bond and/or total bond failure between the coating and the substrate, observed during the tests, is not clear from the preliminary investigations carried out, precautionary measures, like the use of silane coupling agents, are sought to improve the adhesion between the selected polymeric material and the silica optical fibre. A more detailed study of the adhesion mechanisms, whilst interesting, are beyond the scope of this work but would form a useful topic for a wider investigation.

Silane coupling agent can be used to improve the adhesion at the polymer/silica interface as it reacts chemically with the glass substrate and the thin polymer film to form chemical covalent bonds across the interface [30]. It is a multifunctional molecule which reacts with inorganic materials such as glass at one end and organic polymers or resins on the other end. It has a general chemical structure of R-Si-X_3, which R is a non-hydrolysable chemical group that possesses a functionality that allows the coupling agent to bond with other organic resins/polymers and X is a hydrolysable group used to form a silanol group in aqueous solutions which will react with the hydroxyl group on the glass surface.

The reaction mechanism of a silane coupling agent interacting with both organic polymer coating and inorganic silica substrate can be summarised from the following steps [31], as shown schematically in Figure 4-12.

- Hydrolysis of X groups to form the silanol groups
- Bonding of the silanol groups with the hydroxyl groups on the glass surface
- Condensation between the silanol and hydroxyl groups, giving off water as the by product
- Covalent bonding of the silanised glass substrate to the organic polymer as a result of the reaction between the R group and the polymer.

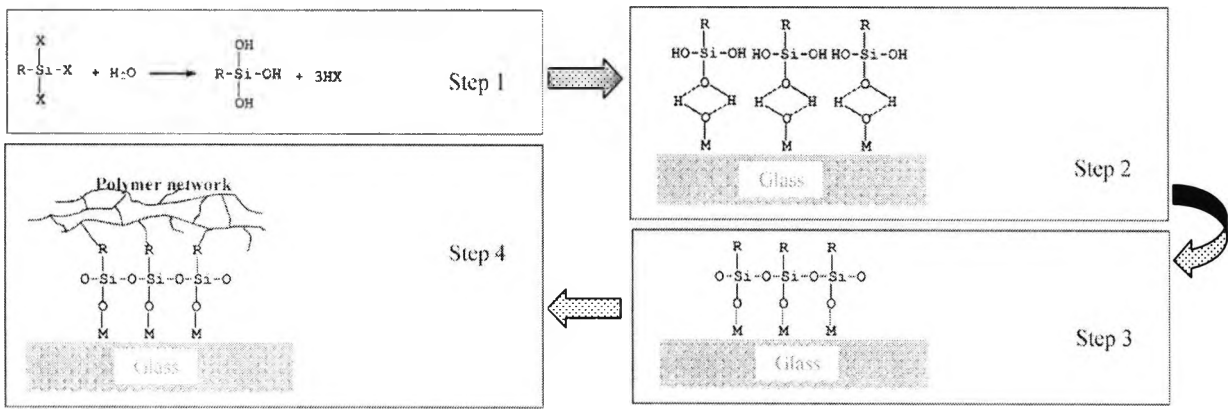

Figure 4-12: The four step process illustrating the reaction mechanism of silane coupling agent. [31]

4.4.2.2. Coating Film Stability

The coating deposition technique that was found most suitable and thus employed in this work involves dipping the optical fibre into a polymeric solution and withdrawing it at a constant speed to leave a thin film on the surface of the substrate. This simple procedure might seem trivial in nature but the process involved in the formation of the fluid film on the fibre is a subject by itself which requires a sound knowledge of fluid mechanics. In-depth discussion on this subject is beyond the scope of this work; however, the aim of this subsection is to highlight the observations and experiments made during the course of this research which can be related to the phenomenon discussed by other researchers [32, 33].

The study of fluid film formation on cylindrical objects such as wires and fibres is important, particularly for practical applications involving textile, fibre or wire related products. This is exemplified by the recent study of spin finish application on fibres carried out by Shim [32] to investigate the film formation phenomenon and various factors that influence the stability of the fluid film formed on synthetic fibres. A detailed discussion with regard to fluid coating on a fibre, through a careful examination of various parameters, defining the thickness of a fluid film entrained by a solid cylindrical substrate, and the general laws of entrainment can be found in the review paper by Quéré [33].

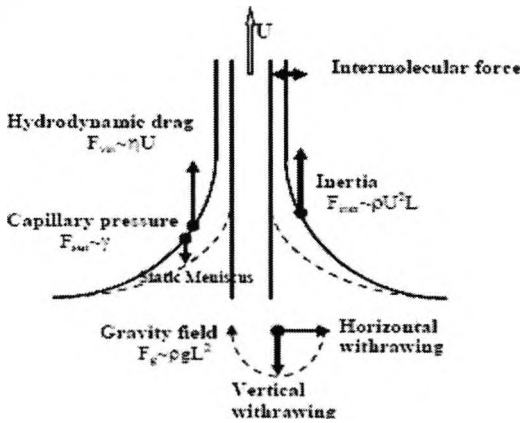

Figure 4-13: Various forces involving the film formation during withdrawal process. [32]

The formation of a fluid film on a fibre is dependent on several factors such as the coating speed, fibre dimension, viscosity and surface tension of the solution [32]. The fluid film entrained on the fibre is the result of the balancing of several forces acting on the dynamic meniscus as the fibre

leaves the solution (see figure 4-13). The forces influencing the film formation become dominant or negligible depending on the various regimes related to the coating speed. Further information on the roles of these forces and the equations governing the film thickness can be found in the literature by Quéré [33].

A uniform fluid coating film on a fibre is generally unstable and it usually collapses into an array of droplets due to the surface tension of the fluid. This is a phenomenon known as the Plateau-Rayleigh instability. The development of instability is independent on various factors including the film thickness, fibre dimension and fluid properties such as surface tension and viscosity. However, these factors can influence the rate at which the instability occurs. Figures 4-14 and 4-15 show some of these pictures excerpt from the thesis by Shim [32] illustrating some of the factors discussed.

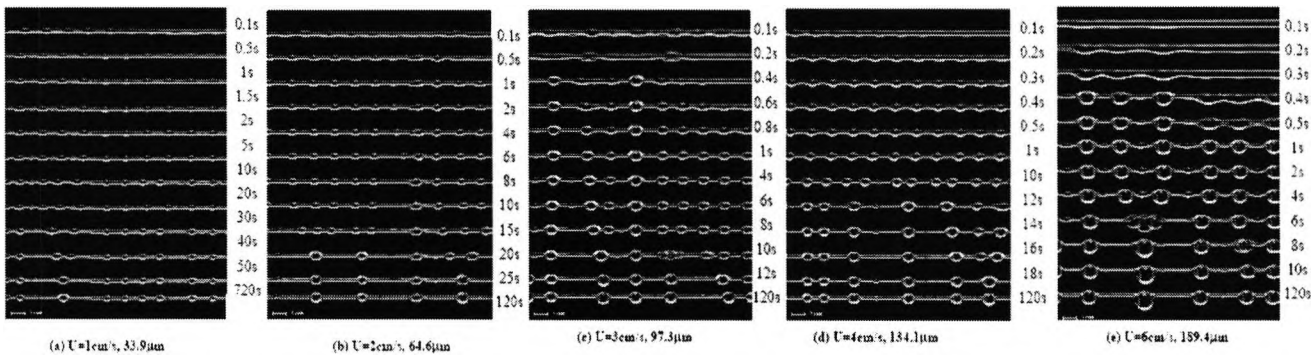

Figure 4-14: Effect of film thickness on the development of instability. Pictures show polypropylene fibres (radius: 100μm) coated with ethylene oxide/propylene oxide fluid. [32]

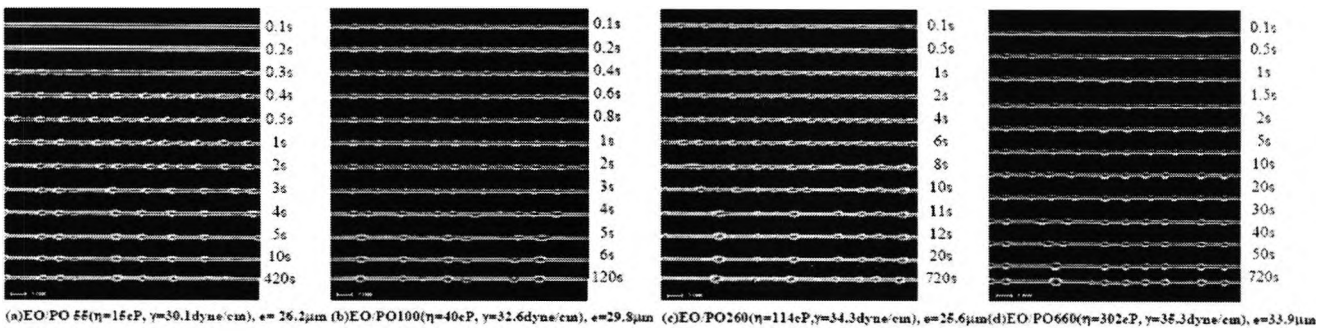

Figure 4-15: The development of instability on polypropylene fibres (radius: 100μm) with a fluid film of various viscosity (η and γ represent the viscosity and surface tension of the fluid and e is the film thickness). With the same film thickness, the rate of instability development was observed to be slower with fluid of higher viscosity. [32]

Similar film instability phenomenon was observed during the fabrication of the coated FBG sensor using highly viscous polymeric solutions. Although it is desirable to achieve a thick coating layer to enhance the sensitivity of the sensor, the fluid nature of the solution in use does not permit a thick polymer film to be deposited onto the FBG through a single dip coating cycle. This can be observed from a brief experiment carried out by coating PI solution onto optical fibres (diameter: 125μm) at different speeds. The problem of instability though cannot be totally eliminated but measures can be taken to minimise this effect.

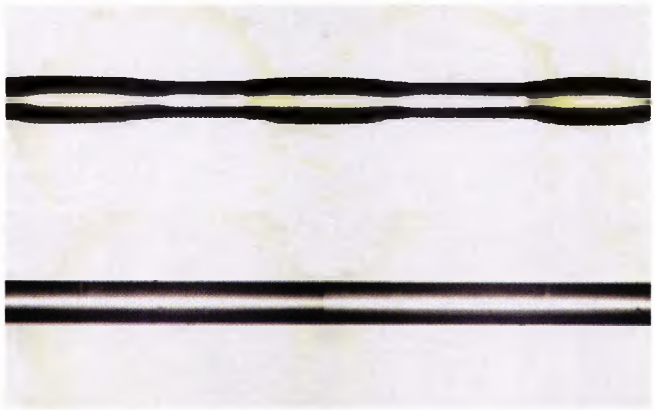

Figure 4-16: Pictures of Corning SMF 28 fibres coated with polyimide solution using different coating speed: (a)48mm/min (Top fibre) and (b)13mm/min (Bottom fibre).

The technique used in this work to minimise the instability problem involves the use of multiple thin layers of polymer film to build up the desired coating thickness. The approach taken to obtain a smooth polymer film is to coat the fibre in PI solution at a very slow speed and then subject it to an immediate short thermal curing process to achieve partial imidisation. This procedure was repeated until the desired thickness was achieved. Although slight ripples can be observed on the polymer film at times, this procedure provides a better controlled solution to the creation of sensors with different coating thicknesses and avoids the possibility of forming random polymer droplets on the FBGs.

4.4.3. Sensor Coating and Assembly

The polyimide used in this work was purchased from HD Microsystems and is sold under the trade name Pyralin® PI 2525. It is primarily produced for the semiconductor microelectronic

industry; however, there are a few variants which were designed specifically for optical fibre and quartz capillary coating [34]. PI 2525 is available as a highly viscous (60 poise) solution with a low curing temperature of 180°C [35]. This is suitable for this work as the normal temperature required for polyimide curing is about 350°C, which may cause the type I FBG written in the B/Ge codoped optical fibre to be erased [23].

The polyvinyl alcohol was obtained from Kuraray Specialities Europe (KSE) and is sold under the trade name Kuraray R-polymer R-3109 (D.H. 98.5%). The R-3109 is a water soluble polymer, supplied in granular form, and is mainly used as a binder for inorganic substance [36]. It also contains silanol groups in the structure which is reactive to inorganic material such as silica or alumina. Therefore, the polymer layer deposited can be bonded chemically to the optical fibre, which eliminates the need for pre-treatment prior to dip coating. PVA solution (15%wt) was produced by dissolving the granular powder in deionised water at 90°C as specified by the manufacturer. The concentration was specifically chosen in order to produce a solution with similar viscosity to the PI solution discussed above. This is to ensure that both solutions are compatible with the procedure using the aforementioned dip coating system.

A general dip coating procedure, as described below, was used in this work to coat the FBGs with the two polymers created above. As there were no specific instructions available from the manufacturers for the purpose of optical fibre dip coating, the procedure was adapted using the information from the technical data sheets provided, with the final process sequence determined after consultations with technical support representatives from HD Microsystems (Mr Michael Knaus) and KSE (Dr Alex Prigrim).

The procedure for the coating developed for and implemented in this work is as follows:

1) Mark and cleave pre-annealed FBG.
2) Soak marked section in isopropyl-alcohol and dry using a lint free tissue.
3) [PI*]Soak marked section into silane solution (0.1% 3APTS in deionised water) for 1 minute.
4) [PI*]Bake optical fibre in oven at 130°C for 15 minutes to activate the coupling agent [37].
5) [PI*]Remove optical fibre from oven and allow it to cool before coating.
6) Dip coat optical fibre with polymer solution. (Withdrawal speed: 13mm/min (PI), 30mm/min (PVA))

7) Bake coated fibre for 5 minutes to partially cure the polymer layer prior to next dip coat. (PI- 150°C, PVA- 80°)
8) Repeat steps 6 and 7 until desired coating thickness is achieved.
9) Bake optical fibre in oven for 60 minutes for final curing. (PI- 180°C, PVA- 80°)

The withdrawal speed used for each solutions were optimised to achieve a thin smooth coating layer. For PI solution, additional surface treatment steps (marked with superscript PI*) were used in order to obtain a pre-silanised optical fibre before coating. This was achieved by using diluted stock solution made from a concentrated 3-Aminopropyltriethoxysilane (3-APTS) silane solution (Pryalin VM651, HD Microsystem) and deionised water. The treated optical fibre was subjected to additional heat treatment as recommended by the manufacturer to activate the silane coupling agent coated onto the surface of the silica substrate.

After the dip coating process, the sensing element, as shown in Figure 4-17, was spliced to a section of standard communication grade fibre (Corning, SMF 28) terminated with a FC/PC connector. The optical fibre sensor was then protected using a perforated stainless steel tube which was fixed to a probe housing using epoxy adhesive.

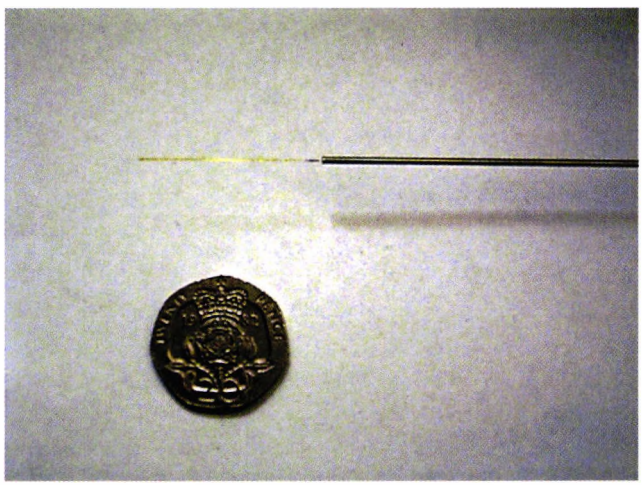

Figure 4-17: Picture of a polyimide-coated FBG.

4.5. Sensor Characterisation

4.5.1. Preliminary Moisture Test

A preliminary investigation to determine the moisture sensitivity of the polymer-coated FBGs was carried out using a PI-coated sensor. The aim was to investigate the swelling phenomenon of the coating layer deposited onto the optical fibre and its influence on the spectral characteristics of the FBG. The test involved subjecting the sensor first to room temperature and humidity conditions, in which the experiment was carried out as before, placing the sensor into a container filled with water. The optical spectrum of the sensor was recorded using an OSA before and after soaking the sensor in the water for 24hrs.

Prior to the coating process, the Bragg wavelength value of the pre-annealed FBGs was also recorded at room condition so as to monitor the influence of the coating process on the sensor. The same measurement process was repeated after the application of the coating so that a comparison can be made between a coated and an uncoated sample. The difference between the two measurements indicates a blue shift in Bragg wavelength of approximately 0.31nm.

The presence of any temperature effect was ruled out first as the likely cause of this discrepancy as the magnitude of the wavelength shift is equivalent to a drop of approximately 30°C in room temperature (approximated based on the temperature sensitivity of the B/Ge FBG). This observation is likely to be attributed by the compressive strain induced on the optical fibre due to the thermal shrinkage experienced by the polymer layer coated onto the fibre.

To verify the above hypothesis, the PI coating on the optical fibre sensor was stripped off by dipping the coated FBG into a hot sulphuric acid bath heated to 150°C. This process was repeated until the coating on the optical fibre was completely removed before rinsing with deionised water to remove any remaining residue and chemicals.

With its coating removed, the FBG sensor was again subjected to the wet condition to test for its moisture sensitivity. The response taken in the form of reflection spectrum using the OSA was plotted together with the measurements taken earlier and are shown in figure 4-18.

The results in figure 4-18 show two key facts developed through the observation of the film:

1) the polymer layer coated onto the FBG sensor is responsive to moisture and is indicated by the red shift in the Bragg wavelength caused by the swelling of the polymer through moisture absorption.

2) the shift in Bragg wavelength is due to the release of the initial compressive strain induced on the FBG as a result of thermal shrinkage experienced during the coating process. Therefore, this implies that the operation of a polymer-coated FBG humidity sensor is based on the release of the compression force induced on the optical fibre as a result of material expansion through moisture absorption.

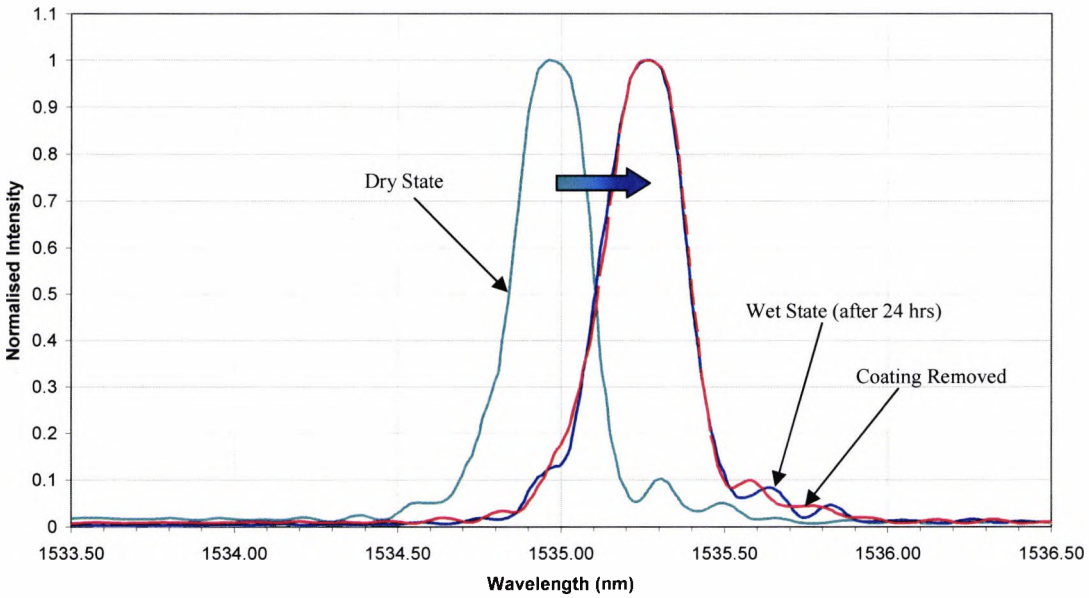

Figure 4-18: Reflection spectra of PI-coated FBG sensor taken at dry and wet state and with coating removed.

4.5.2. Comparison of Polymeric Materials

In order to compare the performance of different types of polymers for sensor applications, FBG sensors coated with PI and PVA were created and tested to investigate the influence of each polymer type on the sensor response to moisture. To perform this investigation, two sensors of

each polymer type with similar coating thickness were fabricated using the procedure discussed in section 4.4.3. The multiple dip coating process yielded an average coating thickness of ~35μm and ~33μm for PVA and PI sensors respectively. This thickness was approximated using a microscope with a 40x objective and a 10x eyepiece. The measuring equipment was calibrated against a standard communication optical fibre (corning, SMF 28) with an outer diameter of 125μm and has a resultant measurement uncertainty of ±3μm.

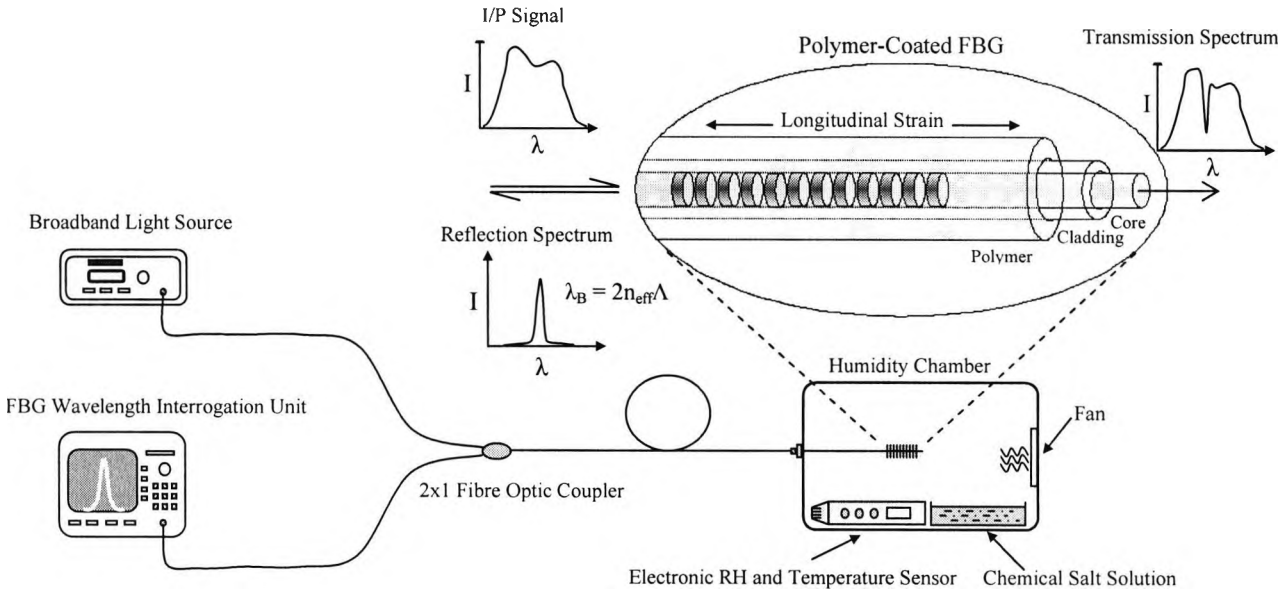

Figure 4-19: Experimental set-up for measuring the moisture response of the FBG sensor.

To conduct the evaluation of the sensors, a purpose-built humidity chamber, as shown in figure 4-19, was used. The humidity chamber consists of an airtight plastic enclosure and a glass Petri dish containing a saturated chemical salt solution [38, 39] used to generate a range of different humidity conditions. A commercial hygrometer with an integrated temperature sensor (accuracy: ±5%RH (40%≤RH≤80%), ±7%RH (RH ≤40% & ≥80%), ±1°C) was used in the chamber to provide a reference RH and temperature readings throughout the duration of the experiment. The time to obtain RH equilibrium in the test chamber was improved by optimizing the solution

surface area to chamber volume and also by installing a fan to generate airflow. The main limitation of using a saturated chemical salt solution for humidity generation is the lack of humidity control during the experiments and it only allows static measurements to be taken: nevertheless, this method is adequate for the purposes of this investigation.

To record the Bragg wavelength shift with respect to humidity, a broadband light source (Opto-Link Cooperation Limited, OLS15 CSF) was connected to the sensor using a 2x1 single mode coupler (Optowaves, SMC-12-155-P-09-1-FC/UPC-50/50) and the reflected signal was monitored using an OSA with a resolution bandwidth of 0.1nm with a measurement uncertainty of ±0.01nm. All experiments performed were carried out at room temperature with fluctuations of no more than ±2°C.

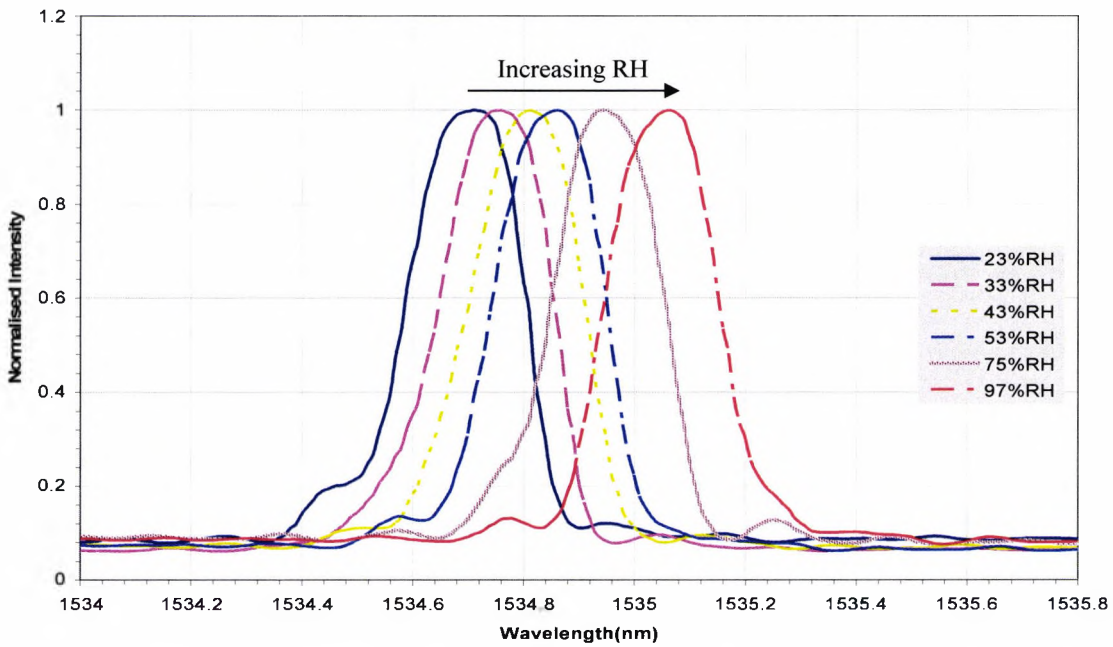

Figure 4-20: Reflection spectra of PI coated FBG sensor at different humidity levels.

The chart in figure 4-20 shows a typical response of the humidity sensor presented in the form of reflection spectrum at various humidity levels. At each humidity level, sufficient time was given to allow the sensors to equilibrate before static measurements were taken. A time period of ~2 hours was found, by experiment, to be generally sufficient for each static measurement; however, it was observed that the PVA-coated sensor reacted very slowly to the test environment (~24hrs). Hence, a longer settling period was used when evaluating the PVA sensor in order to stabilize the

readings. Similar observation on the long equilibrium time required by PVA film was discussed by Penza and Anisimkin [8]. It was reported that with a 1μm PVA film coated on a SAW RH sensor, a time period of more than two hours was required to allow the sensor to reach equilibrium. Therefore, this result validates the use of a long equilibrium period when evaluating the FBG sensor with a 35μm PVA film.

The humidity characteristics of the two sensor types as shown in figure 4-21 were plotted in terms of relative Bragg wavelength shift with respect to humidity change. The solid curves, each containing 6 data points, represent the average response of 2 sensors with the same polymer type and similar coating thickness. The evaluation of each sensor was carried out three times to ensure repeatability of the data and reproducibility of the response trend.

The results in figure 4-21 showed two contrasting response curves obtained using the two sensor types. Examining them closely reveals that the PI sensor exhibits a linear response to humidity change, whereas PVA sensor is non-linear. Both sensors give a similar magnitude in terms of Bragg wavelength shift of ~0.35nm for a humidity change from 23%RH-97%RH and displayed good repeatability and reversibility which indicates that the polymeric materials are not only water sensitive but also water resistive. In comparison to the PI sensor, the response curve of the PVA sensor exhibited a fairly linear response between 23%RH-53%RH and was extended asymptotically as more moisture was introduced to the test environment.

Between values of 23%RH-53%RH, the PVA sensor showed a higher sensitivity than the PI sensor. However, this value decreases with a further increase in humidity level. This suggests that the PVA sensor has an effective sensing range of no more than 60%RH and the strain mechanism becomes ineffective as the polymer coating absorbs more moisture and swells in volume. Though the moisture absorption properties of the two materials are different, with PVA being the more absorbent material, the PI sensor displayed a similar magnitude in Bragg wavelength shift and has a fairly linear response throughout the entire test range. This difference in responses could be due to the interaction between the water molecules and the absorption sites in the polymer coating which changes the film properties. A more detailed investigation of the moisture absorption kinetics and any influence on the material properties is beyond the scope of this work; hence the subject is not developed further in this thesis.

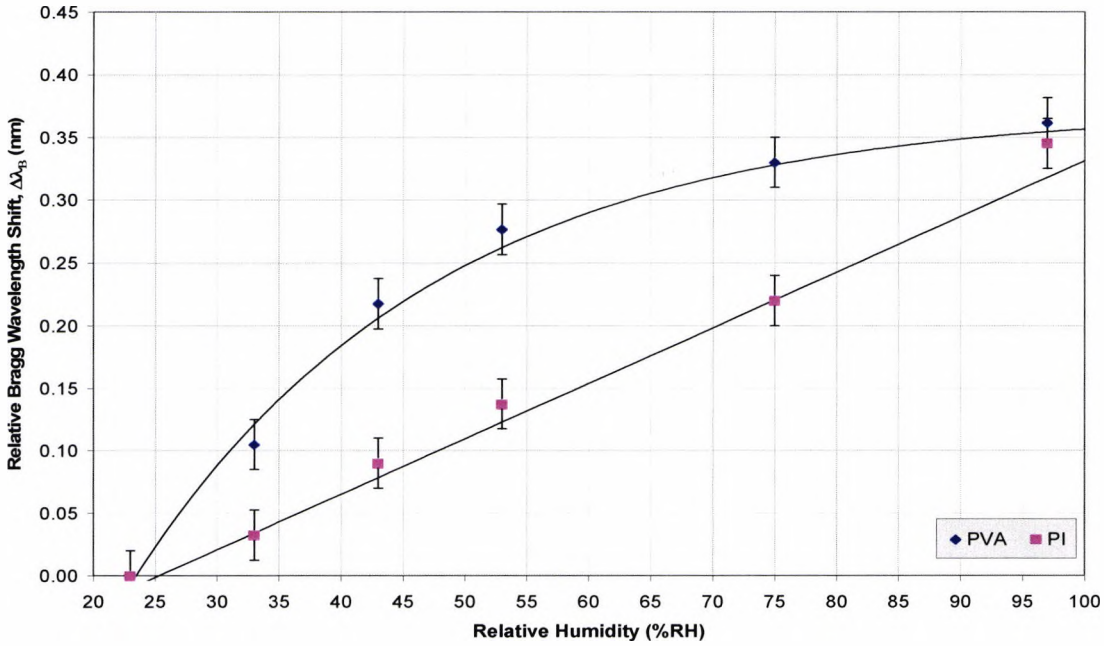

Figure 4-21: Moisture sensing responses of PVA and PI coated FBG sensors.

From this evaluation, carried out to investigate the two selected polymeric materials for FBG-based humidity sensing, it can be concluded that both materials reacted well to humidity changes and showed good repeatability and reversibility. It was anticipated that the sensor being coated with a more absorbent material, PVA, would outperform that with PI in terms of Bragg wavelength change for a given humidity range. However, the observation made during the evaluation proved to be otherwise. It was noted that the strain mechanism employed by the FBG-based sensor does not solely depend on the moisture absorption properties of the material as in the case for other sensing techniques discussed earlier, but also the ability to stretch the FBG as it hydrates. The magnitude of the wavelength shift recorded is similar in both sensors although the PVA sensors had a slightly thicker coating layer. In additional to that, the sensor reaction time is very slow and the nonlinear response curve suggested a lower RH operating range, as compared to that of the PI sensors.

Despite its better moisture absorption properties, the use of PVA as a sensing material in FBG-based sensor does not give any significant advantages over the PI coated sensor. Hence, keeping

the prime objectives of this work (to develop an operational sensor scheme for use in structural monitoring) in mind, it was decided that further characterisation of the sensor, which will subsequently be tested in concrete environment as a moisture ingress sensor, would be focused only on the PI coated sensors.

4.5.3. Effect of Coating Thickness

Equations 4-2a and 4-10, presented in Section 4.2.1, show the dependency of the sensitivity of a polymer-coated FBG on the thickness of the coating layer. The sensitivity of the device can be tuned by varying the coating thickness of the sensing polymer which, has a direct influence on the time response of the sensor and will be discussed later in this chapter. This section examines the effect of coating thickness on both the humidity and temperature response of the FBG sensors. The results obtained through a series of investigations are presented and discussed.

4.5.3.1. Humidity Characteristics

To characterise the effect of coating thickness on the humidity sensing response, a range of sensors with 6 different coating thicknesses were fabricated. The coating thicknesses are 10μm, 17μm, 24μm, 33μm, 37μm and 42μm respectively. In a similar way to the investigation discussed in the section 4.5.2, two sensors were fabricated for each coating thickness hence a total of 12 sensors were used in this evaluation. A set-up, identical to that shown in figure 4-19, was used to subject the sensors to different humidity conditions.

The results obtained were plotted in figure 4-22, showing the Bragg wavelength shift of the PI coated sensors with different coating thickness used. The humidity responses of all the sensors evaluated were found to be linear with increasing RH over the range from 23%RH to 97%RH. The change in the Bragg wavelength observed under a fixed temperature condition indicates the elongation experienced by the grating structure, which causes the Bragg wavelength to shift in response to the changes in the grating period and the effective refractive index value of the FBG due to the photoelastic effect. The linearity of the sensor response is shown by the trend lines that were fitted to all data sets in the plots.

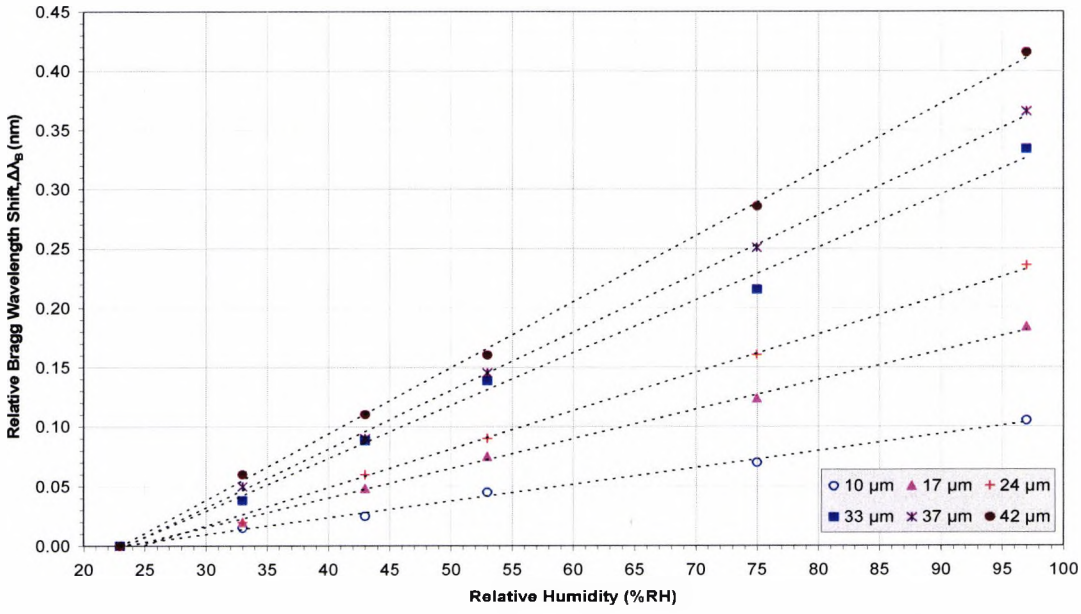

Figure 4-22: Moisture response of the sensors with different coating thicknesses and humidity level (from 23%RH to 97%RH) at constant room temperature.

From the results obtained, it was noted that the magnitude of the strain induced on the FBG due to a change in humidity level is dependent on the coating thickness of the polymer and is in accordance with the expressions discussed in equations 4-2a and 4-10. The slopes of the plots, which represent the sensitivities of the devices, indicate a maximum sensitivity of ~5.6pm/%RH and a minimum of ~1.4pm/%RH were achieved for sensors with PI coating of 42 µm and 10µm respectively.

The sensitivity values of the devices with different coating thickness obtained experimentally were compared with the theoretical values calculated using equation 4-2a. Since the experiments were conducted at a fixed temperature, the temperature related terms in equation 4-2a were omitted and the coefficient of moisture expansion (CME) of the silica optical fibre in equation (4-10) was assumed to be negligible. In order to obtain the theoretical values at different coating thickness, the CME of the polyimide is required. An approximation of the CME of PI (α_{pRH}) cured at 180°C was attempted by back-calculating the value based on the experimental data obtained, together with other known parameters such as the Young's modulus of the materials and the coating thickness of the sensors. However this value does not truly reflect the CME of PI

as the inaccuracy of the value was accumulated during the experiments which encompass instrument and human errors, as well as errors arising from data processing. Nevertheless, the CME obtained allows a simple comparison of the sensor performance to be made theoretically and experimentally.

Comparative data from the literature are difficult to obtain (due to the different experimental situations) but the closest comparison can be drawn from the results published by Sager *et al.* [16]. The value of the moisture expansion coefficient, which represents only the lateral component of the volume expansion, was obtained by using a commercial grade polyimide. The value was found to be in the range between 60-80ppm/%RH and was dependent on the curing temperature. For the same material, the moisture expansion coefficient of the polyimide obtained at a curing temperature of 180°C and a curing time of 30 minutes was reported to be approximately 63ppm/%RH. This value is about two thirds of that obtained in this work herein with a curing temperature at 180°C and curing time of 60 minutes. Given the differing preparation conditions, the complexity of the swelling characteristic of the polyimide and the dependency on material type and the process conditions, the agreement between the two values is satisfactory.

The values of CME calculated using the experimental data obtained from sensors with different coating thickness were found to range from 104ppm/%RH to 82ppm/%RH (see insert diagram in figure 4-23). Although it may be expected that all the sensors would yield a similar value, the variation in the CME, as mentioned earlier, is likely to be caused by cumulative error from the experiments and data fitting.

To calculate the theoretical RH sensitivities, the average value of CME (92ppm/%RH±9ppm/%RH) was used. These values were then plotted together with the experimental values as shown in figure 4-23. It can be observed that both the theoretical and experimental data exhibit the same linear trend in terms of the change in RH sensitivities with coating thickness. The experimental sensitivity values of the sensors with thicker coating layers were found to deviate from the theoretical plot and this may be the result of an ineffective strain

transfer to the FBG as the coating gets thicker, thus placing an upper limit on the coating thickness for effective moisture sensing.

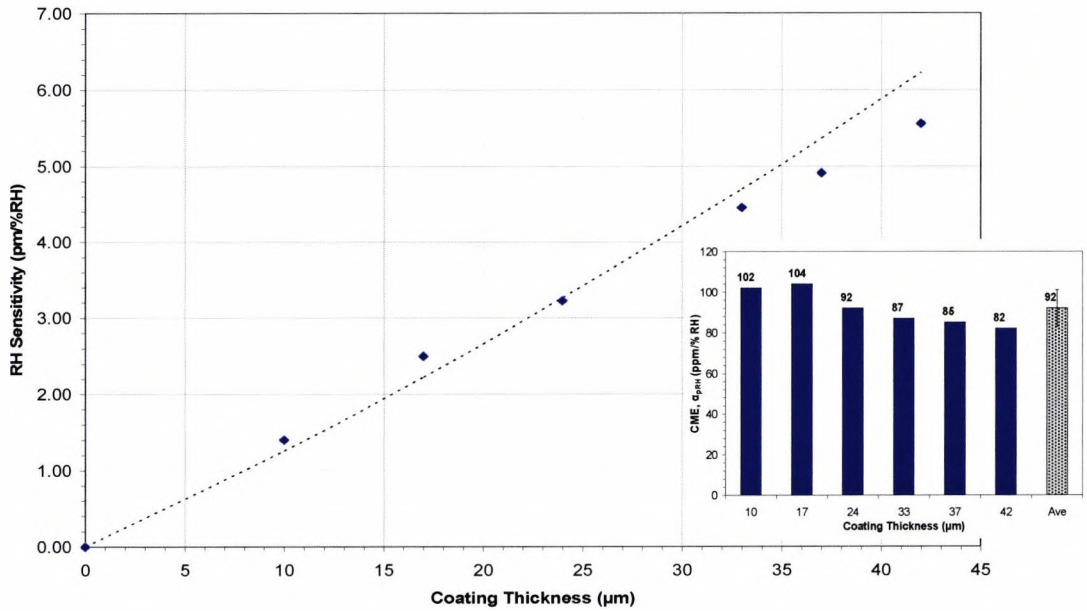

Figure 4-23: Cross comparison of experimental and theoretical values of the moisture sensitivity of FBG sensors with different coating thickness. Inset figure shows the CME of PI cured at 180°C, calculated using experimental data from the sensor calibration.

4.5.3.2. Temperature Characteristics

This section discusses the studies carried out to characterise the temperature response of the PI coated sensors and the effect of coating thickness on the temperature sensitivity. For an uncoated FBG, the thermally-produced Bragg wavelength shift is related to the change in the grating period due to material expansion and thermooptic effect. Referring to equation (4-1), the thermal response of a bare FBG is dominated by the thermooptic effect and has a coefficient value around 15 times higher than the CTE of a silica optical fibre. Hence, the thermally induced strain contribution to the thermal response is negligible. This condition however, is changed when a material with a different value of CTE is coated on the optical fibre. For the case of polyimide which has a CTE value of 40×10^{-6}/°C [35], the thermal response is thus dependent on both the refractive index change and the resultant thermal strain which is scaled according to the coating thickness of the polymer layer as discussed in Section 4.2.1.

To characterise the temperature responses of the PI sensors, a total of 6 sensors with different coating thicknesses, as described in the previous section were used. For the purpose of this investigation, the humidity chamber used in the previous investigation was replaced by a climatic chamber[2] consisting of an oven (Thermotron Industries, Model No.: S-1.2, temperature range: -55°C to 155°C, ±0.1°C) integrated into a humidity generator. As shown in Figure 4-24, the inlet of the oven was attached to a purpose-built gas mixing system formed by a series of liquid and mass flow controllers to generate constant air supply with different moisture content, hence regulating the humidity condition. To monitor the Bragg wavelength of the sensors under test, a detection system consisting of a swept-laser FBG interrogation unit (si-720, loan unit from Micron Optics Inc) interfaced with a PC through a purpose-designed LabVIEW program was used. The system was integrated with a purpose-built sensor probe unit to provide reference humidity and temperature readings.

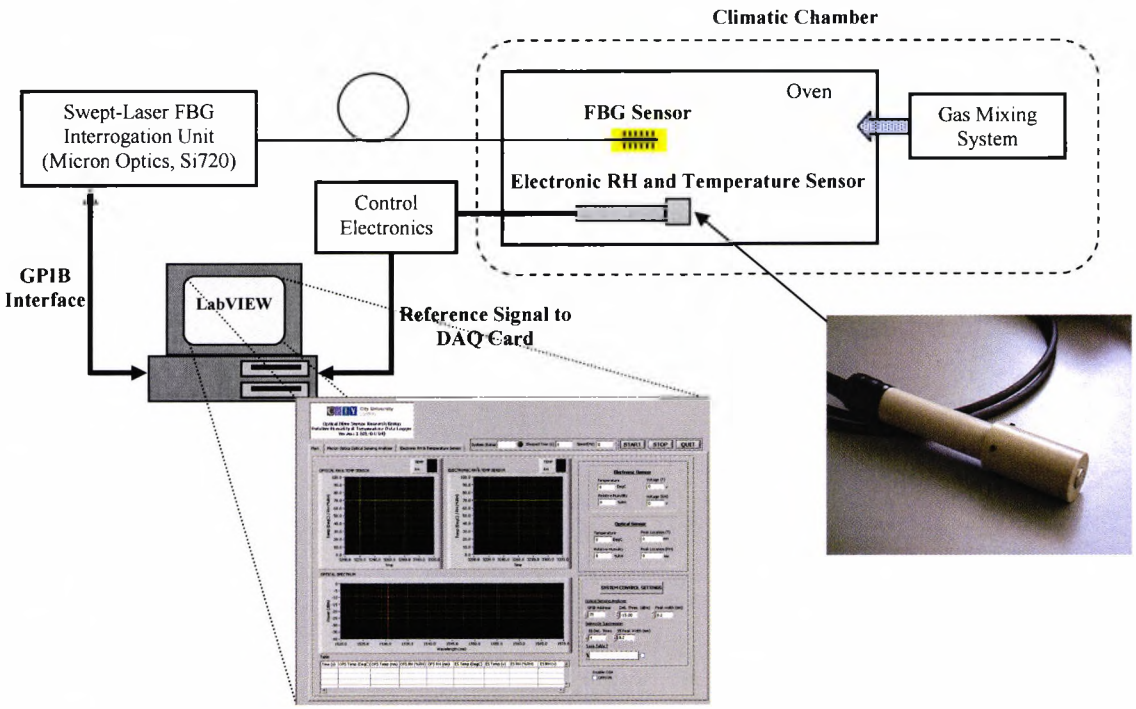

Figure 4-24: Experimental set-up used for temperature characterisation. Inset pictures show screenshot of the LabVIEW interfacing program and photo of purpose-built electronic sensor.

For the investigation of the temperature sensitivity of the devices, the temperature of the climate chamber was varied from 25°C to 65°C. In order to ensure that the readings from the FBG

[2] The climatic chamber was part of the research facilities made available at the premises of the R&D department of Kidde Plc, Colnbrook, UK.

sensors were due to temperature rather than humidity changes, the chamber was purged with dry air (no more than 3%RH) with fixed moisture content throughout the entire experiment duration.

With a constant humidity condition and the temperature in the test chamber varying between 25°C and 65°C, the Bragg wavelength readings of sensors with different coating thickness were obtained and are plotted in figure 4-25. The plots exhibit a similar response trend to that of the RH response, with the same observed effect of coating thickness on the temperature sensitivity. The maximum and minimum temperature sensitivities obtained from the slope of $\Delta\lambda_B$ for 42μm and 10μm were 12.9pm/°C and 9.5pm/°C respectively.

The temperature characteristics of FBGs written in different types of photosensitive optical fibres have been recently discussed by Pal *et al.* [40]. The discussions include the analysis of type I FBGs written into B/Ge photosensitive fibres, which are similar to the fibres used in this work. Thus, the temperature response data extracted from the literature were plotted together with the rest of the results to indicate the base temperature sensitivity of the sensors. The temperature response of the bare FBG was found to be very similar to that of a sensor with a 10μm coating layer. The calculated sensitivity from the data fitting is approximately 9.3pm/°C (For a bare type I B/Ge FBG) and 9.5pm/°C (FBG with 10μm coating).

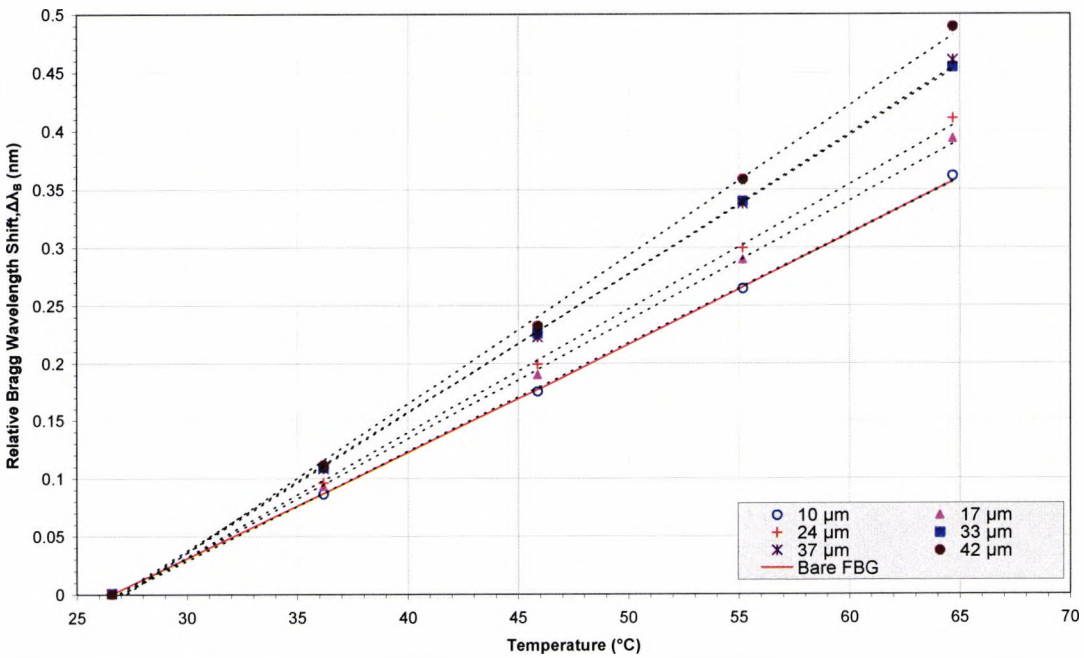

Figure 4-25: Temperature characteristics of the polyimide-coated FBGs with different coating thickness.

The experimental and theoretical temperature sensitivities of the PI sensors were plotted in figure 4-26 to enable a comparison readily to be made. Based on the same approach as discussed in the previous section, the theoretical temperature sensitivities were obtained using an average CTE value of ~59ppm/°C±5ppm/°C. From the chart, it can be observed that the experimental data points clustered around the theoretical plot, showing good agreement between the two sets of data.

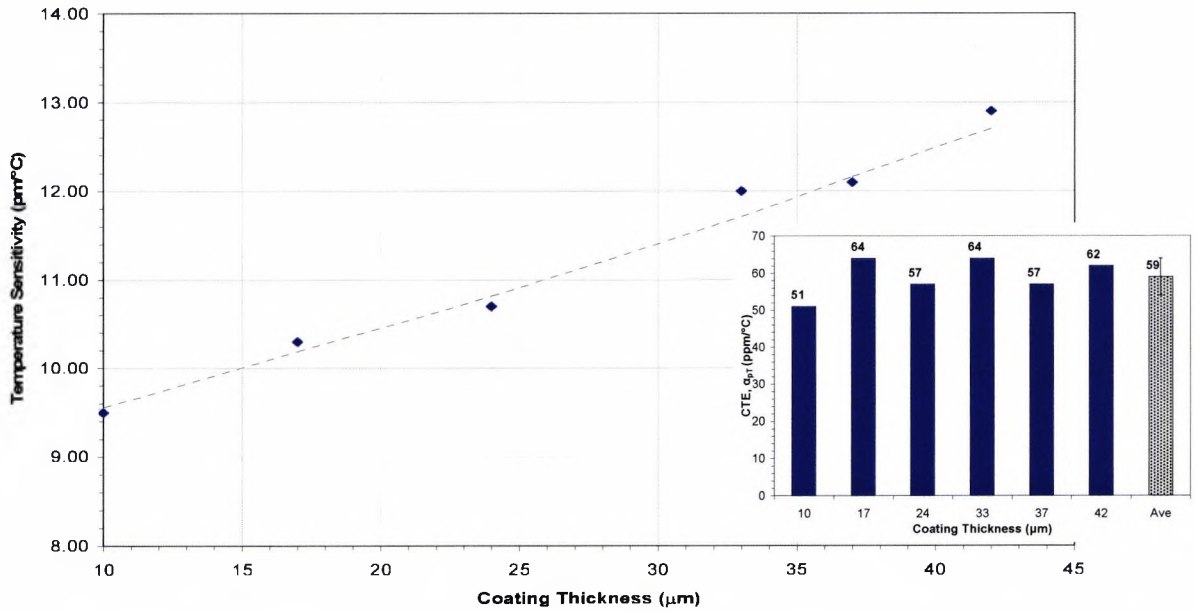

Figure 4-26: Experimental and theoretical values of the temperature sensitivity of FBG sensors with different coating thickness. Inset figure shows the CTE of PI cured at 180°C, calculated using experimental data from sensor calibration.

4.5.4. Time Response and Hysteresis Effect

This section examines the time responses as well as the effect of hysteresis experienced by the PI sensors. The time response is dependent on a number of factors, including the diffusion rate of the water molecules in the polymer, the rate of swelling and the thickness of the sensing material.

To determine the time response, the sensors were subjected to a step humidity change of 42%RH at a constant room temperature of 23°C. This was achieved by using two airtight enclosures of a similar capacity pre-saturated at 33%RH and 75%RH using different chemical salt solutions. The sensors were first allowed to equilibrate at 33%RH in an enclosure containing $MgCl_2$ solution before transferring it to the other pre-saturated enclosure containing NaCl solution. The same

procedure was repeated in the reverse order to investigate the recovery time of the sensors. All time response measurements were recorded using the detection system as discussed in the previous section. The data acquisition speed of the FBG interrogation unit was set to 1 Hz and all data were logged into a PC through a LabVIEW interface program.

In this work, the response time (t_{90}) and recovery time (t_{10}) are defined as the time taken for the sensors to reach 90% and 10% of its final equilibrium value respectively and were determined from the response data curves as shown in figures 4-27 and 4-28. A response time of approximately 45 mins and 18 mins was observed for the sensors with the thickest and the thinnest coating. Reversing the step humidity change yields a recovery time of approximately 28 mins and 4 mins, respectively.

In figure 4-28, it was observed that the recovery time of the sensors is not in the same order as thickness trend - the time required for a sensor with a 33μm coating is longer than that for a sensor with a 42μm coating. As shown in both figures, the clustering of the time response curves of several sensors was also observed. Although the reason for this observation is unclear, a possible explanation could be due to the diffusion kinetics of the water molecules in and out of the polymeric material that resulted in a non-linear dependence of the coating thickness on the time response of the sensors.

The desorption curve of the sensor with a 10μm PI layer was found to be slightly different from that for the rest of the data curves. In that particular response, the Bragg wavelength value was found to increase slightly after reaching the lowest point. The temperature variation throughout the duration of the experiment could be a possible cause for this discrepancy but it was later ruled out after a similar trend was observed when the same experiment was repeated. This observation could be due to the rapid desorption rate of the sensor, which is a few orders of magnitude higher than the absorption rate, causing the water molecules from the material to be released faster than they can be reabsorbed to equilibrate at the stable environment.

The hysteresis curves of the sensors with PI coating thicknesses of 10μm, 17μm and 33μm are shown in figure 4-29. All the sensors were placed in a test chamber of a stable temperature environment, with a continuous supply of moist air from the gas mixing system. To investigate

the hysteresis effect, the humidity level was varied from 30%RH to 60%RH in steps of 10%RH in both ascending and descending order. Sufficient time (~45mins) was given at each RH level before the stabilised readings were recorded. For all the sensors tested in this work, a small but acceptable degree of hysteresis(<5%RH) was observed.

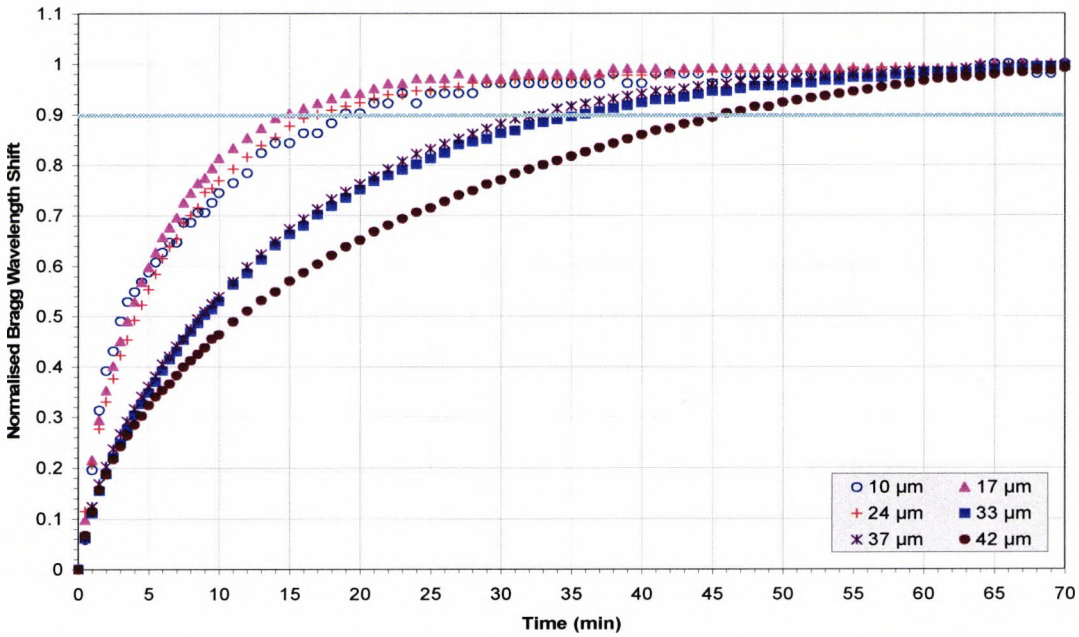

Figure 4-27: Reaction time of the sensors when exposed to an abrupt step change in humidity level from 33%RH to 75%RH.

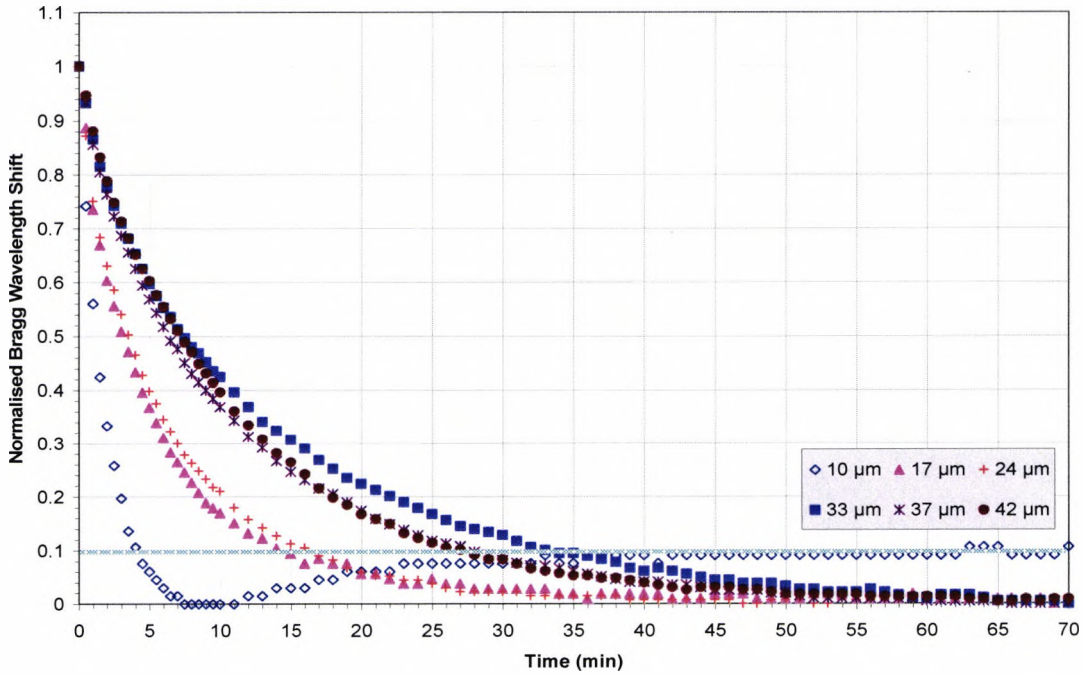

Figure 4-28: Recovery time of the sensors when exposed to an abrupt step change in humidity level from 75%RH to 33%RH.

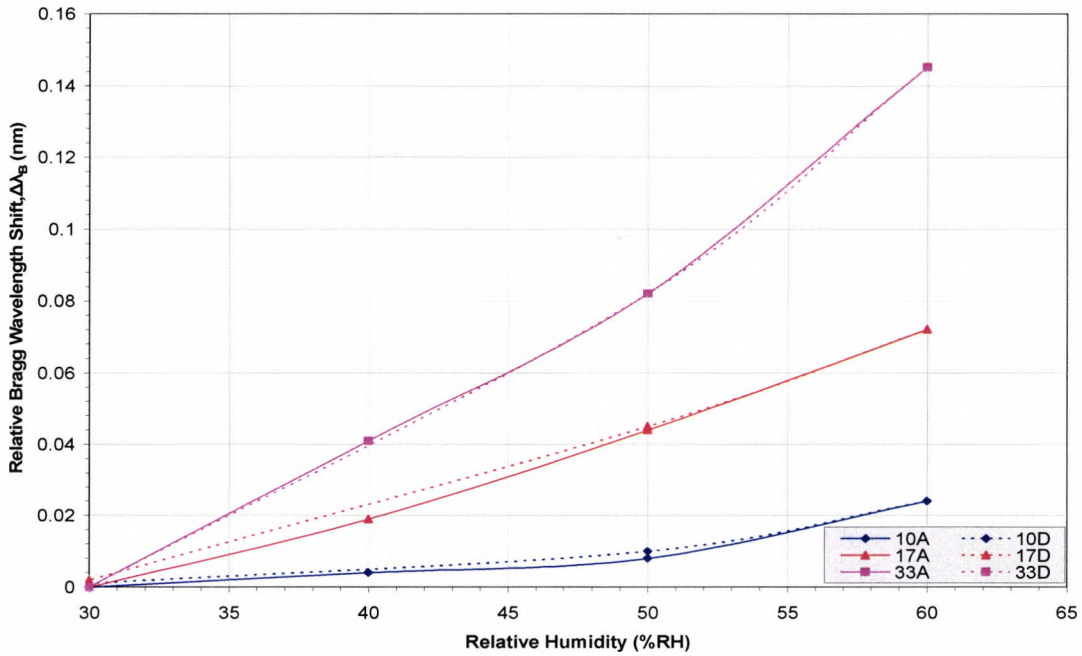

Figure 4-29: Hysteresis characteristics of the PI sensors (A: ascending; D: descending)

4.5.5. Further Investigation on the Influence of Test Environment on the Temperature Response

A common procedure to determine the temperature sensitivity of a humidity sensor is to subject the sensor to a range of temperature levels at a fixed RH level. However, by changing the test temperature, for example increasing the temperature level, the saturated water vapour pressure in the test environment increases and this consequently reduces the RH level. In order to maintain the same RH values at a higher temperature, higher moisture content is required. This will result in the sensor under test being subjected to a test environment with two varying parameters instead of one. For the case of FBG-based sensor, it was anticipated that the Bragg wavelength shift induced at elevated temperatures will be higher than expected due to the moisture induced effect. This investigation therefore examines the influence of different (absolute/relative humidity) test environments on the temperature calibration process.

To carry out this investigation, the same set of sensors was subjected to a similar temperature calibration procedure but with the relative humidity environment set to 50%RH at various

temperature levels. This was achieved by adjusting the mixing ratio of the gas mixing system to maintain the same RH level. In figure 4-30, the calibration data were plotted together with those obtained using a dry environment to illustrate the influence of the test environment. It can be observed that in all the sensors tested, the temperature trend remains fairly linear despite the increase in moisture content at higher temperature. However, there is an offset between the two data sets and has a magnitude which is dependent on the coating thickness of the sensors.

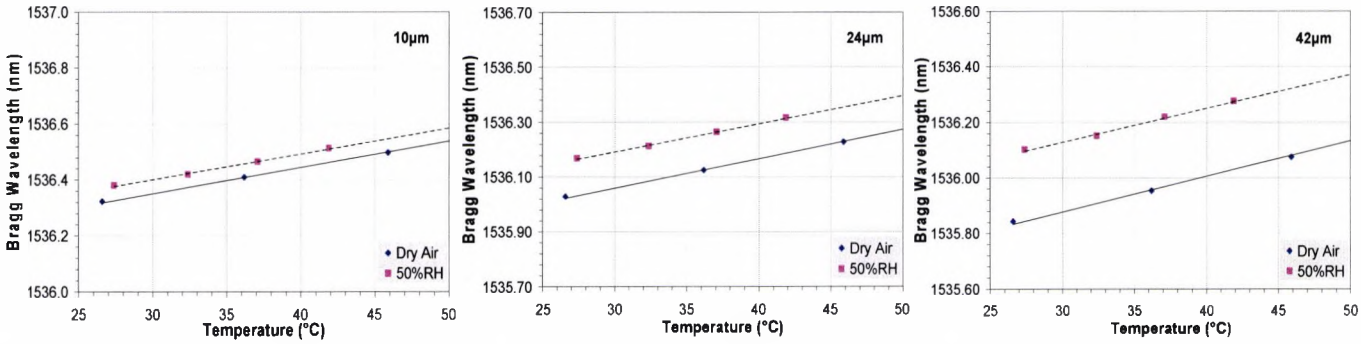

Figure 4-30: Comparison of temperature characteristics obtained in absolute and relative humidity environment.

The observation made in this investigation suggests that the increase in moisture content in the environment to maintain the test condition at 50%RH does, indeed, have an influence on the sensors response, even though the shift in Bragg wavelength did not increase significantly as a result of moisture induced strain at higher temperature. The reason for this observation is not clear but it could be speculated that the mechanical properties of polymer layer could be influenced, which negates the effect of additional moisture absorbed at higher temperature - the change in Young's modulus of the material as a function of temperature and humidity. The swelling behaviour of the polymer film could also be impeded at increasing temperature, a similar effect which was observed in hydrogel films discussed by several authors [41, 42].

The wavelength offset and the difference in RH level between the two sets of data obtained in this investigation allows the humidity sensitivity of the sensors under test to be determined. In figure 4-31, the values obtained were plotted with respect to the coating thickness. The sensitivity values and the trend were found to be very similar to the set of humidity sensitivity values obtained earlier.

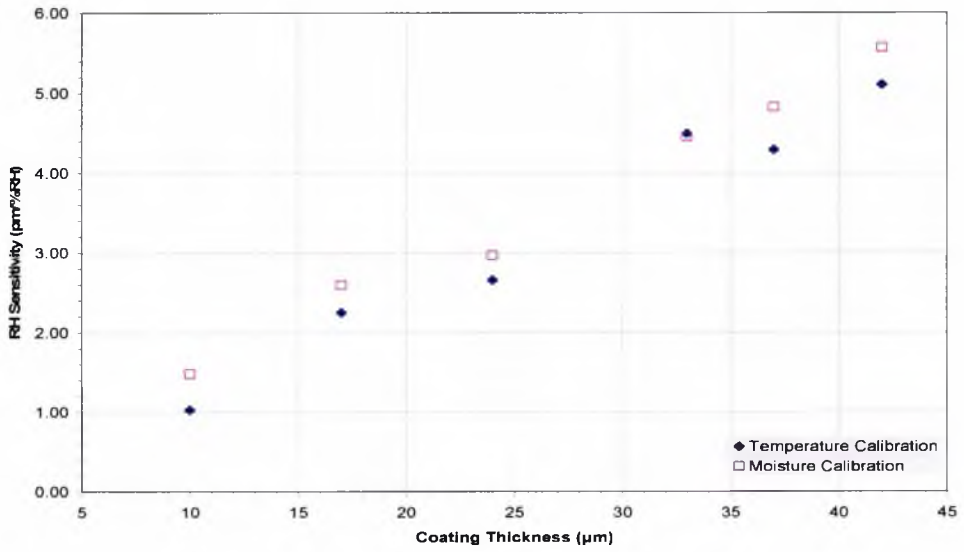

Figure 4-31: Comparison of experimental moisture sensitivities obtained using different calibration environment.

4.6. Summary

This chapter has presented a detailed investigation into the basic operating principles and response details of the FBG-based sensing scheme developed and adopted for humidity detection, as well as the development and characterisation of the sensors developed. Different polymer types, Polyimide (PI) and Polyvinyl Alcohol (PVA), were selected for evaluation as moisture sensitive coating materials. Both materials were found to perform well during the preliminary moisture tests. However, due to its limited operating range, non-linear moisture response and most importantly, the long reaction time observed, PVA was demonstrated to be much less suitable for use in this particular sensing scheme, even though it possess excellent moisture absorption properties as compared to PI.

Detailed sensor characterisation was carried out using the PI-coated sensors, focusing on several key parameters which include the humidity and temperature sensitivity, effects of coating thickness, time responses and hysteresis.

The series of investigations performed showed that the PI-coated sensors exhibit a linear response when tested over a humidity range from 23%RH - 97%RH. The sensitivity of the sensors was

found to increase with the coating thickness of the PI film deposited on the FBG. The experimental data compiled and processed were cross-compared with the theoretical data generated and the results found to be in good agreement.

A maximum sensitivity value of ~5.6pm/%RH and a minimum of ~1.4pm/%RH were observed for PI sensors with a coating thickness of 42 μm and 10μm respectively. Response (T_{90}) and recovery (T_{10}) times were found to be around 45 minutes and 28 minutes respectively for a sensor with a coating thickness of 42μm. For all sensors evaluated, the hysteresis observed is less than ~5%. Although this value is slightly above those of the commercial polymer-based RH sensors which have a typical value of less than 2% [43-45], it is unlikely to have a significant influence on the measurements due to the nature of the tests performed in concrete environment which will be discussed in the following chapter.

Temperature calibration was also performed using the same set of sensors, which are inherently sensitive to temperature. A maximum temperature sensitivity of ~12.9pm/°C was obtained using sensor with a 42μm layer and a minimum 9.5pm/°C was observed using a sensor with a 10μm coating layer. The data obtained thus can be used to remove the temperature effect from the sensor readings by means of a suitable temperature compensation scheme which generally consists of a bare FBG insensitive to moisture.

The sensors developed and evaluated, as reported above, are used in subsequent work to monitor moisture ingress in concrete, as discussed in detail in Chapter 5. The sensor developed was embedded into concrete specimens of different porosity and mix composition. The effectiveness of the sensor was evaluated by using a simple waterbath test in which the samples were immersed in water maintained at a constant temperature.

4.7. References

[1] A. D. Kersey, M. A. Davis, H. J. Patrick, M. LeBlanc, K. P. Koo, C. G. Askins, M .A. Putnam and E. J. Friebele, " Fiber Grating Sensors", *Journal of Lightwave Technology*, 15(1997), 1442-1463.

[2] A. Othonos, "Fiber Bragg Gratings," *Review of Scientific Instruments*, 68(1997), 4309–4341.

[3] J. Case, L. Chilver and C.T.F. Ross, *Strength of Materials and Structure*, 3rd ed., Edward Arnold, 1993.

[4] Valerie Illingworth (ed), "The *Penguin Dictionary of Physics*", 3rd edition, Penguin, 2000.

[5] T. Kuroiwa, T. Hayashi and A. Ito, "A Thin Film Polyimide Based Capacitive Type Relative Humidity Sensor", *Sensors and Actuators B*, 13-14(1993), 89-91.

[6] G. Gerlach and K. Sager, "A Piezoresistive Humidity Sensor", *Sensors and Actuators A*, 43(1994), 181-184.

[7] P. Giaccari, H. G. Limberger, P. Kronenberg, "Influence of Humidity and Temperature on Polyimide-Coated Fiber Bragg Gratings", in *Proc. OSA Trends in Optics and Photonics Series: Bragg Gratings, Photosensitivity, and Poling in Glass Waveguides*, Washington, DC, USA, 61 (2001), BFB2.

[8] M. Penza and V. I. Anisimkin, "Surface acoustic wave humidity sensor using polyvinyl alcohol film", *Sensors and Actuators A*, 76(1999), 162-166.

[9] H. Wang, C. Feng, S. Sun, C. Segre, J. Stetter, "Comparison of Conductometric Humidity-sensing Polymers', *Sensors and Actuators B*, 40(1997), 211-216.

[10] M. Yang, K. Chen, "Humidity Sensors using Polyvinyl Alcohol Mixed with Electrolytes', *Sensors and Actuators B*, 49(1998), 240-247.

[11] R. Jindal, S. Tao, J. P. Singh and P. S. Gaikwad, "High Dynamic Range Fiber Optic Relative Humidity Sensor", *Optical Engineering*, 41 (2002), 1093-1096.

[12] S. K. Khijwania, K. L. Srinivasan, J. P. Singh, " An Evanescent-wave Optical Fiber Relative Humidity Sensor with Enhanced Sensitivity", *Sensors and Actuators B*, 104 (2005), 217-222.

[13] A. Gaston, F. Perez and J. Sevilla, "Optical Fiber Relative-Humidity Sensor with Polyvinyl Alcohol Film", *Applied Optics*, 43 (2004), 4217-4132.

[14] J. J. Licari and L.A. Hughes, "*Handbook of Polymer Coatings for Electronics, Chemistry, Technology and Applications*", 2nd edition, Noyes Publications, pp 55-63.

[15] B.H. Lee, "Polyimide", *Coating Technology Handbook*, 2nd edition, D. Satas and A.A. Tracton(Eds), pp 503-505, 2001.

[16] K. Sager, A. Schroth, A. Nakladal and G. Gerlach, "Humidity-Dependent Mechanical Properties of Polyimide Films and their Use for IC-Compatible Humidity Sensors", *Sensors and Actuators A*, 53 (1996), 330-334.

[17] R. Buchold, A. Nakladal, Gerlach, K. Sahre, K.-J. Eichhorn, "Mechnical Stress in Micromachined Components Caused By Humidity-Induced-In-Plane Expansion of Thin Polymer Films", *Thin Solid Films*, 321 (1998), 232-239.

[18] R. Buchold, A. Nakladal, Gerlach, K. Sahre, M. Muller K.-J. Eichhorn, M. Herold, G. Gauglitz, "A Study on the Microphysical Mechanisms of Adsorption in Polyimide Layers for Microelectronic Applications", *Journal of electrochemical society*, 145(1998), 4012-4018.

[19] http://www.dcchem.co.kr/english/product/p_petr/p_petr8.htm

[20] http://www.poval.jp/english/poval/tec_info/ti_01.html

[21] C. A. Finch (ed), "Polyvinyl Alcohol: Properties and Applications", John Wiley & Sons, 1973.

[22] D. L. Williams, B. J. Ainslie, J. R. Armitage, R. Kashyap and R. Campebell, "Enhanced UV Photosensitivity in Boron Codoped Germanosilicate Fibres", *Electronics Letters*, 29 (1993), 45-47.

[23] S. Pal, J. Mandal, T. Sun and K. T. V. Grattan, "Analysis of Thermal Decay and Predictional of Operational lifetime for a Type I Boron-Germanium Codoped Fiber Bragg Grating", *Applied Optics*, 42(2003), 2188-2197.

[24] K. E. Chisholm, K. Sugden and I. Bennion, "Effects of Thermal Annealing on Bragg Fibre Gratings in Boron/Germania Co-doped Fibre", *Journal of Physics D: Applied Physics*, 31(1998), 61-64.

[25] D. L. William and R. P. Smith, "Accelerated Lifetime Tests on UV Written Intra-core Gratings in Boron Germania Codoped Silica Fibre", *Electronics Letters*, 31(1995), 2120-2121.

[26] S. R. Baker, H. N. Rourke, V. Baker and D. Goodchild, "Thermal Decay of Fiber Bragg Gratings Written in Boron and Germanium Codoped Silica Fiber", *Journal Of Lightwave Technology*, 15(1997), 1470-1477.

[27] T. Erdogan, V. Mizrahi, P. J. Lemaire and D. Monroe, "Decay of Ultraviolet-induced Fiber Bragg Gratings", *Journal of Applied Physics*, 76(1994), 73-80.

[28] S. Pal, "Characterisation and High-Temperature Sensing Potential of Fibre Bragg Gratings in Specialised Optical Fibres", PhD Thesis, City University, 2004.

[29] J. Mandal, "Fibre Laser Development for Sensor Application", PhD Thesis, City University, 2005.

[30] http://www.gelest.com/Library/08Tailor.pdf

[31] http://www.mech.port.ac.uk/zyz/public_html/ENIM/CDRom/Module24/unite%204/related%20materials.htm#reading%202.1

[32] E. Shim, "A Study of Spin Finish Application on Fibers", PhD Thesis, North Carolina State University, 2001.

[33] D. Quéré, "Fluid coating on a Fiber", *Annual Review on Fluid Mechanics*, 31(1999), 347-384.

[34] http://www.hdmicrosystems.com/

[35] HD Microsystems DatasheetPI 2525: http://www.hdmicrosystems.com/conn/pdfform.html

[36] http://www.poval.jp/english/poval/s_grades/sg_r.html

[37] HD Microsystems Datasheets VM65: http://www.hdmicrosystems.com/conn/pdfform.html

[38] L. Greenspan, "Humidity fixed points of binary saturated aqueous solutions", *Journal of Research of the National Bureau of Standard*, 81 (1977), 89-96.

[39] ASTM E104-85, "Standard Practice for Maintaining Constant Relative Humidity by Means of Aqueous Solutions"

[40] S. Pal, T. Sun, K .T. V. Grattan, S. A. Wade, S. F. Collins, G. W. Baxter, B. Dussardier, G. Monnom, "Non-linear Temperature Dependence of Bragg Gratings Written in Different Fibres, Optimised for Sensor Apllications Over a Wide Range of Temperatures", *Sensors and Actuators A*, 112(2004), 211-219.

[41] A. MacLean, W. C. Michie, S. G. Pierce, G. Thursby, B. Culshaw, C. Moran and N. B. Graham, " Hydrogel/Fibre Optic Sensor for Distribution Measurement of Humidity and pH Value", *SPIE Proc.* Vol. 3330 (1998), 134-144.

[42] P. Kronenberg, B. Culshaw, G. Pierce, " Development of a novel fiber optic sensor for humidity monitoring", *SPIE Proc.* Vol. 3670 (1999), 480-485.

[43] http://content.honeywell.com/sensing/prodinfo/humiditymoisture/009012_2.pdf

[44] http://www.sensirion.com/en/pdf/product_information/Data_Sheet_humidity_sensor_SHT1x_SHT7x_E.pdf

[45] http://www.cweb5.com/ohmic/pdf/UPS-500.pdf

Chapter 5:

Application of a FBG-Based Humidity Sensor for *In-Situ* Moisture Monitoring in Concrete

5.1. Introduction

This chapter presents results obtained from a series of experiments performed to demonstrate the use of FBG-based humidity sensors for moisture detection in concrete. The experiments discussed, mainly as "proof of principle" investigations, were carried out working together with colleagues from the civil engineering department to provide valuable advice on the materials used and to enable comparisons to be made with the results of 'standard' tests used in industry.

5.2. Moisture Detection in Concrete Using FBG Humidity Sensor: Initial Evaluation of the Sensor

The aim of this experiment was to investigate the use of the humidity sensor for the detection of moisture ingress in concrete [1, 2]. To monitor the moisture ingress in concrete, the sensor was embedded in concrete samples of different water to cement (w/c) ratios* (taking advice from civil engineering colleagues) which were then immersed in a water bath. A direct indication of the

* Water to cement (w/c) ratio refers to the weight ratio of the water and cement used in a concrete mix. It is a design parameter used to control the properties of concrete including strength, workability and porosity. A high w/c ratio, for example 0.7, results in a mixture that flows easily hence improves its workability, however, it also yields low strength concrete with high porosity and making it more permeable to water.

humidity level within a sample was given by the shift of the Bragg wavelength caused by the expansion of the humidity-sensitive material coated on the FBG.

5.2.1. Experimental Arrangement for the Test carried out

5.2.1.1. Sensor Probe Fabrication

The fragile nature of the fibre into which the FBG was written and the need to use it as a robust probe requires an appropriate way to protect the sensor from possible damage when used in the concrete specimens. A suitable approach to overcome this problem was to use a perforated metal protection sheath which was formed by a thin metal tube with holes drilled along each side to allow the free circulation of fluids. A picture of the probe assembly with the protection sheath is shown in figure 5-1. In practice, the FBG-based sensor requires some form of temperature compensation to remove the temperature effect from the humidity measurements. This can be achieved by simply adding another uncoated FBG to the sensor probe to function as a temperature sensor. Together with temperature calibration data of the humidity sensor, humidity readings can be retrieved by applying temperature compensation to eliminate any temperature variation experienced during the measurements. However, the tests performed in this work were carried out in a water bath, at controlled temperatures: hence this minimizes the need for correction and maintains comparable conditions for the different concrete samples evaluated.

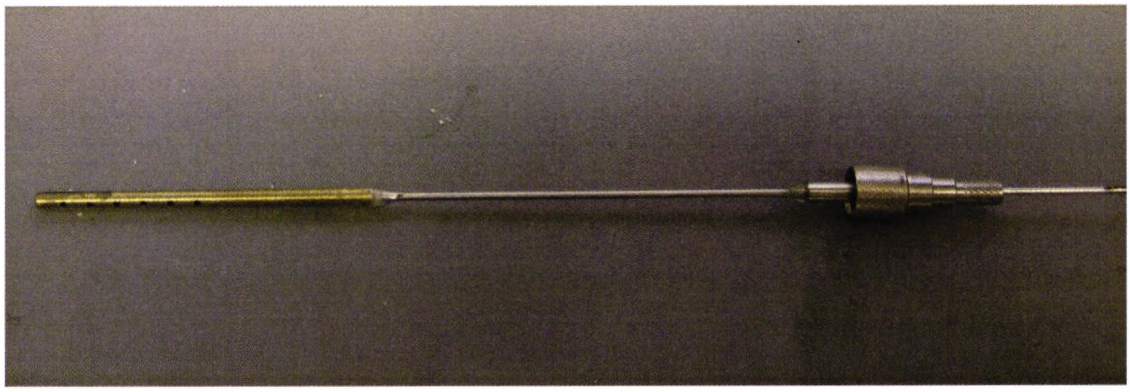

Figure 5-1: Picture of the FBG sensor with perforated metal protective sheath.

5.2.1.2. Concrete Samples

Standardized cylindrical samples of concrete were made with a diameter of 100 mm and depth of 100 mm (as shown in figure 5-2 (a)). They were cast with a 4 mm diameter hole at the centre, with a depth of 80 mm into which the sensor could be placed. On the advice of the civil engineers, the mix was manufactured using ordinary Portland cement (OPC) CEM-I 42.5 conforming to BS EN 197 Part 1 [3], manufactured by Lafarge (previously Blue Circle Cement Ltd.). The mix designs of the specimens were based on the guidelines from the BRE (Building Research Establishment) in the UK [4] and details of the mix proportion for different specimens are given in table 5-1. Sharp sand with a maximum coarse size of 5 mm was used as the fine aggregate and river gravel with a maximum coarse size of 10 mm was used as the coarse aggregate.

	Mix number		
	1	2	3
Water/Cement ratio (w/c)	0.5	0.6	0.7
Water (kg)	205	205	205
Cement (kg)	410	342	293
Sand (kg)	760	826	885
10mm Aggregate (kg)	967	969	959

Materials quantities per $1m^3$ of concrete

Table 5-1: Details of the concrete mix proportion.

To allow for different response time in saturating a specimen, three different mixes were made, with water/cement (w/c) ratios of 0.5, 0.6 and 0.7 respectively. The concrete cylinders were removed from their casts after a period of 24 hours, after which they were left to cure in a water tank for 7 days at ~20°C and finally, removed and left to dry under laboratory conditions with an average temperature of ~16°C until tested.

Four cubes (Dimensions:100 mm x 100 mm x 100 mm as shown in Figure 5-2 (b)) from each mix were cast and their compressive strengths after 28 days were measured using a compression test machine as a means of quality control of the samples used (see figure 5-3(a)). The compressive test results obtained are shown in figure 5-3(b).

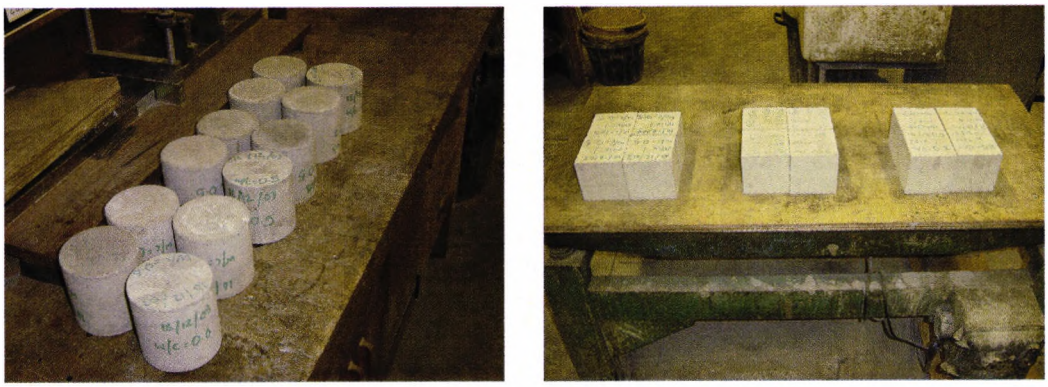

(a) (b)

Figure 5-2: Pictures of the concrete samples cast for the experiment.

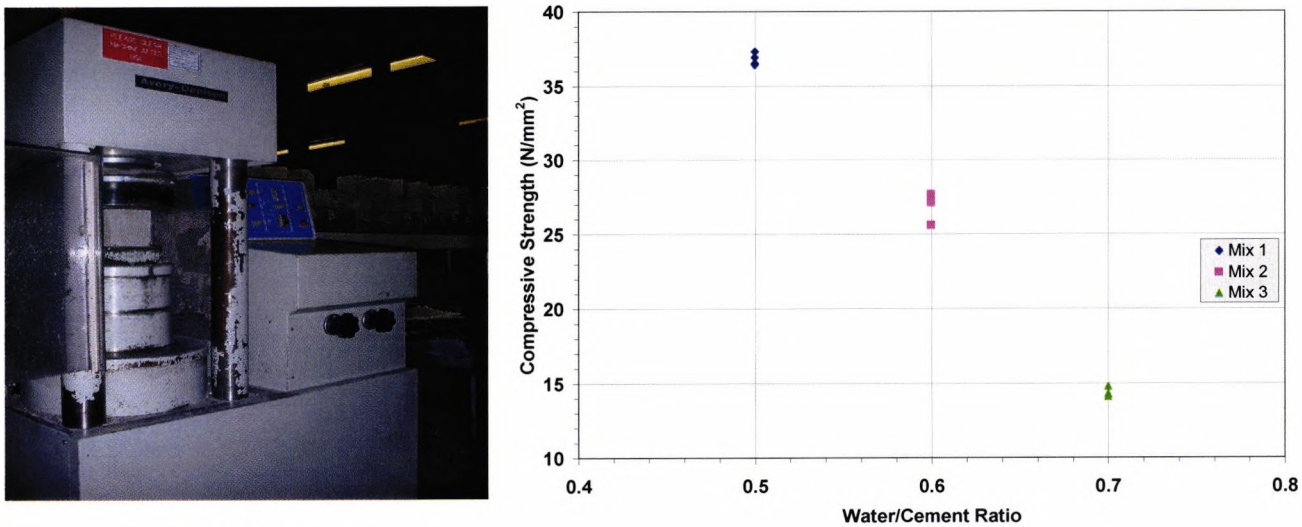

(a) (b)

Figure 5-3: (a) Picture of the compressive strength test machine. (b) Plot of the compressive strength data obtained using samples of three different mixes.

5.2.1.3. Experimental Set-Up: Moisture Ingress Tests

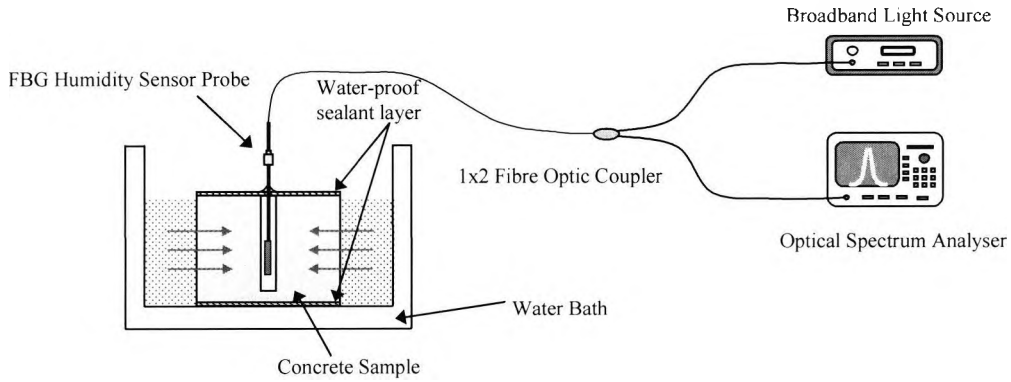

Figure 5-4: Schematic of the set-up used for the moisture ingress test.

The diagram in figure 5-4 depicts the experimental set-up used to monitor the ingress of moisture in concrete. The concrete samples with the embedded humidity sensor were placed in a water bath held at constant temperature. The tops and bottoms of the concrete cylinders were coated with a layer of water-proofing wax to allow only radial absorption of water. For each test, a concrete sample was set up with the probe placed in the centre of the cylinder. The entry point of the probe position was then filled with the malleable wax and sealed with liquid wax, in order to prevent any water seeping in and to prevent the room humidity having any effect. The cylinder was then left for at least an hour, to allow the sensor to reach equilibrium, after which it was placed in the water bath with the water level near to the surface of the concrete and the temperature set at 23°C. The water level in the bath was constantly monitored and topped up as and when necessary. The probe was connected to the optical spectrum analyser (OSA) to determine the characteristic wavelength of the FBG (and thus the measurand).

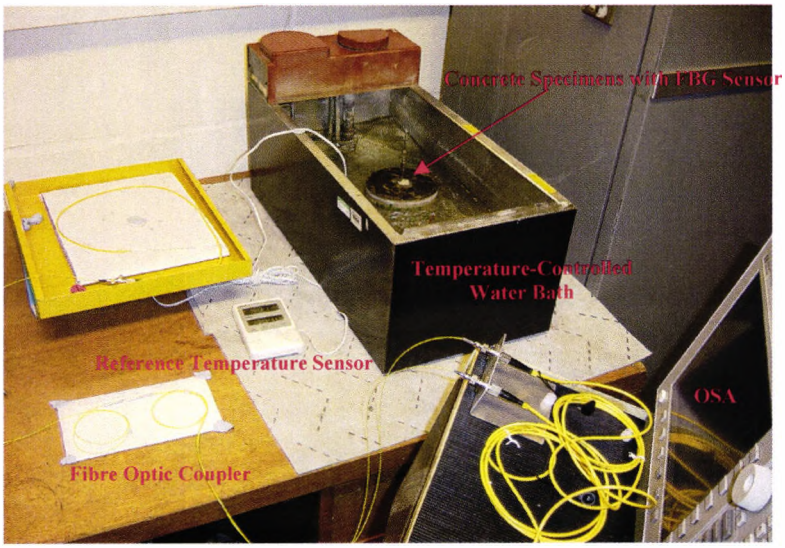

Figure 5-5: Picture showing the experimental set-up used

5.2.2. Results and Discussions

Initial tests carried out using samples dried in the laboratory at room conditions showed a high moisture content within the concrete even before they were immersed in water. This is evident from the readings taken as soon as the sensor was embedded in the samples. This observation was consistent with all three different specimens and was most significant in the 0.5 w/c ratio samples, which indicated a relative humidity (RH) level of 92% as shown in figure 5-6.

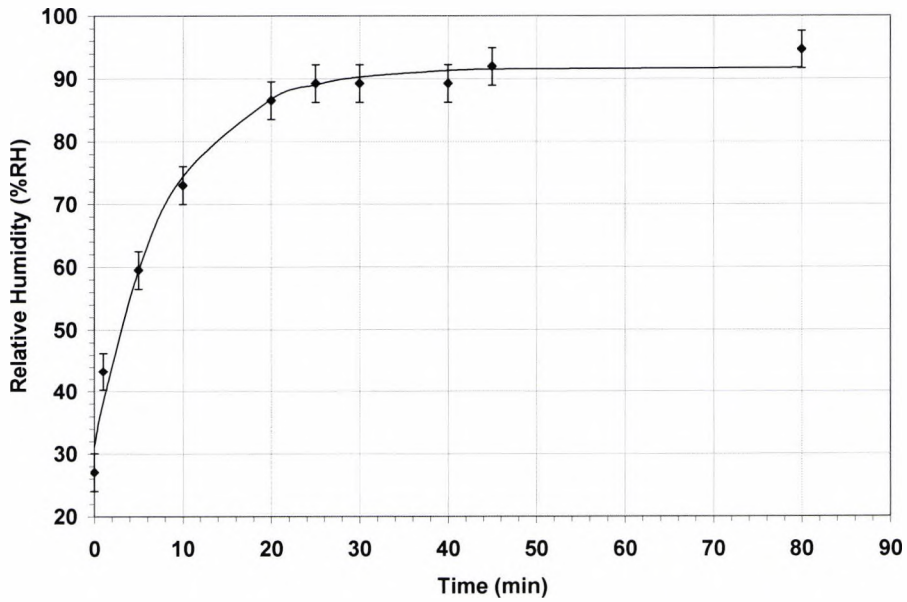

Figure 5-6: Response of the FBG sensor when placed in a fresh concrete sample (0.5 w/c ratio).

It was therefore decided to dry the concrete cylinders in an oven before further testing. Despite the further drying, a high RH level in the samples was still observed. For example, after drying a sample (0.5 w/c ratio) at 80°C for 24 hours (following the recommendation of BS 1881 Part 208, 1996 [5]), the sensor showed a saturated reading of 79%RH. In order to achieve a significant change in RH level during experimentation, a lower starting RH was sought and after drying the sample for 48 hours at 95°C, a reading of 62% RH (for sample with w/c: 0.5) was obtained. This observation shows that the so-called 'drying' of a concrete sample does not remove all, or even most, of the absorbed water. The recommendation for the test method for determination of water absorption (BS 1881 Part 122, 1983 [6]) is to dry samples for 72 hours before testing. This confirms the fact that even after 48 hours of drying, some moisture will still be present.

The moisture ingress experiment was carried out using the remaining concrete samples with w/c ratios of 0.5 and 0.7. When the samples were placed in the water bath, the measurements from the sensor remained fairly stable, showing initial readings of ~62%RH (w/c: 0.5) and ~16%RH (w/c: 0.7). This was followed by a rapid increase in RH detected at approximately 250 minutes later for the 0.5 w/c ratio sample and 240 minutes for the 0.7 w/c ratio sample (see figures 5-7 and 5-8). The approximate 10 minutes difference in the measurement between the two samples could be attributed to the fact that the sample with a w/c ratio of 0.5 contains more cement and hence is less porous than the sample with a w/c ratio of 0.7. Therefore, it requires a longer time for the water to penetrate. However, as both samples had a different starting relative humidity level, a direct comparison was more difficult. Ideally, in light of these results, a better sample pre-treatment in terms of the drying regime and the pre-conditioning of the sample at a defined humidity level prior to moisture tests would be preferable.

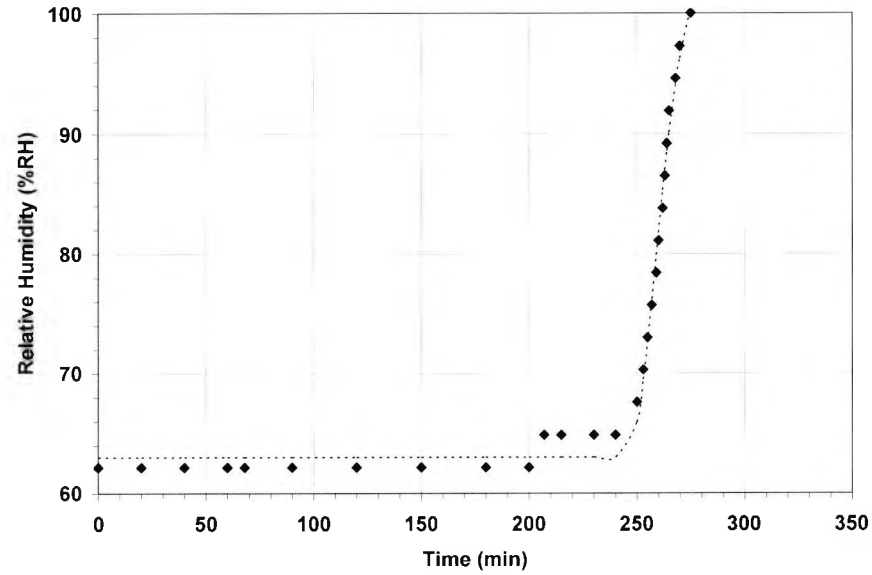

Figure 5-7 Response of the FBG moisture sensor embedded in 0.5 w/c ratio concrete sample, pre-conditioned at 95°C for 48 hours.

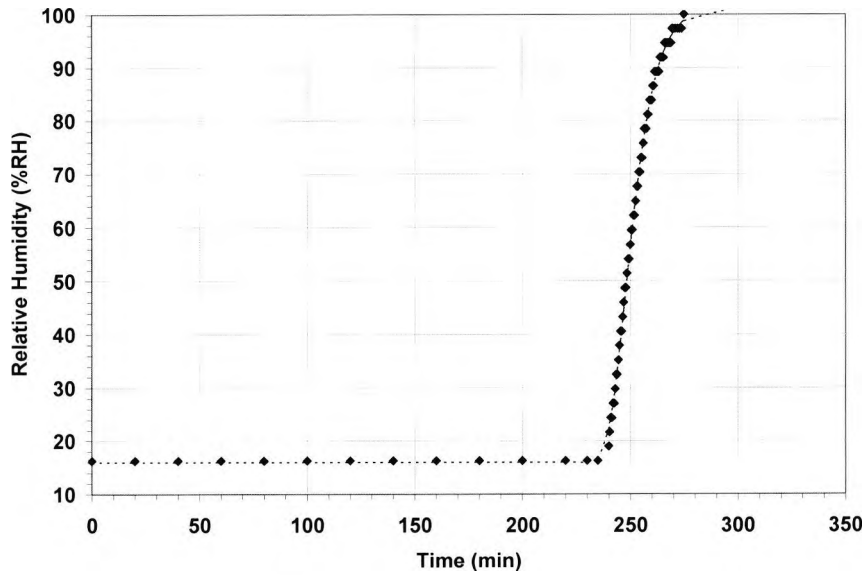

Figure 5-8 Response of the FBG moisture sensor embedded in 0.7 w/c ratio concrete sample, pre-conditioned at 95°C for 48 hours.

The sharp increase in humidity level readings observed was caused by the water reaching the core of the concrete samples. The gradient of the curve for both samples was very similar and this suggests that the time response is dominated by the sensor reaction time rather than the actual

rate of saturation. Upon reaching saturation, which was indicated by the wavelength reading which corresponds to 100%RH, the samples were left in the water bath for a further 24 to 48 hours. Even though saturation had been reached, the readings from the sensor continued to rise slightly to give a higher value. This could have been due either to a small change in temperature or possibly to condensation on the sensor, causing a change in its response to give a wavelength reading that corresponds to a RH higher than 100%RH. Water droplets were found on the metal protection sleeve when the sensor was removed from the test specimen and hence verifying that liquid water could reach the FBG sensor. To confirm this, a final test was done by placing the sensor directly into water with temperature maintained at 23°C and figure 5-9 shows the result of such a test.

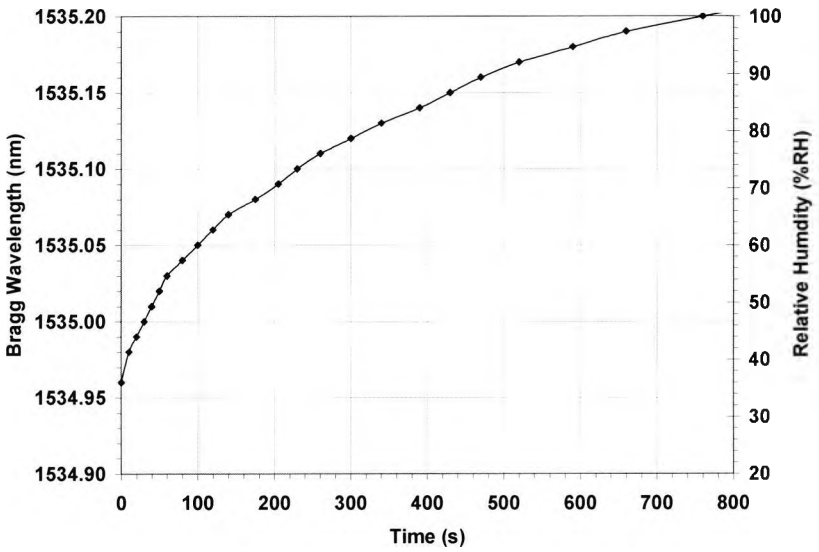

Figure 5-9 Response of the FBG sensor when the probe was immersed in water. The secondary axis shows the corresponding RH readings calculated based on the calibration data.

From this investigation, it was shown that the FBG-based humidity sensors can be used effectively to monitor moisture changes in concrete. This was demonstrated through the experimental data produced using several different concrete samples subjected to water ingress. However, as a result of the sample drying procedures used, the data presented were not able to show the difference between samples of different w/c ratio through the responses obtained from the sensor. Nevertheless, the experience gained during the course of this preliminary

investigation has addressed several key issues such as sensor protection, probe mounting and in particular sample preparation and the appropriate drying regime necessary to perform the moisture ingress tests.

5.3. Monitoring of Moisture Ingress in Different Structural Concrete: Comparison Between Pure OPC and OPC-PFA Blend

PFA or pulverised fuel ash is a by-product generated by the burning of pulverised coal in power stations. It is extracted from the flue gases by mechanical or electrostatic precipators and is generally in the form of very fine powder (typical diameter 1μm-100 μm) with spherical shape [7]. PFA can be used to replace part of the commonly used OPC cement mix and a typical guideline given for the mix proportion is between 25%-40% (by weight) replacement for use in concrete in most purposes [8, 9]. The addition of PFA in concrete is reported to impart properties such as improve workability, enhanced strength (long term) and reduced permeability which influence the resistance to chloride attacks and water penetration [8, 10]. In view of these added properties, particularly, the reduced water permeability, a second experiment was performed to compare the rate of moisture ingress between samples of pure OPC mix and OPC with 30% PFA blend [11, 12].

5.3.1. Experimental Work carried out

5.3.1.1. Concrete Samples

The concrete samples used were constructed from 4 different mixes (as shown in table 5-2), taking into account that the higher the cement content with a reduction in water, the less permeable are the samples and this is reflected in the time of migration of the moisture within the concrete. For each mixture, four 100mm cubes and one 150mm cube were made. The 100mm cubes were used for compressive strength tests as a means of quality control for the samples used in this investigation and the 150mm cubes were designed for the moisture ingress tests.

	Mix number			
	1	2	3	4
Cement Type	OPC	OPC	PFA	PFA
Water/Cement ratio (w/c)	0.5	0.7	0.5 30% PFA	0.7 30% PFA
Maximum coarse aggregate size (mm)	20	20	20	20
Water (kg)	1.62	1.62	1.44	1.44
Cement (kg)	3.24	2.31	2.55	1.88
PFA (kg)	-	-	1.09	0.77
Sand (kg)	5.78	6.10	5.79	6.15
10 mm aggregate (kg)	3.58	3.78	3.58	3.18
20 mm aggregate (kg)	7.16	7.56	7.16	7.61
Total mix volume (m^3)	0.009	0.009	0.009	0.009

Table 5-2: Details of the OPC and PFA replacement concrete mix proportion.

Similarly, all cast concrete cubes were placed in a curing tank after a period of 24 hours as discussed in Section 5.2.1.2. The 100mm concrete cubes were cured and crushed at 7 and 28 days from casting, giving the compressive strength data as shown in figure 5-10. The 150 mm cubes were removed from curing at 7 days (mix 1-2, OPC) and 14 days (mix 3-4, PFA) where samples of different cement mixes achieved approximately 2/3 of their ultimate strength in 28 days. The curing period used was determined from the compressive strength tests performed previously and it was used mainly to standardize the sample preparation for all specimens (to enable cross comparisons readily to be made). Prior to the moisture ingress tests, all samples were placed into a heated oven at ~95°C for a period of 48 hours.

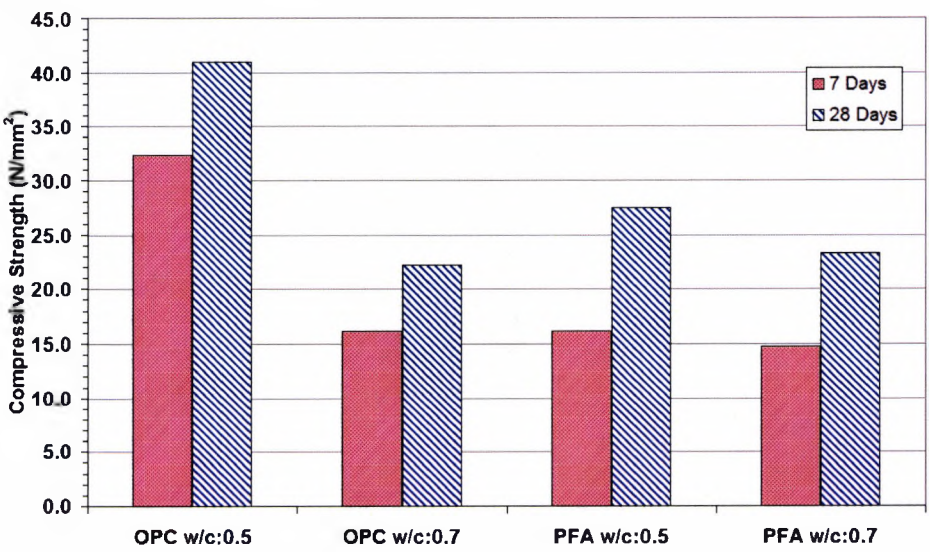

Figure 5-10: Average compressive strength of OPC and PFA samples obtained at 7 days and 28 days.

To facilitate the investigation of moisture migration using the humidity sensors, holes with a diameter of 4mm and a depth of 80mm were cast in the 150mm concrete cubes. A bitumen layer was coated on the surface of the sample cubes, except for the one face where moisture was introduced. Samples with w/c ratio of 0.7 had sensors positioned at 25 mm and 75mm (position 1 and 3) away from the uncoated face whereas for samples with a w/c ratio of 0.5, sensors were installed at 25mm and 50mm (position 1 and 2). These positions were selected to ensure all tests were carried out over a reasonable time scale and that sufficient data were obtained to allow useful comparisons to be made between all the specimens used. Figure 5-11a shows a diagram of the cube design used and the positions cast for the placement of the probes. A photograph of the set-up, illustrating the sensor probes in position is shown in figure 5-11b.

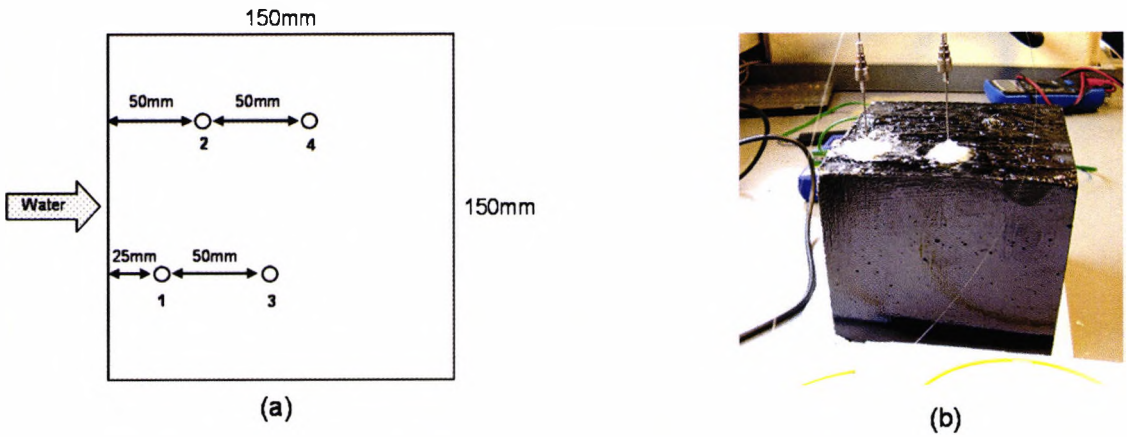

Figure 5-11 (a) Schematic of a standard concrete cube used in this work, showing holes for placement of sensors. (b) Picture of the concrete specimen with embedded FBG humidity sensors.

5.3.1.2. Experimental Set-Up

Moisture ingress experiments were carried out using the set up illustrated in figure 5-12. A broadband light source was used to provide the input signal to the humidity sensors through a fibre optic coupler and the return signals were monitored using an optical spectrum analyser (OSA), together with a personal computer (PC) for data acquisition. The two humidity sensors of similar sensing characteristics as shown in figure 5-13 were installed at different positions in the concrete samples and sealed with watertight wax. The sensors were then allowed to equilibrate in

the sealed environment within the concrete cube before the samples were placed into a temperature-controlled water bath set to 23°C.

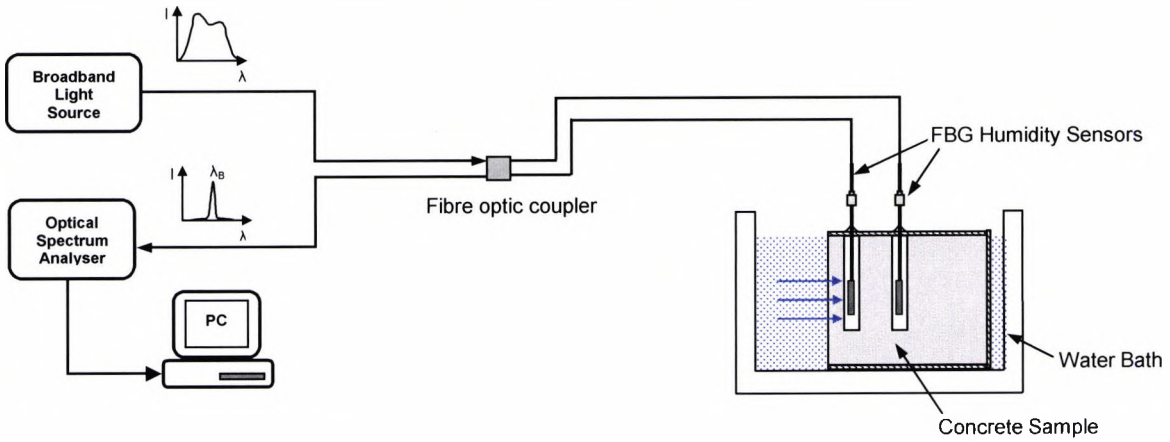

Figure 5-12: Experimental set-up for moisture ingress experiments.

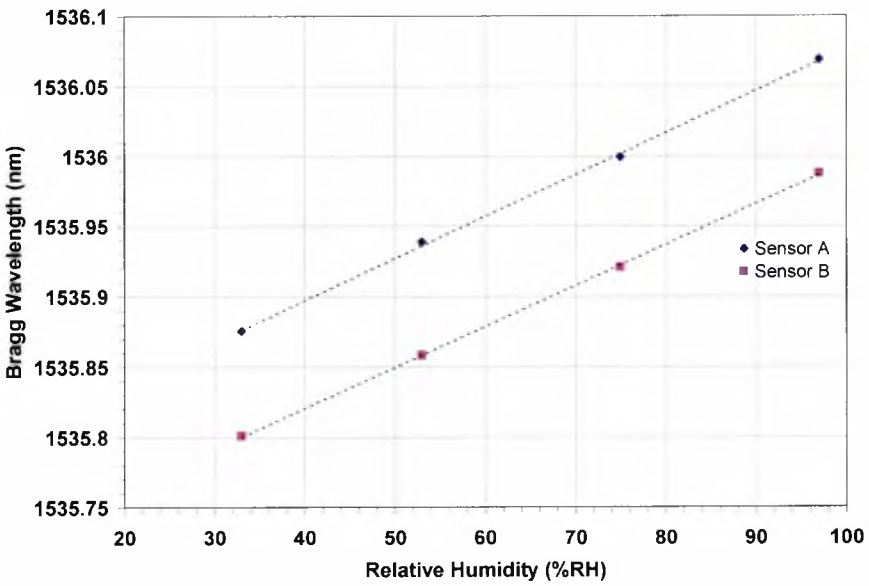

Figure 5-13: Calibration of the humidity sensors at constant room temperature of 23°C.

5.3.2. Results and Discussions

Figure 5-14 shows the results of moisture ingress measurements for mix 1 (OPC, w/c: 0.5), where the sensors were placed at the following positions from the cube edge: position 1 for sensor A and position 2 for sensor B. To eliminate the effect of the differences in the wavelengths associated with the 'dry' and 'saturated' wavelength values, the responses from the sensors were normalized to their respective 'plateau' values. The readings taken at the beginning of the tests showed a variation in the RH level at various positions in the concrete cube. This observation, which is consistent for all the samples tested, reveals a lower RH level at position 1 as compared to other positions further into the centre of the cube. The likely cause of this uneven distribution of moisture within the concrete cube is due to the drying process used prior to the experiments. Nevertheless, the results presented in this work show the effective operation of the sensors when used for measurements on the concrete samples.

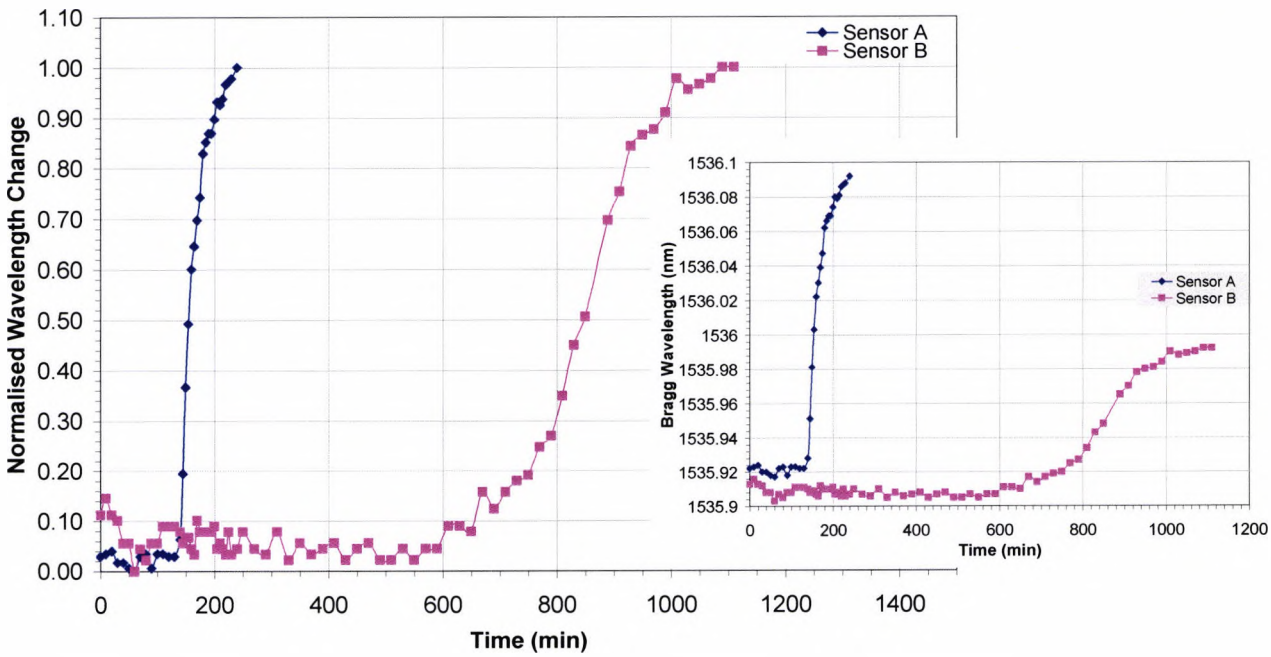

Figure 5-14 Measurements taken from sensor A and B in mix 1 (OPC, w/c: 0.5) with data normalised to unity at the peak wavelength detected for each sensor. Inset shows the wavelength measurements from the same sensors.

Figure 5-15 shows the typical results for mix 2 (OPC, w/c:0.7), where this time sensors were placed at 25 mm and 75 mm (positions 1 and 3), illustrating, as expected a longer time before the moisture ingress was detected at sensor B, this being manifested as a change in wavelength. This result shows the differences in the times of the moisture reaching sensor A and sensor B (at their respective different positions). The time observed could be attributed to both the permeability of the concrete cube and the sensor position for the moisture ingress propagating through the sample.

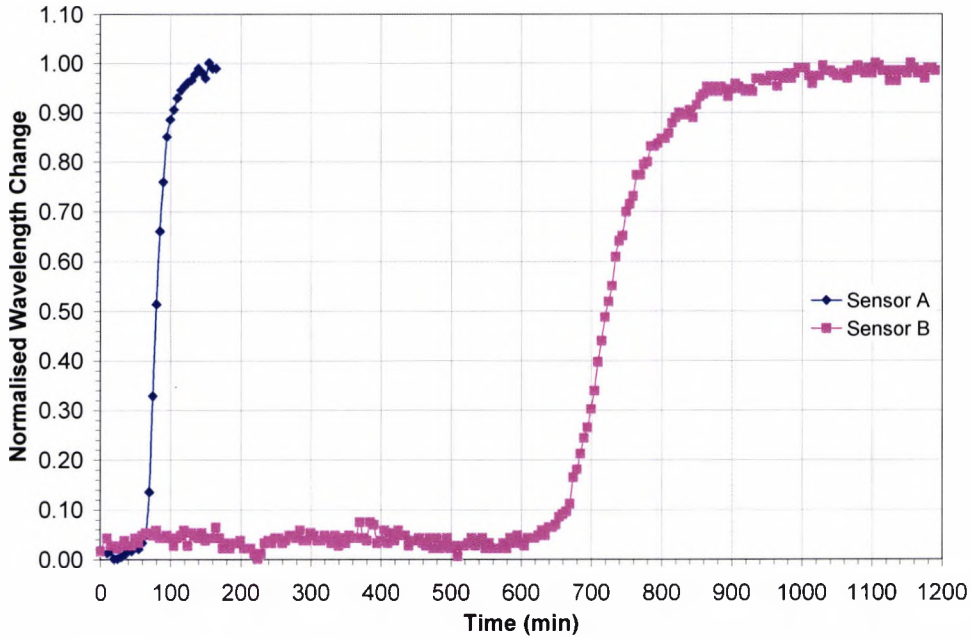

Figure 5-15 Normalised time response plots of OPC sample (w/c: 0.7) taken at different probe positions.

Using the 5% reference point of the normalised plots for different concrete samples and the placement of the sensors, a simplified data analysis was made by calculating the moisture ingress velocity through the different sample cubes. These values, together with the time response of the sensor at different positions were tabulated in table 5-3. The data shows, for example, a higher velocity of water ingress for w/c: 0.7 when compared to w/c: 0.5 for the OPC cube (i.e. comparing mixes 1 and 2), showing the influence of the w/c ratio.

Mix number ,Type, w/c ratio	Sensor A – time to 5% response at 25 mm (min)	Velocity of water ingress to Sensor A (mm min^{-1})	Sensor B – time to 5% response at various positions (min)	Velocity of water ingress to Sensor B (mm min^{-1})
Mix 1 OPC (w/c:0.5)	130	1.9×10^{-1}	590 (at 50 mm)	8.5×10^{-2}
Mix 2 OPC (w/c:0.7)	65	3.8×10^{-1}	625 (at 75 mm)	1.2×10^{-1}
Mix 3 PFA (w/c:0.5)	215	1.2×10^{-1}	>1200 (at 50 mm) not fully saturated	$<4.2 \times 10^{-2}$ not fully saturated
Mix 4 PFA (w/c:0.7)	110	2.3×10^{-1}	2230 (at 75 mm)	3.4×10^{-2}

Table 5-3: Summary of the response time representing the moisture ingress rate and the calculated velocity of water ingress for sensors A and B (at different placement points in the samples), using the 4 different concrete mixes.

Further examination of the data obtained from the experiments also allows comparisons to be made between the responses of the OPC and PFA samples. For example, data recorded for sensor A using both OPC and PFA (mixes 1-4), as shown in figure 5-16 illustrates a clear difference between the time taken for the sensor to react to the moisture as it migrates through the different concrete types. When similar measurements were taken at 75 mm (position 3) from the cube face (see figure 5-17), the data obtained show that the differences in the mechanisms of migration between mixes 2 and 4 become more apparent with depth into the concrete. Data obtained also show that the rate of water ingress reduces by a factor of ~ 2 when mix 2 (OPC) is replaced by mix 4 (PFA) for sensor A (25 mm, position 1). Further into the material (at 75 mm, and using sensor B) the PFA material shows an even slower rate of water ingress, with the calculated velocity being only ~ 30% of that for the OPC (mix 2). In the case of 0.5 w/c (mixes 1 and 3) and making a comparison at 25mm (position 1), the PFA again shows a slower velocity of water ingress, slightly under the factor of 2 seen for mixes 2 and 4.

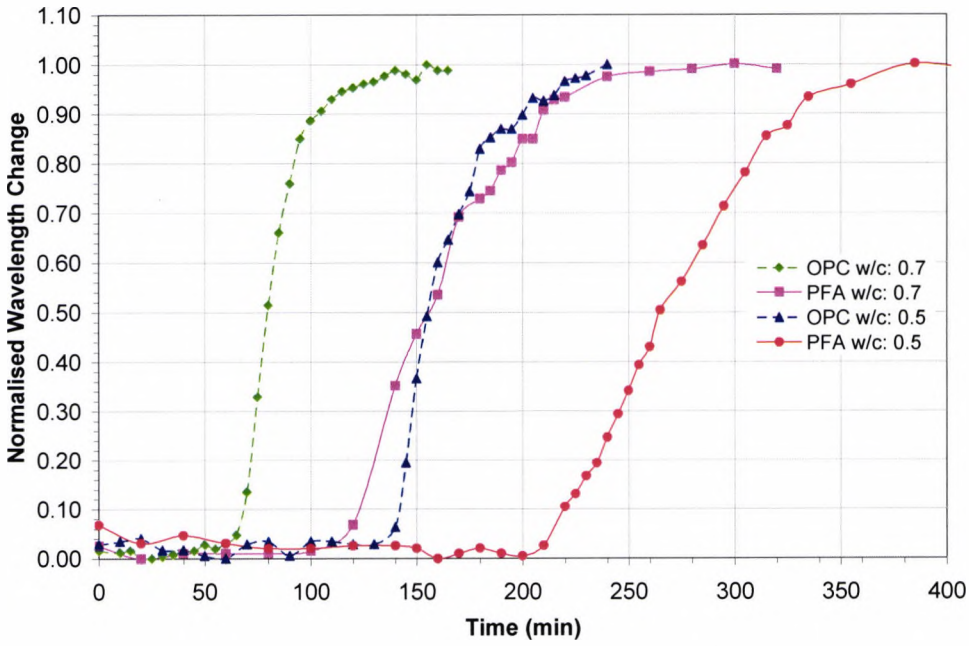

Figure 5-16: Normalised time response plots taken from sensor A (25mm from cube face) for mix 1-4.

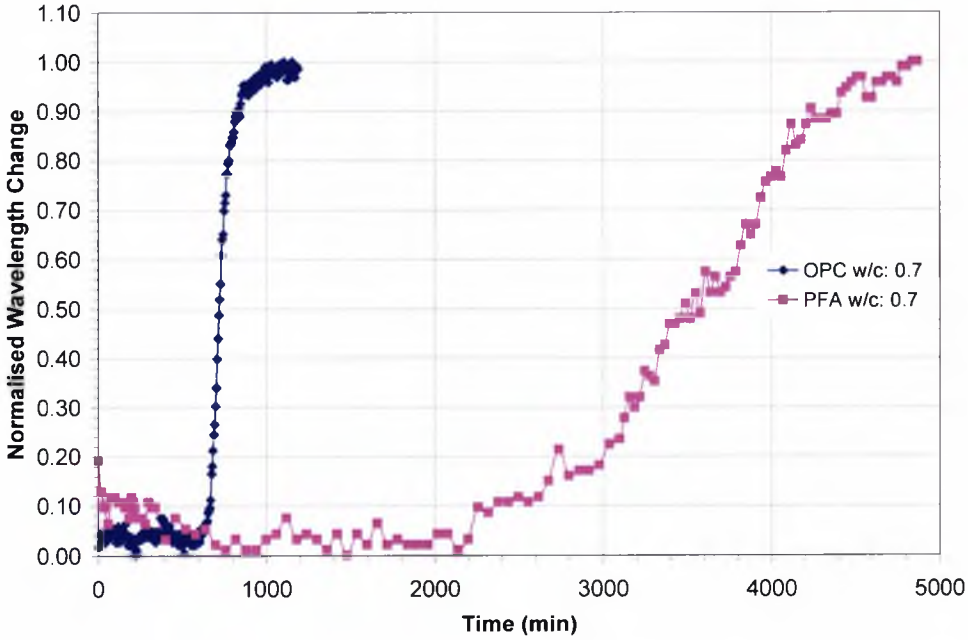

Figure 5-17: Comparison of time responses taken from sensor B positioned at 75mm from the cube face using mix 2 and 4.

In this investigation, results obtained from a series of experiments using standardized concrete samples, of different w/c ratio and cement mixture have shown that useful measurements of the

rate of moisture ingress can be obtained using the humidity sensors developed in this work. The set of data obtained has enabled the determination of simple *in-situ* sensor parameters such as response time and the average velocity of propagation of moisture through the different concrete samples used. These results give useful insights into the effects in the concrete samples of different porosity and the construction of the experiments has enabled simple measurements of the average rate of migration of water (or more importantly water-borne contaminants) between the two sensors when placed at known distances apart in the sample cubes. Data thus obtained can be linked to information on the compressive strength of the samples for optimum material choice. Though these measurements are obtained under standardized laboratory conditions, it does show the potential of the sensor developed for use in structural monitoring.

5.4. Investigation of Freeze/Thaw Effect on Moisture Transport in Concrete

The freeze/thaw effect is one of the damage mechanisms that accounts significantly for the deterioration of concrete. It occurs when the concrete structure is saturated with water and subjected to repeated freezing and thawing cycles which is common in a cold climate environment [13]. The freezing of the water trapped in the capillary pores result in the formation ice. The expansion in volume as a result induces pressure on the concrete and if the pressure acting on the concrete is higher than its strength it leads to the formation of microcracks. This consequently facilitates the transport of water into concrete and it also accelerates the penetration of chloride ions which will result in the onset of corrosion processes in steel reinforcement concrete. The deleterious effect of freeze/thaw action causes a feature known as 'spalling' and scaling of the concrete surface and it is a cumulative process that will induce further damage to the structure.

In this brief investigation, an experiment was carried out to investigate the effect of freeze/thaw action on the rate of moisture ingress in OPC concrete samples [14]. The structure of the experiment is similar to the one described in section 5.2, but it was carried out using samples subjected to various freeze/thaw cycles.

5.4.1. Concrete Samples and Experimental Set-Up

The samples for this investigation were made using the same mix design, dimensions and curing process as discussed in Section 5.2.1.2. The water/cement ratio was set to 0.7 in order to give samples that are low resistance to frost attack. A total of 8 concrete cylinders for the moisture test and 4 cubes for compressive strength test were cast for this investigation. After 28 days of curing, the cubes were crushed to determine their various compressive strengths (see Table 5-4) and the cylinders were subjected to various freeze/thaw cycles to induce crack formation within the samples. Three of the eight cylinders were subjected to three freeze/thaw cycles and another three were subjected to nine cycles. The freezing and thawing process was carried out using cycle of freezing at -16°C (10 hours) and thawing at 23°C (14 hours), thus requiring a total of 24 hours for one complete cycle. The samples were placed in a container filled with water throughout the whole process with the aim to induce a more severe deterioration. After the freeze /thaw process, all the samples (including the remaining two undamaged cylinders which were used as control samples) were then oven-dried and stored in airtight containers before tests.

Sample	1	2	3	4	Average
Compressive Strength (N/mm^2)	12.9	11.9	13.5	13.6	13.0

Table 5-4: Compressive strength value of the OPC (w/c: 0.7) sample cubes.

Due to the limited time constraint for this test, samples were only subjected to 3 and 9 freeze/thaw cycles. Although there is no standard method to perform freeze/thaw resistance test, it is not uncommon to use tens to hundreds of cycle in order to induce a significant damage in concrete [13] and on this occasion it was not possible to conduct such an extensive test (although this is likely to be the subject of continuing work). For example, in the method suggested by ASTM [15], freeze/thaw process can continue up to 300 cycles. However, in this investigation, the number of cycles defined for the samples was based on the time allocated to carry out this investigation, with such limitations as that may impose on the results obtained. Whether this will be sufficient to indicate if signification variations arising from the moisture ingress tests will be seen and if it will yield a response as a result of the freeze/thaw damage induced in the samples under test is an important outcome of the work, for the planning of future tests.

For the moisture ingress tests, a set-up similar to that shown in figure 5-4 was used. In brief, the top and bottom of the samples were coated with a layer of waterproofing material. The FBG sensor with known characteristics as shown in figure 5-13 (Sensor B) was embedded in the centre of the concrete cylinder and sealed with wax. The sensor was allowed to stabilise in the concrete before being placed in a water bath regulated at 23°C.

5.4.2. Results and Discussions

The plots in figure 5-18(a)-5-18(c) show the results on the moisture ingress characteristic obtained from a series of samples prepared as discussed in the previous section. In all the responses presented, a similar trend was observed where the beginning of the plots shows a stable and relatively flat response which indicates the humidity level of the cavity in which the sensor was positioned. This was followed by an increase in the sensor reading which is reflected by the red shift in the Bragg wavelength value as a result of water reaching the centre of the concrete samples. In order to perform a comparative analysis using the data obtained, the same approach as discussed in section 5.3.2. where the time taken to reach the position of the sensor is defined by the 5% increment of the total wavelength shift observed in the tests and these values are tabulated as shown in Table 5-5.

From the data presented, the values (based on 5% total wavelength increment) obtained from the 0 and 3 freeze/thaw cycles samples as shown in Table 5-5 were found to cluster in the same time region, giving a small variation which is insignificant to indicate the difference between the two sample groups. The average time taken for the water to penetrate to the centre of the cylindrical samples for 0 and 3 freeze thaw cycles is ~243 minutes and ~240 minutes respectively. This could be due to the low number of freeze/thaw cycles used which is insufficient to induce significant damage in the concrete cylinders, hence changing its water absorption properties.

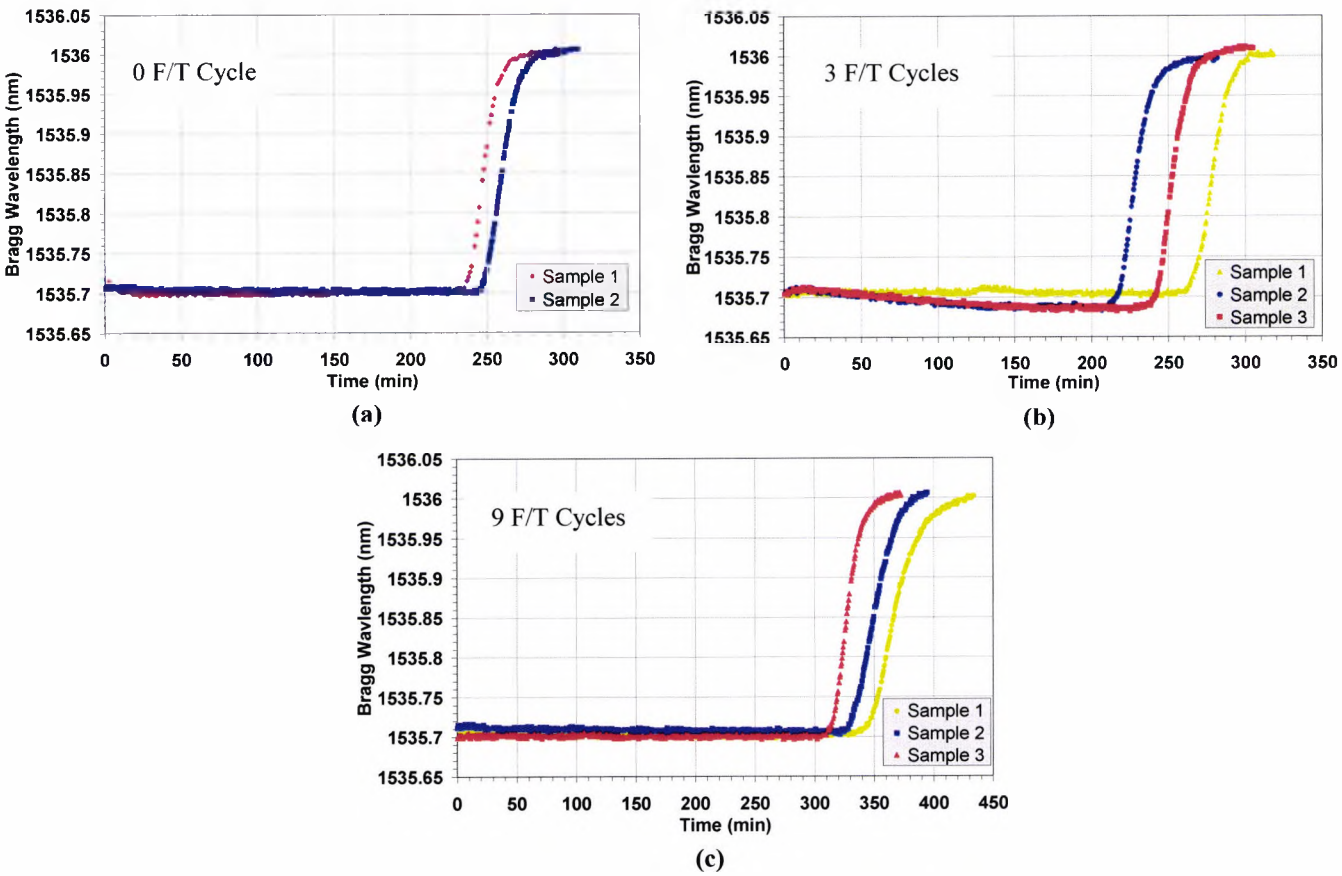

Figure 5-18: Moisture ingress responses of various concrete samples. (a) control samples without freeze/thaw damage, (b) samples with 3 freeze/thaw cycles and (c) samples with 9 freeze/thaw cycles.

Sample	0 Cycle		3 Cycles			9 Cycles		
	1	2	1	2	3	1	2	3
Time to 5% response (min)	237	248	264	216	241	345	331	314
Average (min)	243		240			330		

Table 5-5: Data comprising the different time period (represented by the 5% increment of the total Bragg wavelength shift) for moisture to penetrate to the centre of various concrete samples under test.

Due to this reason, comparative analysis for this investigation was limited only to 0 and 9 freeze/thaw cycles samples. Referring to Table 5-5, the average time response difference between these two sample groups is ~90mins which indicates a much longer time period than the comparison made earlier and the magnitude is also larger than the variation observed within each

sample group, clearly showing, through the measurements obtained from the FBG sensor, the influence of the freeze/thaw action on the concrete samples. However, the results also reveal that the 9 freeze/thaw cycles samples have a slower water penetration rate than the control samples. The microcrack formation as a result of freeze thaw action is known to accelerate water absorption within the concrete which is contrary to the trend observed in this investigation. This observation may be due to the complex random crack formation within the concrete structure, for example cracks that are formed orthogonally to the direction of moisture ingress, which could possibly impede the penetration of the water to the centre of the sample. The main reason for this observation however is not clear and detailed discussion on this observation requires more in-depth discussion on the properties of concrete with structural engineers. However, the tests carried out have set the scene for further research into the freeze/thaw mechanisms using the probe developed.

5.5. Summary

This chapter has discussed the potential applications of the FBG humidity sensor developed in this work for moisture detection in concrete, carrying out a series of experiments as "proof of principle" investigations where the results presented have shown the effectiveness of the sensor in detecting the ingress of moisture in concrete samples of different w/c ratio, mix composition and subjected to various freeze/thaw cycles. Although the sensor was employed as a point sensor in these investigations, multiple sensing elements can be easily cascaded to form a sensor network and coupled with several advantages such as ease of installation and multiplexing, small size, immunity to electromagnetic interference, remote sensing, etc, it offers a potentially more attractive alternative for civil engineering application as compared to its electronic counterparts. The work is clearly a preliminary investigation to give confidence to civil engineering colleagues on the value of the sensor for measurements routinely made in the laboratory by using 'conventional' techniques and this has been achieved. This investigation hence sets the scene for on-going investigations in this area.

5.6. References

[1] D. Eckstein, "The Application of Fibre Optic Sensors in Structural Monitoring", Final Year Project Report, Department of Civil Engineering, City University, 2004.

[2] T. L. Yeo, D. Eckstein, B. McKinley, L. F. Boswell, T. Sun and K. T. V. Grattan, "Demonstration of Fibre Optic Sensing Technique for the Measurement of Moisture Absorption in Concrete", *Smart Materials and Structures*, 15(2006), N40-N45.

[3] BS EN 197-1:2000, "Cement composition, specifications and conformity criteria for common cements"

[4] BR106, Building Research Establishment Report, "Design of normal concrete mixes", Revised Ed. 1988.

[5] BS 1881-208:1996, "Testing concrete. Recommendations for the determination of the initial surface absorption of concrete"

[6] BS 1881-122:1983, "Testing concrete. Method for determination of water absorption"

[7] A. M. Neville, "Cementitious Materials of Different Types" in *Properties of Concrete*, Chapter 2, Fourth edition, Addison Wesley Longman Limited, 1997.

[8] A. M. Neville, "Concretes with Particular Properties" in *Properties of Concrete*, Chapter 13, Fourth edition, Addison Wesley Longman Limited, 1997.

[9] G.F. Blackledge and R. A. Binns, "Concrete Practice", Third Edition, British Cement Association, 2002.

[10] "The Use of PFA in Concrete (Blue Circle Part 1 Ash)", Lafarge Cement, UK.

[11] M. A. C. Cox, "The Use of Fibre Optic Sensors in Monitoring Structural Concrete Application", Final Year Project Report, Department of civil Engineering, City University, 2005.

[12] T. L. Yeo, M. A. C. Cox, L. F. Boswell, T. Sun and K. T. V. Grattan, "Optical Fiber Sensors for Monitoring Ingress of Moisture in Structural Concrete", *Review of Scientific Instruments*, 77(2006), 055108-1 – 055108-7.

[13] A. M. Neville, "Effects of freezing and thawing and of chlorides" in *Properties of Concrete* , Chapter 11 , Fourth edition, Addison Wesley Longman Limited, 1997.

[14] Y. Yuan, "Use of Optical Fibre Sensor to Measure The Properties of Concrete After Freeze/Thaw", Final Year Project Report, Department of Civil Engineering, City University, 2006.

[15] ASTM C666-92, "Standard Test Method for Resistance of Concrete to Rapid Freezing and Thawing", *American Society for Testing and Materials Standards.*

Chapter 6:

Conclusions and Future Work

This chapter gives a summary of the work presented in this thesis and discusses the significance of the results obtained during the course of the research programme undertaken, examining the conclusions in light of the aims and objectives set out in Chapter 1.

6.1. Major Conclusions of the Work Done

The primary objective of this thesis was to conduct an experimental-based research programme aimed towards the initial development of FBG-based humidity sensors and their use for *in-situ*, online monitoring of moisture levels in structural concrete materials. The motivation of this work stems from the need for a fibre-optic-based solution for detecting the water-borne deleterious agents responsible for the corrosion of steel reinforcement bars embedded in concrete structure, with moisture being the key agent which is involved in most structural damaging attacks such as carbonation and chloride ingress. There are currently various fibre-optic based techniques available for the detection of moisture, the most popular is the evanescent wave sensing method which involves stripping of a portion of the optical fibre cladding and re-depositing a measurand-sensitive overlay that would interact with the evanescent field which extends beyond the fibre core. This technique, however, weakens the fibre and is not compatible with the FBG-based SHM system employed in civil structure applications to distributed strain monitoring, for

example. In addition, it adds complexity to what is considered a simple and better optical sensing solution in a SHM system that shows considerable potential to integrate both physical and chemical sensors to provide measurements that together reveal more comprehensive information on the health condition of a civil structure. This hence sets the research work in the direction of developing an effective FBG-based moisture sensor scheme for the purpose of such application.

The humidity sensor as discussed in Chapter 4 was developed using a FBG sensing element coated with an overlay of moisture-sensitive polymeric material. The sensing principle was based on the swelling of the polymeric coating material which stretches the FBG when the humidity level increases, thus causing the Bragg wavelength of the sensing element to shift in response to humidity change. The elegant simplicity of this design lies in the use of a FBG which essentially operates as a strain sensor that was configured to translate the humidity level in the test environment to the applied strain as a result of polymer swelling. The series of characterisation tests performed in this work indicates a reversible sensor response and it also reveals the dependency of coating thickness on the responses of the FBG humidity sensor which is shown by the sensitivity values extrapolated from the calibration plots obtained using saturated chemical salt solutions. For example, a FBG sensor with a coating thickness of ~10μm exhibits a sensitivity value of ~1.4pm/%RH: however, this can be increased to ~5.6pm/%RH with a coating thickness of ~42μm. The optimum sensitivity of the sensor system is dependent on the sensor design used taking into account the spectral resolution of the detection unit employed to analyse the spectral signal of the optical sensor. The thickness of the polymeric coating material clearly also influences the response time of the sensor. Hence these factors need to be taken into consideration when selecting an appropriate coating thickness value for a specific application, in light of the data reporting in this work.

The effectiveness of the FBG-based humidity sensor was evaluated in a concrete environment. The evaluation, which was carried out through a series of "proof of principle" investigations, showed promising results. In the investigations described in Chapter 5, the sensor was embedded in a number of oven-dried concrete specimens with different w/c ratios and mix compositions and immersed in a water bath held at a constant temperature. The sensor in the concrete specimens responded well in distinguishing the different concrete specimens through the time response plots obtained, hence showing the potential of the sensor developed as a useful tool for moisture

detection in concrete environment. Although the sensor used in the series of laboratory-based tests was employed to give point measurements, an array of such sensor elements can be multiplexed to form a sensor network, using the wavelength interrogation nature of fibre Bragg grating-based sensors and offering a non-intrusive detection method that is compatible with the other FBG-based SHM systems employed in civil structure applications.

Thus in summary, with reference to the aims and objectives set out in Chapter 1, all the following were achieved:

- A FBG-based sensor scheme for moisture monitoring, suited to the needs of structural monitoring, was designed and evaluated
- An experimentally-based programme of research, with the objective of developing and characterising FBG-based sensors for the purpose of moisture detection and relating the data to the corrosion process analysis, was carried out and reported in this thesis
- An interdisciplinary programme of research, involving civil engineers to test the sensors in concrete samples as a proof of concept and to evaluate the effectiveness of the FBG-based moisture sensor developed in highly alkaline concrete environment, was undertaken and reported in the thesis
- Relevant conclusions on the effectiveness of the sensors developed were drawn and reported in the thesis
- The results obtained have been, and continue to be reported in the peer reviewed literature and at Conferences (co-authored with civil engineering colleagues to reflect their input to the research programme)

6.2. Future Work

Although the FBG-based humidity sensor evaluated has shown its potential in civil structural applications, the tests carried out in this work however, were performed in a laboratory-based environment, but using samples representative of materials employed 'in the field'. As such, further work is required to look into various aspects pertaining to the durability of the sensor when employed to provide a long term, *in-situ*, online monitoring of moisture level in a concrete structure. The highly alkaline concrete is a very corrosive environment that may affect the

operation of the sensor, especially when it is in direct contact with the sensor materials and polymers such as polyimide has been shown to degrade when cast in concrete. Although no significant degradation in sensor performance has been observed through the repeated tests carried out in this work as the sensor was embedded into a pre-cast cavity to provide non-contact measurements, it is imperative to look into various ways in which the sensor can be protected from this harsh environment (for example, polymeric membranes that are chemically inert) without impeding the measurement of moisture level in concrete. Other practical issues such as sensor packaging should also be considered in order to ensure its robustness against the environment in which the sensor is employed.

Keeping these practical considerations in mind, extended field trials can then be carried out to evaluate the usefulness of the sensor in concrete environment for a range of applications. For example, an array of FBG moisture sensors can be employed to give a moisture profile of newly built concrete floor in new developments in order to ensure the material is sufficiently dry prior to applying floor covering. Standard methods currently employed to yield such measurements involve using broad plastic sheets taped onto the concrete floor or calcium chloride tests performed on specific locations and more recently, the use of relative humidity probe to provide in-situ measurements which requires holes to be drilled into the concrete floor. All these tests can be very tedious, time consuming and may not yield measurements that truly reflect the moisture profile of the area, as what an optical fibre sensor network can do.

Further development of the FBG-based chemical sensor can be extended to look into the detection of pH level and chloride ions, the two parameters which are equally important in corrosion monitoring. The use of coating materials such as hydrogels for pH monitoring (pH level 3-6) and saline concentration measurements have been explored and demonstrated for use in different environment. Further work can be carried out to explore the issues involved in integrating these chemical sensors with the moisture sensor developed to form an all-fibre FBG-based corrosion monitoring network suitable for a range of civil structure applications. This work would not just require an appropriate selection of suitable sensing materials but also optimisation of the sensor design which can effectively transfer the change of measurands to corresponding FBG wavelength shifts based on various transfer mechanisms. For example, a set of ring clamps can be used on each end of the FBG so that the coating can push against the clamps, thus

stretching the sensor as it swells or the sensor can be placed in a housing to restrict the radial expansion of the coating layer, hence induces a pressure in axial direction and consequently stretching the sensor.

Moving beyond civil structural application, the current sensing principle can be extended to explore the use of polymer-coated in-fibre grating devices (FBG or LPG) in gas/vapour sensing application. There has been a considerable amount of research work carried out in the field of chemical gas sensing technologies, particularly the use of gas sensor array based on a variety of chemical-selective polymers which swell reversibly when exposed to target analytes. Various technology platforms (for example, surface acoustic wave and resistance sensing) are used together with these polymeric materials to create an assortment of gas sensors to function as artificial olfactory system which has been demonstrated to detect volatile organic vapours, toxic gases and even chemical signatures associated with explosives. Studies can be carried out to investigate the potential of using such a technology in a FOS platform and applied in areas where the existing electronic-based sensing methods may be deemed unsuitable.

List of Publications

Journal

T. L. Yeo, T. Sun, K. T. V. Grattan, D. Parry, R. Lade and B. D. Powell, "Polymer-Coated Fiber Bragg Grating for Relative Humidity Sensing." *IEEE Sensors Journal*, 5(2005), 1082-1089.

T. L. Yeo, T. Sun, K. T. V. Grattan, D. Parry, R. Lade and B. D. Powell, "Characterisation of a Polymer-coated Fibre Bragg Grating Sensor for Relative Humidity Sensing", *Sensors and Actuators B*,110(2005), 148-156.

T. L. Yeo, D. Eckstein, B. McKinley, L. F. Boswell, T. Sun and K. T. V. Grattan, "Demonstration of a Fibre-optic Sensing Technique for the Measurement of Moisture Absorption in Concrete", *Smart Materials and Structures*, 15 (2006), N40-N45.

T. L. Yeo, M. A. C. Cox, L. F. Boswell, T. Sun, K. T. V. Grattan, "Optical Fiber Sensor for Monitoring Ingress of Moisture in Concrete Structure", *Review of Scientific Instruments*, 77(2006), 055108-1 – 055108-7.

T. L. Yeo, Y. Yuan, L. F. Boswell, T. Sun and K. T. V. Grattan, "Optical Fibres Sensor for the Measurement of Concrete Sample Properties following Exposure to Freeze/Thaw tests", *to be submitted to Sensors and Actuators B Chemical*, 2007.

Conference

T. L. Yeo, T. Sun, K. T. V. Grattan, D. Parry, R. Lade and B. D. Powell, "Characterisation of a Fibre Bragg Grating-Based Relative Humidity Sensor", Photon 04, Glasgow, UK, 2004.

T. L. Yeo, D. Eckstein, B. McKinley, L. F. Boswell, T. Sun and K. T. V. Grattan, "Fibre Optic Sensor for the Monitoring of Moisture Ingress and Porosity of Concrete", 17th International Conference on Optical Fibre Sensors, Bruges, Belgium, 2005.

T. L. Yeo, M.A.C Cox, L. F. Boswell, T. Sun and K. T. V. Grattan, "Monitoring of the Moisture Ingress in Structural Concrete Using FBG-based Sensors", Photonex05, Coventry, UK, 2005.

K. T. V. Grattan, **T. L. Yeo**, M.A.C Cox, L. F. Boswell and T. Sun "Monitoring Ingress of Moisture in Structural Concrete Using a Novel Optical-Based Sensor Approach", International Conference on Optical and Laser Diagnostics(ICOLAD), London, UK, 2005.